NASA TECHNICAL TRANSLATION NASA TT F-15,749

SOLAR PROCESSES AND THEIR OBSERVATION

Yu. M. Slonim
(Editor-in-chief)

Translation of "Solnechnyye protsessy i ikh nablyudeniya". Tashkent, "FAN" Press, 1973, pp. 1 - 125.

(NASA-TT-F-15749) SOLAR PROCESSES AND THEIR OBSERVATIONS (Scientific Translation Service) 190 p HC $12.50 CSCL 03B

N74-34262

Unclas
G3/29 50383

NATIONAL AERONAUTICS AND SPACE ADMINISTRATION
WASHINGTON, D. C. 20546 OCTOBER 1974

STANDARD TITLE PAGE

1. Report No.	2. Government Accession No.	3. Recipient's Catalog No.
NASA TT F - 15,749		

4. Title and Subtitle	5. Report Date
SOLAR PROCESSES AND THEIR OBSERVATION	October 1974
	6. Performing Organization Code

7. Author(s)	8. Performing Organization Report No.
Yu. M. Slonim (Editor-in-chief)	10. Work Unit No.
	11. Contract or Grant No. NASw-2483
9. Performing Organization Name and Address SCITRAN Box 5456 Santa Barbara, CA 93108	13. Type of Report and Period Covered Translation
12. Sponsoring Agency Name and Address National Aeronautics and Space Administration Washington, D.C. 20546	14. Sponsoring Agency Code

15. Supplementary Notes

Translation of "Solnechnyye protsessy i ikh nablyudeniya". Tashkent, "FAN" Press, 1973, pp. 1-125.

16. Abstract

This collection contains investigations of the physics, dynamics and interrelations of processes which develop in active regions of the Sun, and also an analysis of apparatus applicable for solar observations and the conditions of the observations themselves. One of the articles of the collection is devoted to the development of a model of the inhomogeneous chromosphere.

The collection is intended for scientific workers, graduate students and students specializing in the area of solar physics.

17. Key Words (Selected by Author(s))	18. Distribution Statement
	Unclassified - Unlimited

19. Security Classif. (of this report)	20. Security Classif. (of this page)	21. No. of Pages	22. Price
Unclassified	Unclassified		

TABLE OF CONTENTS

	Page
Annotations	iv
Solar Flares and Processes in Active Regions. Yu. M. Slonim .	1
Proper Motions of Spots in Multicenter Groups. Z. B. Korobova, B. M. Tishchenko, A. A. Tskhay and V. V. Baturin	89
Relation Between Sporadic Chromospheric Processes and the Evolution of Sunspot Groups. K. F. Kulashova	117
On a Model of the Solar Chromosphere. A. Sadikov	121
Laser Testing of the ASP-20 Spectrograph. I. Sattarov	137
Transmission of Interference-Polarization Filters for H-alpha and CaII K Lines. Z. B. Korobova	163
Study of Image Quality from the Photometric Profile of Mercury on the Solar Disk. I. Sattarov	173

ANNOTATION

This collection contains investigations of the physics, dynamics and interrelations of processes which develop in active regions of the Sun, and also an analysis of apparatus applicable for solar observations and the conditions of the observations themselves. One of the articles of the collection is devoted to the development of a model of the inhomogeneous chromosphere.

The collection is intended for scientific workers, graduate students, and students specializing in the area of solar physics.

SOLAR FLARES AND PROCESSES IN ACTIVE REGIONS

Yu. M. Slonim

ABSTRACT. The relation between flares and phenomena at the photospheric, chromospheric and coronal layers of an active region is considered on the basis of observations over 30 years. The problem of the spatial localization of flares is also investigated.

These investigations have led to the following conclusions: 1) a flare is a natural event in the evolution of an active region; 2) flare activity is determined by the initial reserve of magnetic energy of the region, and is a function of the number of poles and its field intensity; 3) particularly active flare centers are characterized by two specific features which, in combination, lead to the formation of multipolar groups: recurrent activity and large-scale vortex motions. These motions are hydrodynamic in nature and borrow their energy from the convective zone; 4) flares are divided into two independent types, which differ by the nature of their development, the physical and dynamic features, the height of origin and time of appearance in a region; 5) the evolutionary and physical features of a flare depend on its initial altitude, i.e., on the level at which it ignites; 6) the flare event develops in an analogous manner in the optical and radio ranges. The initial localization and direction of propagation of the optical phenomenon coincide with those of the radio burst; 7) flares are genetically related with all the sporadic and stationary processes of the upper layer of an active region.

Introduction

The relation between flares and phenomena of the lower (photospheric) and particularly the upper (chromosphere and coronal) layers of an active region is considered in this investigation. The questions of the spatial localization of flares and the dependence of their physical characteristics on the level of their origin, which are closely linked with the fundamental problem, are also considered. The works of the author [1 - 20], which are summarized and generalized in this investigation are based on original observations of photospheric and chromospheric processes, which were carried out at the Astronomical Institute AN UzSSR using a meniscus photoheliograph, a chromosphere telescope, and a spectrohelioscope over thirty years (1937 - 1967). In addition, some summarized materials of the Solar Survey, published in [21 - 24], were drawn upon for solving individual problems, principally statistical in nature. /3*

Historically, the representation of flares, which had accumulated during the first half of this century, depicted this complex and contradictory phenomenon in a very simplified form. A flare was considered as a static process localized in the chromosphere [25]. It was interpreted as a local enhancement of the brightness of the chromosphere (an ignition of a floccular component). Some researchers adhere to this point of view even now (cf., for example, [26]), artificially separating the flare from the processes accompanying it. Meanwhile, the occurrence of a flare is inherently linked with a combination of phenomena, which develop in the photosphere, as well as (particularly) in the chromosphere and in the corona.

The relation of flares with photospheric processes has long escaped observers. The long-observed correlation between the frequency of flares and the number of spots [2, 3, 27] was an indirect indication of its existence. But this relation became clearly perceptible only as a result of a combination of investigations carried out at the Crimean Astrophysical Observatory by A. B. Severnyy and his colleagues. These investigations showed that the localization

*Numbers in margin indicate pagination in original foreign text.

of flares in an active region and the probability of their appearance are caused by the structure of the photospheric magnetic fields and their variations in time. A. B. Severnyy established that the field of a group becomes complicated and stronger before a flare, and is simplified and weakened after [28, 29, 30]. Flares are accompanied by motions of spots and magnetic humps [31]. Finally, a significant rearrangement of the groups themselves, which is displayed in the repulsion of nuclei of like poles, occurs for intense (proton) flares [30, 32].

The relation between flares and chromospheric phenomena is expressed, on the contrary, so clearly that only the prevailing concept of the statistical nature of flares and, in part, the limited possibilities of the instrumentation used in the early years (spectroheliographs and spectrohelioscopes) prevented its discovery. Motions in flares were first discovered by A. B. Severnyy [33], and then were discussed in detail by him, together with Ye. F. Shaposhnikov, in [34] and [35]. These investigations drew the attention of observers to the type of flares, similar to prominences in the nature of development. The intensive observations of the IGY and IQSY programs aided the study of flares and prominences and revealed many characteristics of their relationship. For example, the author established the genetic relationship of flares with ejections of chromospheric plasma and with discharges of jets down from the corona [4, 6]; V. G. Banin showed that flares at the limb, in fading, degenerate into prominences [36]; Roberts [37], Menzel [38] and V. A. Krat [39] demonstrated the identity of flares and loop systems; the author was also first to show that flares are transformed into loop prominences [6]. /4

The results of investigations carried out over the last 25 years have established without a doubt the generality of the nature of flares and prominences near spots, or the so-called "fast processes" [12, 13]. Their interdependence and mutual conditionality, originally traced using re-entering ejections as an example [4, 6, 40, 41], is confirmed by the relation of flares with the phenomena of the

activation and explosions of stationary filaments (in active regions themselves, as well as beyond them) [2, 3, 14, 15, 42, 43], and confirmed by the effect of the regeneration of flares in systems of loop prominences [1, 6, 7, 8, 9, 44, 45, 46].

The physical nature of the relationship between flares and prominences near spots and the generality of their nature are emphasized by the repeatedly recorded similarity of their spectra [47, 48, 49, 50] and by the similarity of their shapes and motions.

The enumerated reasons attest to the direct relationship of the occurrence of a flare with a combination of phenomena, which develop in the upper layer of an active region. However, this relationship is not exhausted by only single fast processes — it also extends to stationary formations; the definite tendency for flares to develop along the routes of the stable filaments of a region was recently established [10, 11, 12, 13, 51].

The relation of flares with phenomena of the upper layer of an active region can be traced not only by prominences, but also directly by coronal formations. V. A. Krat and V. M. Sobolev [52] and Zirin [49] have described cases when a flare developed as a result of the sudden collapse of coronal condensation. Zirin is generally inclined to consider the phenomenon observed in H α as only a secondary reflection of a flare process actually occurring in the corona [53]. The hypothesis of the coronal origin of flares in itself is not new; it was advanced by I. M. Gordon [54] long before Zirin. We will return later to the little-studied question of the altitude localization of flares, in §8. It should be pointed out here that flares can ignite over a very wide range of altitudes. Judging from the appearance in white light of some of them, they can affect not only the chromosphere and corona, but also the photosphere. There are even indications of the existence of sub-photospheric flares [55].

The genetic relation of flares with re-entering ejections indicates that in many cases flare process is propagated from below upwards, from the chromosphere into the corona [12]. In some cases, /5

the flare process is even accompanied by a removal of photospheric material into the upper layers [9, 56]. On the other hand, flares related to coronal prominences, and particularly with large stationary filaments, actually originate in the corona and propagate downward, into the chromosphere [13]. This conclusion is confirmed by the stratification of elements in many limb flares [39, 57], and by the sequence of ignition of the lines of hydrogen, helium, metals and the rare earths [58]. Finally, the descending motions accompanying the initial phase of a flare is indicated, in the opinion of V. G. Banin [59], by the long-known effect of the "red asymmetry" of line profiles [60].

In summarizing all these assertions, we are led to the conclusion that flares originate over a wide range of altitudes, and encompass the chromosphere and corona during their development. Flares and fast processes can be considered as a peculiar mechanism of the interaction of coronal, chromospheric and even photospheric material [4, 6, 9]. The interaction of coronal and chromospheric streams can be evaluated as another indication of the extremely inhomogeneous nature of the chromosphere [61, 62, 63]. Moreover, the similar interaction of the streams speaks in favor of the hypothesis advanced by E. R. Mustel' of the coexistence of hot (coronal) and cold (chromospheric) material in flocculi [64].

I. Flares and Phenomena in the Lower Layer of an Active Region

It has been established in the works of the author [2, 3, 10, 16, 17] that the occurrence of a flare represents a natural phenomenon in the development of an active region; the distribution of flares inside an active region has also been studied in these works, their relation with the characteristics of the region have been investigated, and some features of particularly active flare centers have been developed. We will consider the obtained results.

§1. The flare as a normal symptom of region evolution. The first observations of flares performed with spectroheliographs created for observers a false concept about the exclusiveness of these phenomena. However, the results of patrolling with spectrohelioscopes later showed that these are actually very frequent, ordinary occurrences. In summarizing these results, d'Azambuja [65] expressed the assumption that the appearance of flares should be considered as a natural stage in the evolution of an active region. The correctness of a similar point of view was demonstrated statistically by us in [2, 3] by comparing the average daily patrol duration D with the number of groups (active regions) B in which flares were recorded for twelve years (1937 - 1948). As a result, it was shown that:

$$\frac{D}{24} \approx \frac{B}{A}, \qquad (1)$$

where A is the total number of groups in each of the years under consideration (for the whole twelve year interval, A = 1867 and B = 763).

Equality (1) implies that for the diurnal patrol, flares would be recorded in every group. However, the authors of a comparatively recent monograph [26] arrived at a contradictory conclusion; according to their data, the number of flare-active groups is at most the order of 40%.

Since the question of whether a flare is a natural or a random event is of fundamental importance from the point of view of the theory of the process itself, we have re-analyzed it in [16] by using /6 the uniform data of IGY, that is, the "summer" synodic rotations of 1958 No. 1398 - 1404, corresponding to April - September [22]. The probability of observing a flare, as will be shown in §6, is the greatest in the early stage of the life of a region, when it increases in less than one synodic rotation. Thus, young centers generated in the visible hemisphere were selected from the data of [22]. There were 103 such young floccular regions; flares were observed in 76 of them, i.e., in 74% of the cases. But in the materials used [22], as well as in the summaries published in [21], sub-flares do not appear. The far from complete consideration of the latter, based

only on the lists presented in [24], increases the number of flare-active regions to 86, i.e., to 83%. These statistics indicate that a flare should actually be considered as a natural event in the life history of a region, just as natural as the appearance of spots and pores in them, noted in only 88% of the cases, according to the same original data [22].

§2. Distribution of flares in an active region. In the works of the author [2, 3], the position of 1720 flares was studied with respect to two coordinate origins: the group center, and the center of the floccular field. In order to eliminate the effects of perspective compression and projection, only regions located within the longitudes $\lambda \leq \pm 50°$ from the central meridian were used. The completed investigations led to the following conclusions about the distribution of flares in an active region:

1) flares are concentrated within the floccular field within an oval area corresponding in dimension to the normally developed spot group;

2) with respect to the center of the group, their average longitude is observed shifted by $0°.6 \pm 0°.1$ to the east, and the average latitude is shifted by $0°.3 \pm 0°.1$ toward the corresponding pole;

3) with respect to the center of the floccular field, their average longitude is observed shifted by $0°.3 \pm 0°.1$ to the west.

These data are easily interpreted on the basis of the intimate relation of flares with spots, more precisely, with the processes of their formation and decay. The eastern part of a group is always less stable than the western. The processes of formation, division and disintegration of spots occur more often here; the magnetic field configuration is very irregular here. Thus, the eastern part of a group is the predominant flare area. Actually, of the 1720 flares under consideration, 897 (52%) were recorded to the east of the group center, and only 621 (36%) — to the west (the remaining 12%

are localized at the same longitude as the group center). This surplus of "eastern" flares also explains the shift of their average longitude to the east. Thanks to the inclination of the group axis to the parallel, the predominance of the eastern flares leads, at the same time, to a shift of their average latitude toward the pole. This shift is a direct consequence of the greater activity of the eastern, "high-latitude" part of the group. The correctness of such conclusions follows directly from the following data, where the shift of the flares toward the pole ($\Delta\phi$) is shown as a function of their longitude relative to the group center ($\Delta\lambda$):

Longitude from group center $\Delta\lambda$	Shift toward pole $\Delta\phi$
3°.5 toward E	0°.49
0.0	0.04
3.5 toward E	0.06

The shift in longitude to the west relative to the center of floccular field is also explainable, assuming the intimate relati of flares with spots. As was noted in [66], the group center does not usually coincide with the field center; in a majority of cases, the group is shifted towards its western boundary. We evaluated the magnitude of this shift from the data of 540 regions; it was found to be equal to 0°.9. Consequently, the group center is shifted with respect to the field center by + 0°.9 (to the west). But the flares are related to the group, and are concentrated predominantly in its eastern part. Their average longitude with respect to the group center is - 0°.6 (to the east). As a result, their average longitude with respect to the field center must be: /7

$$+0°.9\,(W) - 0°.6\,(E) = +0°.3\,(W),$$

which is actually observed.

§3. Flares and the lifetime of a region. The first indications of a correlation existing between flare activity and the lifetime of a floccular region were presented in [65]. A detailed investigation

c the question, which we performed in [2], revealed that the number of flares y originating in the region is related to the time of its existence t by the simple dependence:

$$y = t^2,$$

where t is expressed in synodic rotations, and y is the total number of flares in the first transit of t' region across the solar disk.

However, the selectivity of the material used undoubtedly affected the form of this dependence. A re-analysis (cf. [16]) based on the more massive and uniform materials of IGY [21, 22], that is, on 162 regions, indicated that the investigated relation actually has a linear, and not a parabolic nature:

$$y = kt \approx 9t. \qquad (2)$$

This refined dependence (Figure 1) indicates that the flare activity is directly proportional to the lifetime of the region. The very intimate relation of the lifetime of a region with the number of generated flares was emphasized recently in [67].

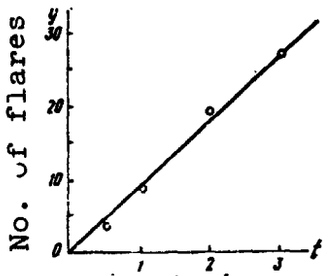

Figure 1. Relation between frequency of flares and lifetime of the region

If it is assumed that the time of existence of a region, i.e., its stability, reflects the scale of the magnetic center producing it, then theoretically:

$$t = \frac{4\pi\sigma l^2}{c^2},$$

where t is the attenuation time of the field H, l is the characteristic dimension of the region in which the variation of the field occurs, σ is the conductivity. In practice, the lifetime of a region and, consequently, its flare activity are determined by the reserves of magnetic energy of the center producing it. This conclusion follows from the dependence, which we established in [16], relating the existence time of a region with the maximum initial field intensity,

i.e., the field of the spot group formed in it (the average age of these groups generated in the visible hemisphere is 0.25 synodic rotation). The dependence (Figure 2) is based on materials of the catalog of magnetic fields of IGY [68] and data of [21]. It was obtained from 161 regions. We note in passing that, according to this dependence, the fields of the shortest-lived groups, i.e., the very short-term and, consequently, very small pores, must be no less than 1000 G. This coincides completely with recent determinations performed in [69]. /8

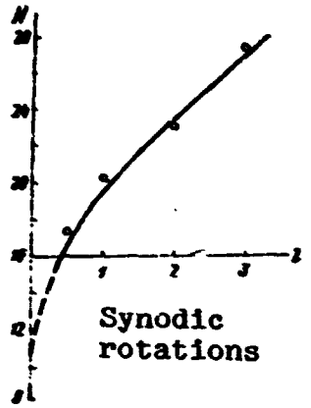

Figure 2. Relation between the lifetime of the region and initial field intensity (H is given in 10^2 G)

§4. Flares and spots. It follows from the preceding paragraph that the frequency of flares in a region must be correlated with the magnetic fields of the spots in which the initial flux is concentrated. The possibility of such a dependence is also indicated by the fact that the frequency of flares is correlated with the area of the spots [2, 3, 70], and the latter, in turn, is rather intimately related with the field intensity in the spot [71, 72]. Giovanelli, who first compared the frequency of flares with the field intensity of the group, did not find a dependence between them [70]. On the basis of more extensive material [73] and by differentiating the groups according to polarity type, we have shown that the dependence exists, and that it is linear [2, 3]. It is true that the obtained correlation coefficients were small in view of the great dispersion of the data (the value of r is 0.51 for the groups βγ and γ, and was even less for the groups β and α). However, the application of the well-known statistical criterion [74]:

$$\frac{|r|}{\sigma_r} = |r|\sqrt{n-1} > 3$$

indicated that the relation between the number of flares in a region and the maximum field intensity H is real, nonetheless [2, 3].

At present, the existence of reliable and detailed magnetic characteristics [68] permits the solution of this problem rather uniquely. As a result of the repeated investigations [16], carried out on the basis of 161 regions (i.e., the material used in the preceding paragraph) and without dividing the groups according to polarity types, we were led to rather reliable results. They indicate that the number of flares in a region is related to the field intensity of the group by an exponential dependence:

$$y = ae^{kH} \approx 0.37\ e^{0.16H}. \tag{3}$$

This dependence is represented in Figure 3. We recall that, as previously, H is the maximum field intensity of the group expressed in 10^2 G, and y is the total number of flares during the first transit of the region across the solar disk.

On the other hand, the frequency of flares in a region is certainly correlated with the number of poles of the group (nuclei and pores). Here again, the parabolic relation, which we found previously in [2, 3] has been transformed into a linear relation [16] with the use of the IGY data:

$$y = kf \approx 0.85f, \tag{4}$$

where f is the average number of poles in the group in the Soviet Solar Service system assumed by us [24].

Dependence (4), which is based on the material of 124 groups, is characterized by a high value of the correlation coefficient ($r = 0.77 \pm 0.04$), which indicates that the investigated relation is rather close. It is significant that the straight line reflecting the dependence (Figure 4) passes through the origin of the coordinates. /9 This can be interpreted as an additional verification that flares are a natural display of the activity of a region, a display as natural as the spots themselves.

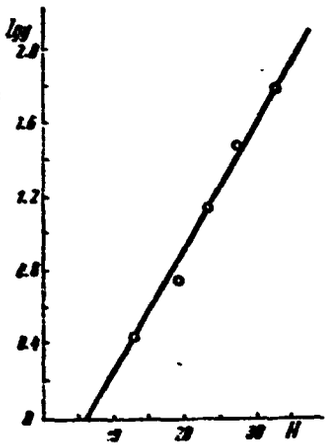

Figure 3. Relation between the frequency of flares and the maximum field intensity of the region

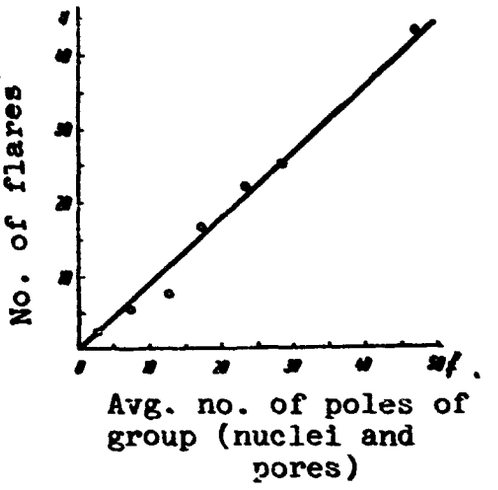

Figure 4. Relation between the frequency of flares and the number of poles of the group

As a result, the frequency of flares in a region is a function of the number of poles and the field intensity. It is also a function of the distance between the poles, since groups, which are characterized by a close proximity of spots or nuclei of unlike polarity [3] are particularly flare-active.

§5. Particularly active flare centers. It has been asserted for a long time [2, 3, 70] that multipolar groups (the types βγ and γ) are the most flare-active. According to the calculations performed by us in [2, 3], in 1937 - 1948, the average number of flares over a synodic half-period is by groups: α — 3.1, β — 5.0, βγ and γ — 16.0.

If, on the other hand, one turns to purely external geometric criteria, then they indicate [2, 3] that particularly active flare centers are characterized by an abundance of poles and by their tendency to group into two definite systems. In the first configuration, numerous fine pole-nuclei are scattered inside a gigantic spot with an irregular "shaggy" penumbra, filling an insignificant portion of its area (spot with a spattered umbra). Examples of such centers are given in Figure 5 (VI, X, XIV are the most typical; I and IX are also rather representative). In the second configuration, the poles (spots and pores) extend in a long chain or in two parallel chains

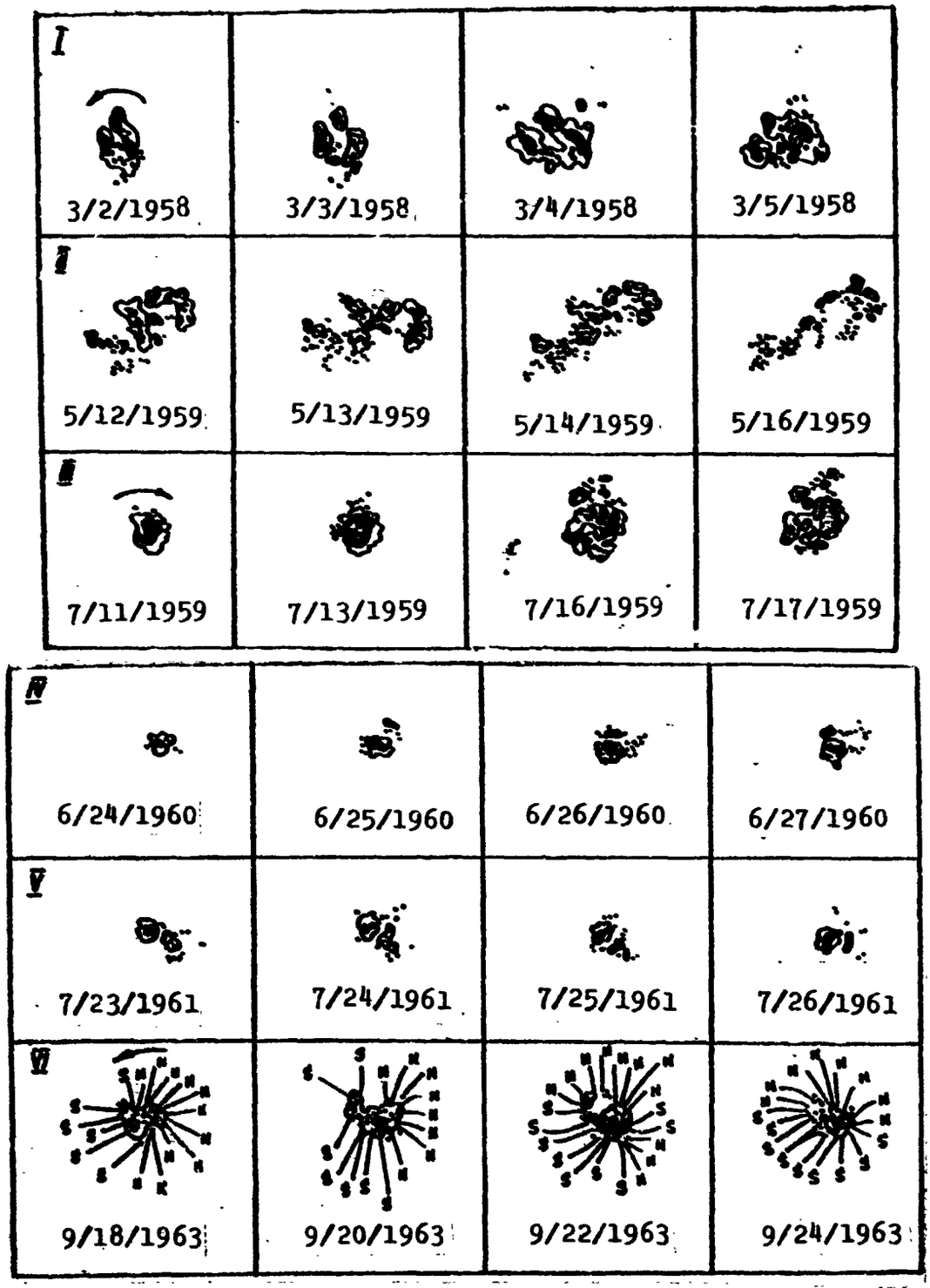

Figure 5. Particularly active flare centers:
I — group № 111, $\varphi = -16°$, $l = 10°$, 44 flares;
II — group № 251, $\varphi = +17°$, $l = 57°$, 72 flares;
III — group № 379, $\varphi = +10°$, $l = 330°$, 76 flares;
IV — group № 255, $\varphi = +20°$, $l = 60°$, 46 flares;
V — group № 208, $\varphi = +6°$, $l = 359°$, 27 flares;
VI — group № 101, $\varphi = +13°$, $l = 310°$, 87 flares;

(Figure continued on following page)

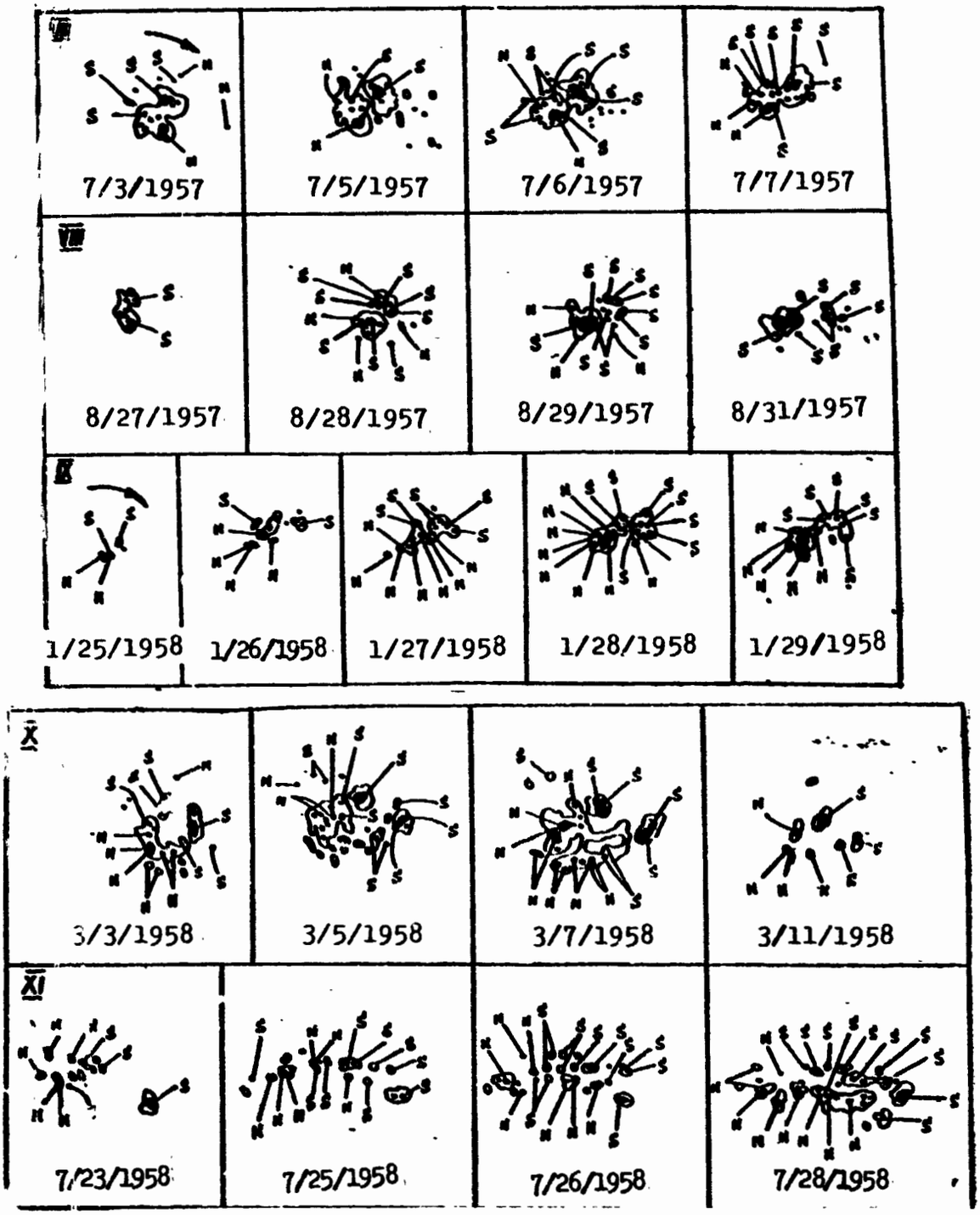

Figure 5. (continued)

VII — group № 295, $\varphi = -30°$, $\ell = 8°$, 25 flares;
VIII — group № 393, $\varphi = -20°$, $\ell = 336°$, 56 flares;
IX — group № 54, $\varphi = -10°$, $\ell = 160°$, 11 flares;
X — group № 111, $\varphi = -16°$, $\ell = 16°$, 44 flares;
XI — group № 384, № 387, $\varphi = -17°$, $\ell = 315°$, 99 flares;

(Figure continued on following page)

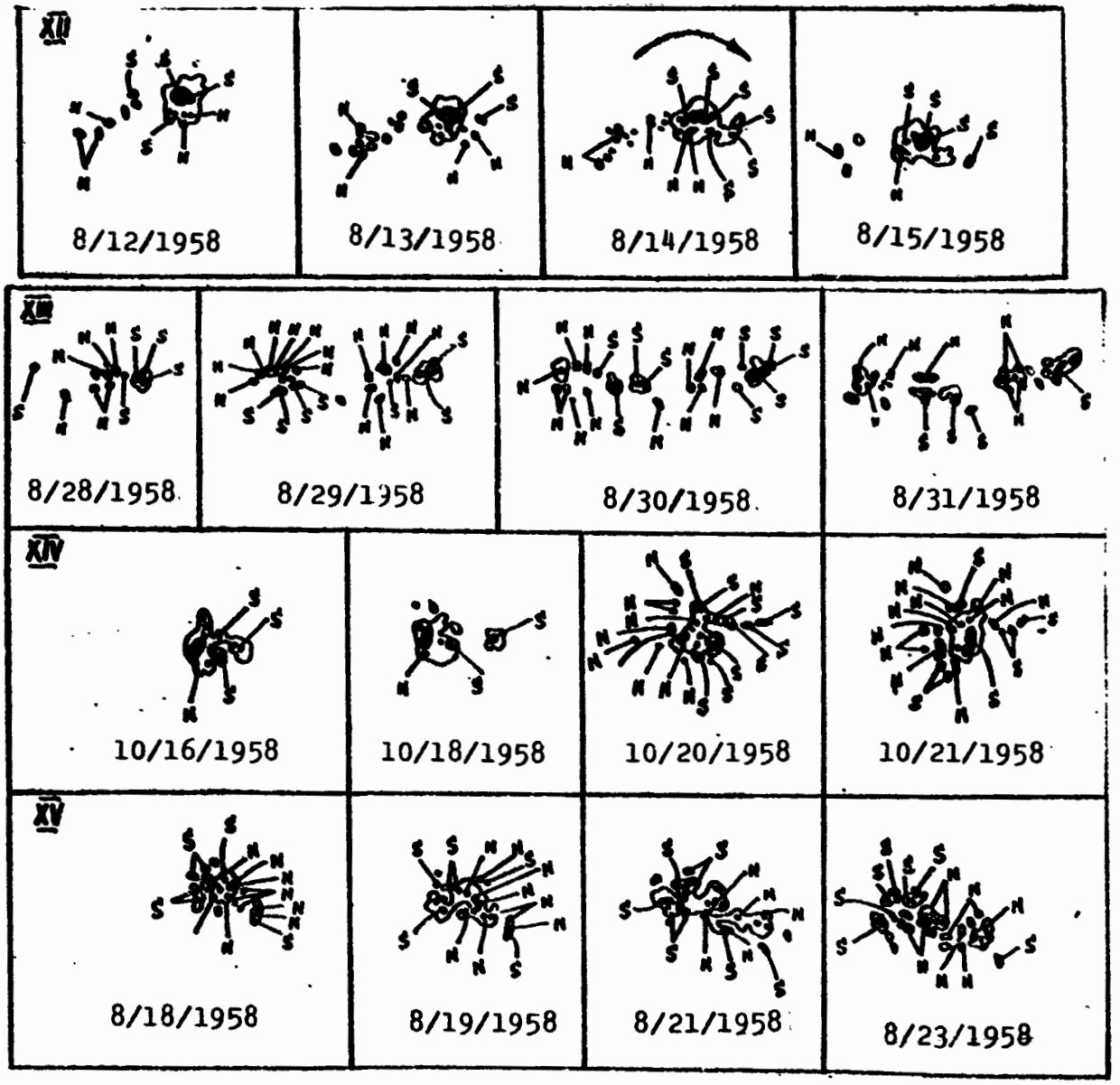

Figure 5. (continued)

XII — group № 417, $\varphi = -14°$, $l = 86°$, 66 flares;
XIII — group № 458; $\varphi = -8°$, $l = 196°$, 44 flares;
XIV — group № 554; $\varphi = -4°$, $l = 258°$, 50 flares;
XV — group № 414; $\varphi = +18°$, $l = 323°$, 67 flares

(Figure 5: II, XI, XIII). In the last case, we encounter two (or more) interfering and intertwined groups. In the opinion of several investigators [75, 76], it is just this structure, characterized by two parallel chains of nuclei of opposite polarity, which is most effective and generates, in particular, proton flares [77, 78]. However, judging from [79], both these configurations are equally typical for proton flares.

Actually, the purely external morphological features of active flare centers conceal the deeper evolutionary features, which make both these configurations related. Active flare centers are regions /15
with recurring (often repeatedly) activity [5, 9, 10, 80]. The "reprises" of activity appear: 1) in the reactivation of extinct groups; 2) in the renewal of the fading activity of groups; 3) in the generation of new young groups within already existing spot-forming centers with unrevealed decay features (cf., for example, Figure 5, XI). In the last case, the generation of a "fresh" formation in the background of the old is easily distinguished by the appearance of a striking compact floccular field superimposed on the weaker and more diffuse field of the previous center.

The regeneration of activity indicates the renewal of activity of the generating spot of an intense center, and the emergence of new systems of magnetic field tubes into the outer layers of the Sun. Activity in such regenerating centers is, on the average, twice as great as in the ordinary [17]; according to our calculations based on 125 groups (data of IGY), the number of flares in regenerating and ordinary centers are 19.2 and 10.0, respectively.

The second feature of particularly active flare centers, which was developed by us in [10, 17], involves the peculiar dynamics of their development. The spots in such centers do not have a circular, but a vortex structure; their penumbra is "shaggy", i.e., it is cut into tongues and inlets, it often has even a ring or horseshoe shape (cf. Figure 5: I, II, IX, X, XIV). The spots themselves display the effects of rotation (cf. I, III, VII, X in Figure 5); nuclei and

pores are thrown off from them along spiral trajectories (the groups III, IV, V, VI, VIII, XIV). These spiral chains sometimes close again in the spot which ejected them, but enter at another part of its penumbra (cf. IV V, VI, VIII in Figure 5). The effect of the ejection of nuclei of like poles, described in [32] for a proton flare, is evidently one of the displays of this process. In some cases (cf. VI, VII, IX, X, XI, XII), it is possible to trace the behavior of the poles of the group, which are dragged by the general "whirlpool", and circumscribe the circular or spiral trajectories inside the region.

All the enumerated facts indicate that large-scale rotational or vortex motions occur in groups, which are similar in nature with those developed first in [81], and studied in [82, 83]. These motions must originate in sub-photospheric layers.

The described evolutionary features of the centers under consideration (their regenerating spot-forming activity and their peculiar dynamics leading to "intermingling" of poles) also produce groups of complex multipolar structure in them. In other words, the multipolarity of groups is not the origin of the high-frequency of flares in these centers, but is the effect of these specific evolutionary features, as is their flare activity itself.

Both features of particularly active flare centers being emphasized are possibly interrelated. The twisting of the field lines must contribute to an increase of buoyancy, since the magnetic pressure inside such a field rope is inversely proportional to the fourth power of its diameter [84]. Thus, the twisting can lead to the emergence of new tubes or strands of field lines onto the surface, i.e., to the reprises of activity observed in such centers and to the formation of new "fresh" groups within those already existing.. The actual cause of the high flare activity of these centers evidently lies in their recurring activity, stimulating, in the chromosphere and in the corona, interactions between the systems of field lines already existing here and the new field emerging from the sub-photospheric layers [9, 11]. We established in [9] that some intense /16

flares are actually accompanied by the emergence of photospheric material into the chromosphere and into the corona; an analogous conclusion follows from [56, 85]. Moreover, flares are sometimes related to the appearance of weak photospheric loops [11, 86]. Finally, as was shown by the author in [9], and later verified by Krivsky in [87, 88], the evolution of strong flares is coupled with the ejection of magnetic field arches from the photosphere into the corona.

All the described phenomena should be evaluated as indications of the escape into the upper layers of the Sun of new tubes or strands of force lines. Their emergence can lead to contacts between the new and old fields, to the partial annihilation of fields, and to the conversion of their energy into the radiation energy of flares. Let us point out that a mechanism of the type proposed by Fokker [89] can also be a cause of the emergence of the field into the upper layers, i.e., a gradual emergence of loops of magnetic field lines into the corona caused by the opposite rotation of two dipoles. In the situation of the complex vortex motion observed in active flare centers, such a mechanism is quite possible. The fact that some intense persistent flares actually display the effects of the twisting of ropes in two opposite directions [5, 11] speaks in its favor.

Under the assumptions being discussed, the energy of flares is derived, in the final analysis, from the energy of large-scale vortex motions, i.e., from the energy of the sub-photospheric layers. Whatever the transmission mechanism stimulating the emergence of the field into the upper layers might be, it can be shown that these motions themselves are capable, in principle, of supplying the necessary amount of energy ensuring the flare activity of the flare centers under consideration. This energy can be roughly evaluated on the basis of the following simple considerations. Spot motions in active flare regions do not display a relation with polarities; they can be directed toward like poles, i.e., they have a hydrodynamic, and not an electromagnetic origin [17]. This is easily verified on the basis of data presented in Figure 5. Thus, in the cases VI

(September 22 and 24) and VIII (August 28 and 29), the pores and small spots of polarity S are moving toward the S poles of the main components; and in the cases XI (July 26 and 27) and XV (August 18, 19, and 21), the approach and fusion of spots of the same polarity occurs.

Consequently, these motions are controlled by hydrodynamic forces, overwhelming the effect of the electromagnetic forces. To evaluate the energy of the large-scale hydrodynamic motions, we will use the work produced by them against the field forces [17]. Let us assume that there is some initial field corresponding to a previously generated spot group. We will assume for simplicity that this field is uniform with an intensity H_0. Further, let there be a new bipolar group appearing within the old field under consideration as the result of the emergence of a new magnetic tube from the sub-photospheric layers. Its magnetic dipole moment M is defined as:

$$M = mD, \tag{5}$$

where $m = m_1 = m_2$ is the magnetic pole strength of each of its components, and D is the distance between them. We assume, following [90], that:

$$m = F/2\pi \tag{6}$$

and /17

$$F = \frac{\pi r^2 H}{3}, \tag{7}$$

where F is the magnetic flux, and r is the radius of each of these two spots, and H is the magnetic field intensity at the center of the spot. By taking (6) and (7) into account, we can replace (5) with the expression:

$$M = \frac{HrD}{6}. \tag{8}$$

We finally assume that the dipole representing the new group rotates in the initial field of the old group within which it

appeared. Then the work performed by the hydrodynamic motions against the field forces for the rotation of the dipole by the angle $d\phi$, in a direction approaching like poles, will be:

$$dW = MH_0 \cos\varphi d\varphi.$$

If the dipole rotates by the angle of 90° from a position perpendicular to the field, to a position parallel to the field, the work developed by the hydrodynamic motions, with consideration of (8) equals:

$$W = MH_0 \int_0^{\pi/2} \cos\varphi d\varphi = MH_0 = \frac{Hr^3DH_0}{6}. \quad (9)$$

By taking $H_0 = 3500$ G, $H = 1500$ G, $D = 10^\circ = 0.175 R_\odot = 1.2 \times 10^{10}$ cm, $r = 10^9$ cm, we find that:

$$W \approx 10^{34} \text{ ergs}. \quad (10)$$

According to recent estimates [51, 91, 92], the total energy of a strong Class 3+ flare is the order of $5 \cdot 10^{32}$ ergs, and of a Class 2 flare is the order of $5 \cdot 10^{30}$ ergs. Hence, it follows that even 10 - 15% of the energy expended by large-scale hydrodynamic motions for work against the field forces is quite sufficient to explain the actually observed activity of centers, i.e., to ensure the appearance of up to 100 flares in particularly active groups, including repeated Class 3+ events.

It can be shown that the energy of the considered hydrodynamic sub-photospheric motions is borrowed from the convective zone. Actually, if

$$\frac{\rho v^2}{2} > \frac{H_0^2}{8\pi},$$

then for $H_0 \approx 3000$ G, and the observed rate of motion of poles $v \approx 0.5$ km/sec, ρ must be the order of 10^{-4} gm/cm^3.

This implies that the large-scale hydrodynamic motions derive their energy from the convective zone, where the spots or the magnetic field tubes forming them must go for their "roots".

In concluding this portion of the investigation, we state concisely its basic conclusions.

1. A flare is a natural event in the evolution of an active region.

2. Flare activity is determined by the initial reserves of magnetic energy of the region, and is a function of the number of poles and field intensity.

3. Particularly active flare centers are characterized by two specific features, which in combination lead to the formation of multipolar groups: recurring activity and large-scale vortex motions. /18
These motions are hydrodynamic in nature and borrow the energy from the convective zone.

II. Flares and Phenomena in the Upper Layer of an Active Region

The relationship of flares and phenomena of the upper layer of an active region was investigated by us in [1, 2, 3, 4, 6, 7, 8, 9, 10, 11, 12, 13, 14, 15, 18, 19, 20]. Their relation with the activations and disappearances of stationary filaments was disclosed in [14, 15], and studied in [2, 3, 10, 11]. Their inherent relationship with re-entering ejections is shown in [4, 6, 7], and their relation with coronal types of prominences is also established. It was shown in [6, 7, 8] that flares degenerate in the development process into systems of loop prominences. Finally, an attempt was made in [12, 13, 18, 19] to generalize the obtained results, and to trace the physical relationship and mutual conditionality of the processes of the upper layer of an active region. The problem of the altitude localization of flares was investigated along with this, and the

dependence of their physical characteristics on the level of their generation was considered [7, 10, 11, 12, 13, 20]. We will discuss the results of these investigations.

§6. Two types of flares. Justification was given in [4, 6, 7] for the differentiation of flares into two rather clearly bounded classifications: the pulse type A, evolving as a sudden burst of radiation, and the delayed development type C. The classification was based, in particular, on the luminosity curves of these two types of flares. As Figure 6 shows, the A flares are characterized by an almost instantaneous ignition (a sharp "flash" phase) and a rapid drop of brightness. The swiftness and short duration of the process indicates its explosive nature. The C flares, on the contrary, are characterized by a sluggish increase of brightness, and an even more gradual decrease (cf. Figure 6). Their light curves display repeated maxima, and even repeated ignition of a point (or close, adjacent, almost coincident points). These pulsations of brightness often merge in a continuous uninterrupted chain, which is impossible to differentiate into isolated flares.

Table 1, containing the average characteristics of A and C flares, indicates that they differ not only by the duration of radiation and the ignition rate, but also by their physical features.

TABLE 1.

Flare characteristics	Flare type	
	A (n=31)	C (n=80)
Total duration	28^m	76^m
Rise time of brightness to maximum	4^m	15^m
Width of Hα, Å	5.4	2.8

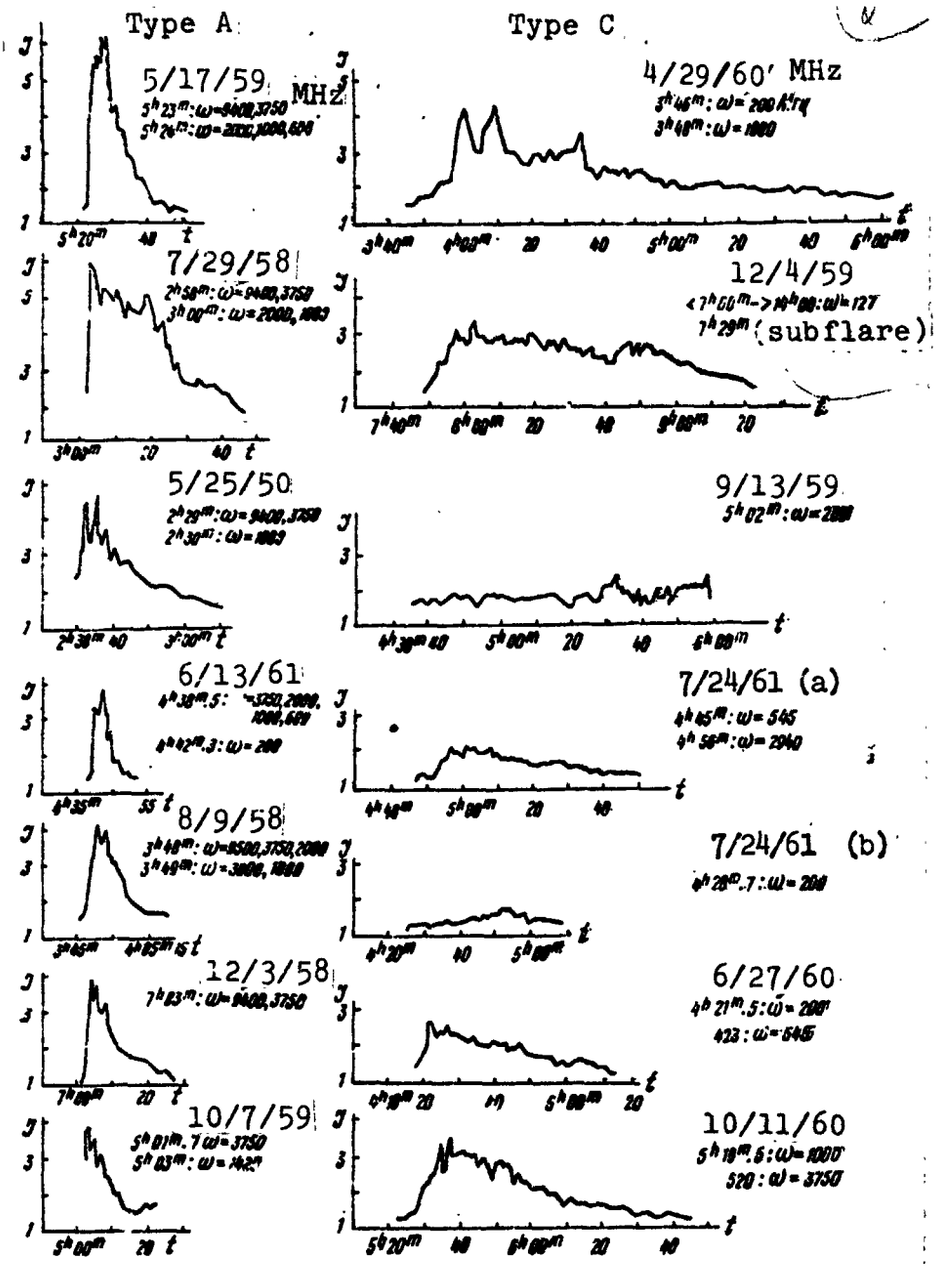

Figure 6. Luminosity curves of A and C flares (t — universal time; I — flare brightness with respect to the adjacent undisturbed chromosphere)

The spectral line is significantly wider for A flares than for C flares [6]. The average extent of the H α wings for the type A ≈ 5.5 Å; for many flares of this type, it reaches 10 Angstroms, and for several of them — even 20. The A flares are compact; they consist of a single center, are usually spiral in form, and degenerate into two close bright nuclei*. Nebulous expanding clouds sometimes propagate from this center, indicating the explosive nature of the process [12]. The C flares, on the contrary, are usually dispersed; they consist of isolated point, often not flaring up at the same time. For intense processes, the points later merge into one band.

Further, the difference between A and C flares verifies the differences in the nature of the accompanying prominences, i.e., of the associated chromospheric and coronal processes [6, 7, 12, 13].

The A flares are accompanied by emissions of plasma jets propagating from the chromosphere into the corona (in particular, by reentering ejections). In complete accordance with the postulated explosive nature of the flares generating them, the ejections of chromospheric plasma are swift and short-term. Their speed reaches 200 - 300 km/sec. The evolution of ejections indicates the partial or complete dispersion of their material into the corona, which is caused by the spontaneous disintegration of the magnetic field containing them (the dynamics of these plasma jets are interpreted in detail in §9). /19

For C flares, on the contrary, long stationary plasma discharges are observed propagating from the corona into the chromosphere. Their speed is small, the order of 40 - 60 km/sec (cf. §10). The stable repeated nature of these discharges conforms well with the prolonged pulsating development of C flares. /20

*Intense A flares are also encountered with band shapes, which are generally typical for events of Class ≥ 3. But these bands (later splitting into two strips) also have a spiral structure.

The following characteristics of the difference between A and C flares is revealed in the behavior of one of the basic physical parameters, the spectral line width. For the A flares, the width of H α is correlated with the area of the emission center [7, 12]. This relation between the area and spectral line width is illustrated by Figure 7, with the data of 24 flares. It can also be interpreted as an argument for the explosive origin of type A. Actually, the total extent of the line wings for A flares reaches 20 Å. Such broadening can be attributed to very intensive motions. Since the effects of these motions appear generally, from the center of the disk even to the limb, they indicate the scattering of the flare plasma by an explosive type process*. The stronger the explosion, the swifter the ejection of material from the flare center and the larger the area over which the process itself propagates. Hence, the relation of the H α width with area observed for A flares. The validity of this interpretation is verified by the dependence between the line width and the radial velocity of the ejection ascending from the A flare [12] (cf. Figure 8, based on the material of 19 processes).

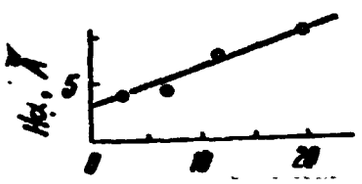

Figure 7. Relation between the area S and the line width of H α for A flares

The C flares, as is indicated by Figure 9 (based on 88 phenomena), do not display a relation between the H α width and the area of the emission center [7, 13]; consequently, their nature differs from the nature of A flares.

Finally, the A and C types are differentiated by the time of their appearance in the active region. The frequency of flares as a function of the age of the region was investigated in [65]; the results obtained in this work are completely verified by us in [2].

*The visible growth of the line width toward the edge is caused, to a significant degree, by the increase of contrast of the flares toward the limb [26], and the statistical selection of the material, i.e., the shortage of small flares at large longitudes from the central meridian.

Figure 8. Relation between the line width of H α and the radial velocity v of the ejection ascending from the flare

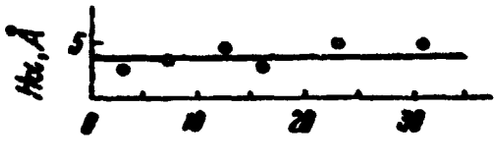

Figure 9. Relation between the area and line width of H α and for C flares

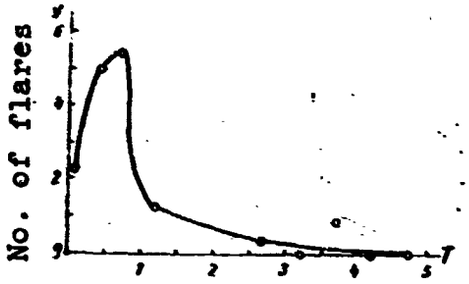

Figure 10. Dependence of the frequency of flares on the age of the active region

They are represented by the dependence of Figure 10, based on extensive statistical material (816 cases), and indicating that an overwhelming majority of flares originate in regions with an age T up to one synodic rotation, and that their frequency reaches a maximum for T = 0.75 rotation, after which it rapidly decreases.

/21

However, a more thorough analysis of the relation of flares with the evolution of groups performed by us in [7] leads to the conclusion that the dependence revealed by Figure 10 is the result of the superposition of two curves corresponding to the two different types of flares, A and C. The frequency of these two types of flares as a function of the age of the group is shown in Figure 11. One of the solid curves represents the evolution of the group area; the ascending and descending branches of the curve are symmetric, so that the age of the group, i.e., the argument T, is expressed as fractions of the growth and decay phase. The other solid curve in Figure 11 corresponds to the frequency of C flares; the dashed curve — the frequency of A flares. This statistical analysis indicates that type C originates mainly in the growth phase of the group and, consequently, of the magnetic field of the region; and type A — in the decay phase of the group and field.

The separation of A and C flares is not exhausted by the factors enumerated above; additional results verifying their differing nature will be presented in the following paragraphs.

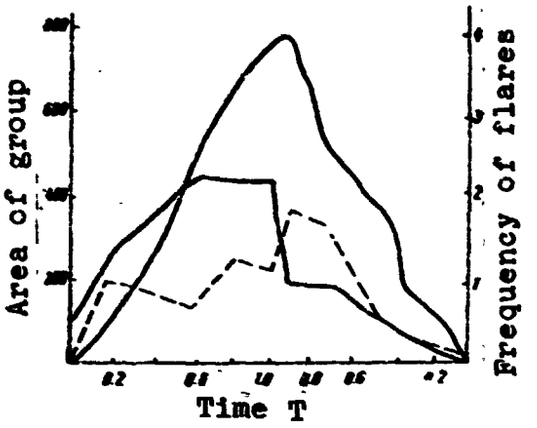

Figure 11. Frequency of A and C flares as a function of the age of the active region

Let us emphasize in conclusion that it is more accurate to speak about two types of flares A and C, since the more complex events and, particularly, intense flares with their successively ignited points can be represented as a combination of these centers.

§7. Flares and stationary filaments. The intimate relation of flares and stationary filaments has escaped observers for many years. The most direct way of studying their relationship, that is, their spatial combination, is laden with obstacles. In fact, with the recording of the phenomenon on the disk, the fact alone of the propagation of a flare along the channel of a filament and even the fact of the interchange of filament and flare still does not indicate their coincidence in space. For observations close to the edge, or at the limb itself, the clarity of the spatial picture of the phenomenon is masked by its specific factors. The perspective contraction and the loss of contrast at the edge of the Sun "erases" the filament. At the limb itself, the filament (prominence) lying at the base of the flare is screened by the foreground of the chromosphere, and by the flare itself, if it is sufficiently extended in longitude. In view of all the enumerated reasons, the interrelation of flares and filaments, which should be evaluated as the key symptom of the physical relationships of phenomena of the upper layer of a region, remained outside the field of view of observers. The fact itself that weak flares propagate along the paths of filaments of a region was noted comparatively recently [34, 93]. Ever-increasing consideration has been given to this fact in recent years. This was caused in part

/22

by the fact that flares entangled with filaments or following along their channels are often sources of meter radiation (noise storms, radio flares of type IV)[94, 95]. According to[77], for example, the presence of a filament and its position relative to the spots of the group are the deciding factor in the question of the appearance of type IV)flares, although according to other data, the role of such a dictating symptom is attributed not at all to filaments, but to the loop prominence rising from the flare [46]. In all the enumerated words, the relation between flares and filaments is considered as some specific peculiarity, and not as a general regularity. The internal relationship of these processes was first noted in [96], where rather extensive material (71 events) is analyzed, and the conclusion is reached that many, if not all, flares are associated with the activation of filaments. Later, the genetic relation of these two processes was emphasized in [51, 97] in which it was stated (to be sure, without a specific basis in observations) that the close similarity of the routes of flares and filaments, the generality of the configuration of their magnetic fields, and the agreement in time of their activity require a combined treatment of both phenomena. Finally, the mutual conditionality of flares and filaments was reemphasized quite recently by Dodson [98], who noted that intense flares (Class $\geq$ 2) appearing with weak features of photospheric activity (with spots completely missing or with only single small pores) develop along filament channels.

We encountered the first indication of the intimate interrelation of flares and filaments in 1945, with the observation of the ignition of bright components close to large stationary flares located far beyond active regions. Five cases of such processes were described in [14] and [15]. A detailed investigation of 19 similar anomalous flares, carried out in [2, 3], led to the following conclusions.

1. Anomalous flares arise close to stationary and usually extended filaments during their activation and decay. Flares preceding the appearance of such filaments should also belong to this same category.

2. Anomalous flares are ignited only on "clean" (undisturbed) parts of the disk, close to filaments or directly in the bright border framing it. In the first case they disappear without a trace; in the second, they gradually dissolve, merging with the weakly glowing frame of the filament.

3. Although anomalous flares are not related to spots, in 20% of the cases they foreshadowed the formation of a group appearing in its place from one to six days later. /23

4. Anomalous flares are not as bright as the ordinary, and their whole process has a more sluggish nature.

5. The duration of anomalous flares is confined to the range from tens of minutes to 2 - 3 hours.

The physical interrelation of flares and filaments revealed by these combined displays of their activity is emphasized by the fact that these simultaneous displays are observed outside active regions, where the combination of the two events under consideration could easily be attributed to a common perturbing factor.

Later we again encountered an indication of the intimate relationship of flares and stationary filaments (this time localized directly in very active regions) in studying the specifics of intense events accompanied by type IV radio flares [10, 11]. It was revealed in the process of these investigations that all such intense flares developed along the route of filaments, which existed, had disappeared or were formed later in the region. A more detailed analysis of the question, based on the materials of 120 flares of Class $\geq$ 1+, showed that they practically always occur along the paths of filaments existing in the region or of filaments which are observed either before or after the date of the flare [12]. Hence, it follows that the intimate interrelation with filaments is typical not only for intense events, but also for flares in general.

The identity of the spatial dimensions of flares and stationary filaments was later established [10, 20]. This conclusion is based on the comparison of their distributions in visible altitude. Two such distributions are compared in Figure 12a. The solid curve is constructed from the altitudes of 99 limb flares measured near the time of maximum brightness. Original filtergrams taken with our chromosphere telescope were used for 74 measurements, and the maps D1 [99] were used for the remaining 25. The dashed curve was obtained from the altitudes of 114 stationary prominences measured on the maps D2 [100]. The selection of the prominences is random; the first dates of eight months of 1958, beginning with January and ending with August are taken.

In Figure 12b, the altitude distribution of limb flares is supplemented by materials published in [101], which permits including 187 measurements in the investigation, instead of 99*. The same data as in Figure 12a are taken for the prominences.

The agreement of the distributions being compared is obvious in both cases. Figure 12a and 12b indicate that flares and filaments are distributed in altitude in a very similar manner. Consequently, both considered phenomena coincide with each other not only in their location in an active region, but also in their altitude localization.

If one turns to specific observations, then it is found that, in spite of the unfavorable factors masking the relation of flares and stationary filaments, recent patrol films convey direct obvious evidence of the spatial agreement of these two phenomena. Cases of ignition of bright points at the tops and crests of previously existing prominences are not rare. Examples of such processes can, in particular, be found in the observational materials published in /24
[102]. Cases of the appearance of intense limb flares in prominences

*The altitudes of the flares in [101] are understated; according to the evidence of the author himself, "bright streamers" and other structures crowning a flare were not taken into account in the measurements.

are described in [79, 98, 103], although they are considered here rather as an exception than as a rule. The intense flares of February 21 and March 7, 1942 [104, 105] are also very indicative, although the observers did not comment on this fact.

We ourselves record-1 repeatedly ignition of bright points in large activated prominences in films of the chromosphere telescope. The altitudes of such points reached 40,000 - 60,000 km. In some of them, actually localized lower (≈ 25,000 km), the observed width of H α (4 - 5 Å) is very typical for flares.

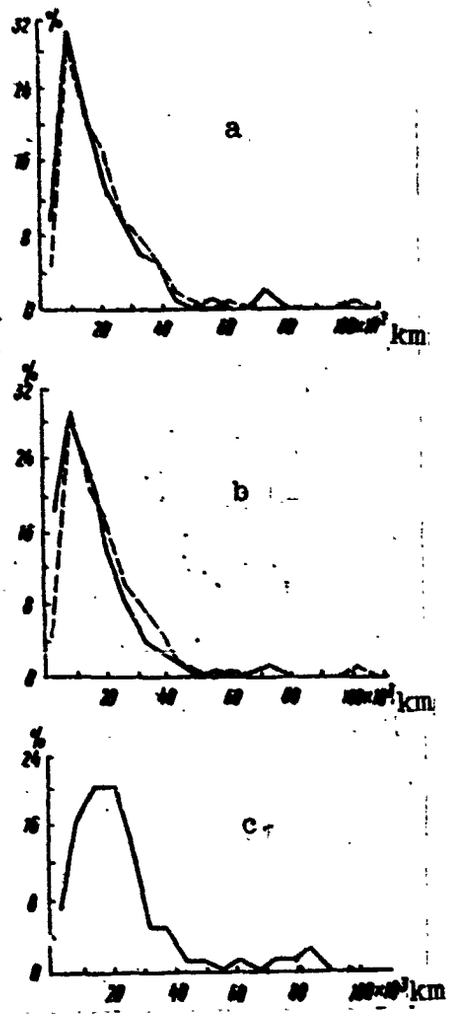

Figure 12. Altitude distribution of flares and filaments

But flares originate most frequently in bright "bulges" of the chromosphere observed above active regions, in projections lying at the base of converging loops and coronal streams [4, 6]. These bulges are projections above the limb of new lower filaments of active regions. According to our estimates, their average height is 14,000 km. Bulge prominences, when flares ignite in them, grow and "inflate", degenerating into loop systems. The degeneration into loops is typical in general for flares, as was first shown by us using the most intense of them as an example [6, 7, 10, 11]. The loop arch formed with the limb flare "straddles" the prominence along its axis (Figure 13, IV-1, VIa - VIc, IXa - IXc). The flare emissions can propagate along the arch from above downward, from the top of the prominence to its base, as has occurred, for example, in the case IV-1 in Figure 13, or in

REPRODUCIBILITY OF THE ORIGINAL PAGE IS POOR

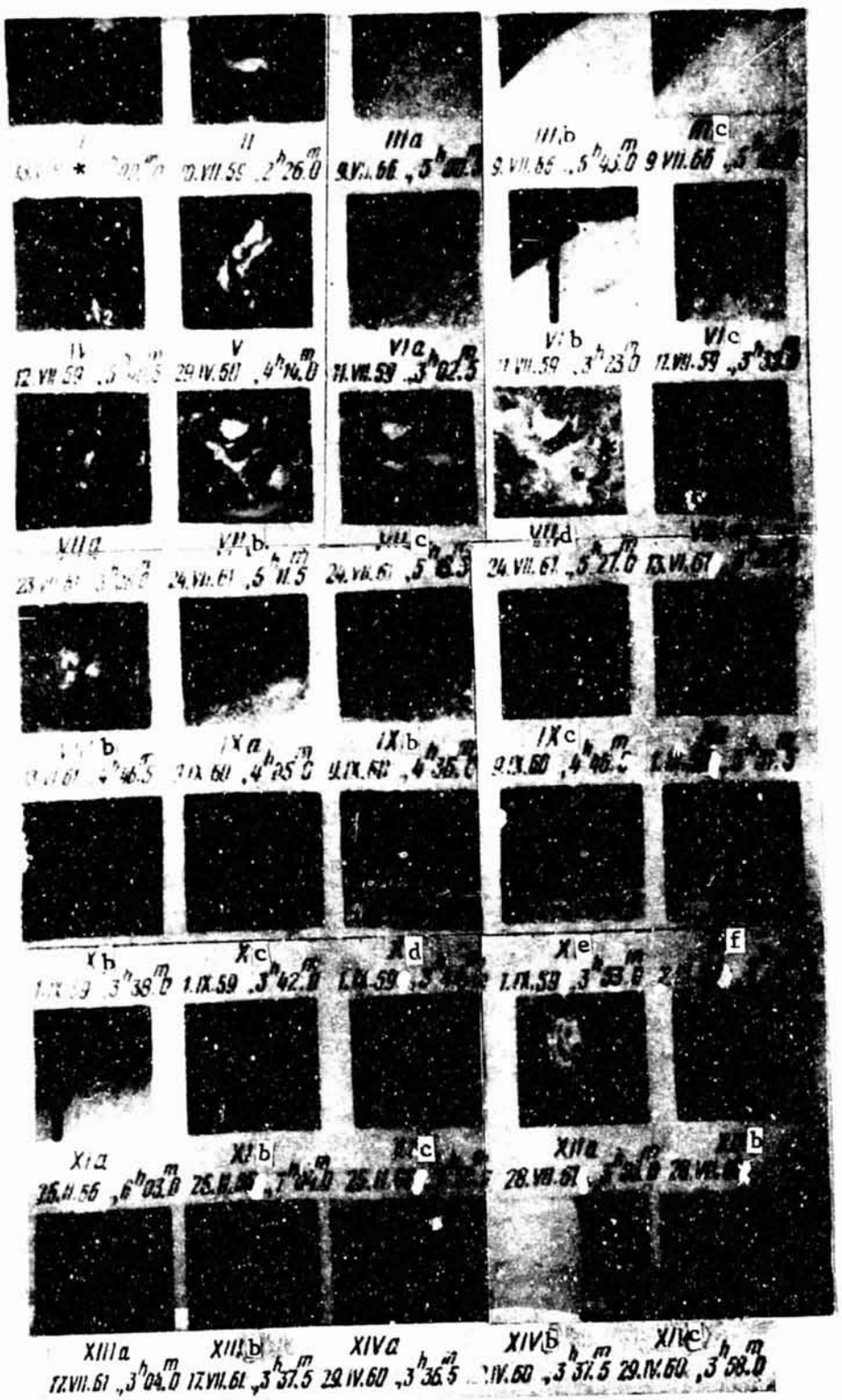

Figure 13. Relationship of fast processes and flares with stationary filaments

* Translator's note: Roman numerals in dates indicate the month, i.e., 13 V 60 is 5/13/60.

the cases of the intense flares already mentioned of March 7, 1942 [105] and May 4, 1960 [79]. But the emission develops more often from below upwards. The emission persists longest at the top of the loop arch, independently of the nature of the propagation. This causes the effect, well-known to observers, of the separation of the flare from the edge, i.e., the appearance of a dark ("white" in the negative) band under it, which separates it from the limb (Figure 13, IXc), and sometimes even a "dent" in the edge. The legs of the loop arch are extinguished more rapidly than its top, which is noted particularly in intense flares, where the points crowning the loop are brightest (Figure 13, IIIa - IIIc).

When a flare generated in a filament is observed on the disk, it changes, i.e., as if it were screened (Figure 13, I, VIIa - VIId, centers 1 and 2).

The combination of all these facts characterizing the development of a flare at the edge and on the disk indicate that it is ignited in the external layers of a filament. The flare carefully draws with its emission the loop sections of some previously invisible envelope shrouding the stationary filament. The axis of such a loop system is oriented along the flare and its loops encircle it [11]. The flare can be intense (cf. Figure 13, I, II) or weak (IV-1, VIa - VIc), its emission can outline the whole loop arch (II, VIb, IXc) or its individual sections (IV-1); the nature of the phenomenon remains the same. Its essence lies in the fact that the flare arch is inherently hollow, and this "hollow" loop cloud ignites around the filament. The hollow structure of flares is particularly well-traced near the edge of the Sun, where, with a favorable orientation, one can sometimes look through its loop shell along the axis (cf. Figure 13, II). The conclusion about the hollow nature about the loop arch of a flare and its localization external to the filament agrees with the results of [106], which indicates that the stationary filaments of a region pass through the loop systems. This conclusion is also verified by a direct comparison of the average heights of the stationary filaments, 50,000 km [107], and the loop systems at the top of their ascent, 83,000 km [46] (cf. more details in §9). The shells enveloping the

stationary filaments can be traced not only by the loop arches (or tunnels, in the terminology of Bruzek [46]) illuminated by flares. Judging from the observational data published in [108], they are also viewed in the coronal arch systems closely encircling the structure of stable prominences over a number of days in H α light, i.e., in the coronal arcs enveloping successive sections of extended stable filaments. Moreover, as was first noted by the author in [9] and verified in [88], and particularly in [109], the loop systems of flares themselves can be traced in the coronal lines, where they repeat the motions typical for H α.

To sum up: flares coincide in space with stable filaments; they evolve into loop systems through which the filaments pass. The loop systems of flares penetrate with time into the corona. They become visible not only in H α, but also in the coronal lines duplicating the dynamic picture observed in H α. Such a succession in the configurations and motions indicates the forming and controlling role of the magnetic field. Only they can dictate the stable loop figure being repeated in the chromospheric and coronal phenomena. It has been traditionally assumed that it is the magnetic field which sets the shapes and routes of the prominences originating in the corona above a region, i.e., their arches, streams, the trajectories of their jets and points [110, 111, 112]. But the loop prominences are particularly closely interwoven genetically with the field structure. Bumba and Kleczek [106, 113] identify them, not without reason, with systems of magnetic field tubes. In following all these arguments, one might suppose that the loop structure of a filament reflects the structure of its magnetic field, some field "shell" enveloping the filament. The term "shell" may be conventional, but it correctly communicates the essence of the phenomenon, consisting of flares originating in the field configurations, which generate stationary filaments, and evolving into systems of loops, which enclose these filaments. The validity of this term is verified by the investigations of Rust [114], who, as a result of simulating the field of stationary filaments, arrived at a very similar loop configuration of the field lines around it.

In fact, the presence of a magnetic field shell with filaments /26
was predicted by I. S. Shklovskiy [115], beginning with the necessity of their effective heat shielding. Grounds for an analogous concept were given in [116]. It is difficult to explain the persistent existence of these stable formations without such a field envelope. It performs the function of a heat shield for the filament, protecting it from heating in the hot coronal medium. The field shell evidently also plays an essential role in the mechanism of supporting the filament above the solar surface.

Of course, flares also arise without stationary filaments present. However, as we have already noted, observations of the disk indicate that a filament either did exist there previously, or would be formed later. Observations at the limb indicate that at the point on the edge, where a flare ignites, converging coronal streams or loops anticipating it often appear. They are typical symptoms of the presence of the fields which produce filaments. All these facts emphasize the key role of the filament magnetic field in the flare mechanism. Kiepenheuer [51] suggested that flares and filaments should be considered as two effects of the process of condensation of coronal material, differing only in the time scale. But, on the basis of the picture of the interrelation of these phenomena documented above, we are inclined to consider that the flare process itself develops in the external layers of the filament, i.e., in the envelope of field lines surrounding it.

The stationary filaments, along which flares are ignited, can be situated along a neutral line of the longitudinal field (a line separating polarities, cf. Figure 13, V), or proceed from a region being covered by the latter only at the end closer to the spot (inside) (Figure 13, XIIIa - XIIIb), or finally encircling a spot, as is observed in compact groups of type α, and more complex magnetic structure including γ (Figure 13, VIIa - VIId, filament 2, and also XIIa).

The magnetic fields of filaments are clearly related with the photospheric fields. This relation is particularly clearly traced in the example of several compact groups, where the loops of the

flare replacing an annular filament are focused in the spot itself (Figure 13, XIIa - XIIb). The close relation of the percursory fields of filaments with the photosphere is also indicated by the region of their origin. According to [117], all stationary filaments are formed in spot zones, i.e., in practically continuous belts of strong photospheric fields outlined by chains of calcium flocculi [118, 119, 120]. Filaments generated directly in groups arise in the close vicinity of spots, their closer end being oriented toward them, as if the magnetic field producing them emerges from the spots. The filament fields are capable of quickly re-establishing their configuration. This is seen from the repeated regeneration of the structures of the homologous flares related to them. It is possible that the cause of such rapid regeneration of the filament fields lies in their close relationship with the stable photospheric fields.

It is natural to assume that filaments reflect the escape of a magnetic field of a region into the outer layers of the solar atmosphere, an "island" of concentrated field in the corona, where the intensities can reach hundreds of gauss, according to [121, 122, 123, 124, 125]. The structure of the magnetic field of a flare is practically unstudied. Its loop "braid" illuminated by the flare ignited within it evidently reveals the presence of a toroidal component of the field. It is possible that there exists a poloidal component directed along the axis of the filament. Its presence is often indicated by the observed motions of gas moving along the filament toward a center of attraction located in the chromosphere and, in particular, an "absorption" of the filament into spots. In confirmation of the suggested field structure, one can refer to the results of B. A. Ioshpa [123] and Rust [114]. The first proceeded from indirect determinations, and the second — from direct recordings of the fields of quiet prominences; and both of them observed axial as well as transverse field components in filaments. This specific magnetic field structure, characteristic of filaments, was completely verified recently by Harvey [126]. /27

Filaments are the most persistent and long-lived symptoms of active regions, outlasting all other optical features of its activity. The lifetime of stationary filaments is estimated at tens of synodic rotations [127]. Perhaps this is another argument in favor of the non-force nature of the field in the upper layer of an active region, which has been supported recently [128, 129, 130, 131].

§8. Phenomena in the radio range and the altitude localization of flares. We will now consider the observed in the radio range for flares of types A and C [12, 13].

The initial burst of radio emission of the type A flares is usually confined to the centimeter range, or simultaneously encompasses the centimeter and decimeter ranges (which is explained by its high rate of motion). In an overwhelming majority of cases, the frequency of the burst decreases with time, i.e., the burst is propagating from below upwards.

Thus, for 41 investigated flares, we arrived at the following results:

Total flares studied	41 (100%)
With initial burst in the centimeter or the centimeter and decimeter range	32 (78%)
Of the 41 flares considered, propagation of burst observed in	34 (100%)
With propagation of burst from chromosphere into corona (frequency decreases)	22 (65%)

According to this summary, the initial bursts of 32 flares out of 41 were localized within the limits mentioned, and for 22 flares out of 34, the frequency of the burst decreases with time. In 12 cases, the propagation of the burst is anomalous. However, in 4 of them, it originated in the range of 3750 - 1420 MHz, and shifted subsequently in the direction of decreasing as well as increasing frequencies, which is naturally expected for the explosive nature of the process and the higher localization of the flare itself.

In our interpretation of the phenomena stimulated by flares in the radio range, we proceed from the hypothesis of I. S. Shklovskiy [132], i.e., we assume that the sporadic radio emission of the Sun is caused by the natural oscillations of the chromospheric and coronal plasma. The relation between the altitute of the ignition of a flare and the frequency of the initial burst generated by it, which is established below, serves as the strong verification of this hypothesis. Consequently, the presented data can be interpreted in the sense that A flares are generated low in the chromosphere, rather than at its upper boundaries. Moreover, these data indicate that the flare process propagates from below upwards; from the chromosphere into the corona. A complete analogy with the phenomena accompanying the A flares in the optical region is observed here; the typical ejection of plasma jets also erupts from the chromosphere into the corona (cf. §6).

Let us now discuss the picture of radio phenomena for C flares. The initial frequency of the radio emission for these flares is significantly lower than for A flares. In an overwhelming majority of /28
cases, it is $\leq$ 1000 MHz. This frequency can be considered as a reference criterion for differentiating A and C flares; it is the dividing line, beginning with which (and lower) the relation between the area of the luminous center and the width of H α disappears, which serves exactly as the typical feature of the C type (cf. Figure 9).

We have studied the appearance and propagation of the bursts for 92 type C flares. The obtained results are summarized in the following:

Total flares studied	92
Accompanied by phenomena in the radio range	51 (100%)
With initial burst $\leq$ 100 MHz	38 (75%)
Of the 51 flares considered, propagation of burst observed in	21 (100%)
With propagation of burst from corona into chromosphere (frequency increases)	15 (71%)

The pattern being observed in this case in the radio range indicates according to our interpretation that, firstly, C flares are generated above the A flares; secondly, that for C flares, the propagation of the burst (i.e., the process) is typically from above downward; from the corona into the chromosphere. The last conclusion follows even more clearly from the statistics of intense events. Thus, of 55 large flares with initial burst $\leqq$ 1000 MHz, the propagation of the burst was observed from above downward for 48, i.e., 87%. Such motion of the burst from low frequencies to high, which agrees completely with the phenomena accompanying the development of C flares in the optical range, that is, with stationary discharges of plasma from the corona into the chromosphere (cf. §6).

The radio data permits another illustration of the difference of the basic physical features of A and C flares. The frequencies of the initial radio bursts are written next to the luminosity curves of the two flare types presented in Figure 6, and, where it was possible, the direction of motion of the burst is indicated. The radio data indicate that in these cases the division of flares according to the luminosity curves is practically equivalent to their differentiation according to the initial frequency criterion. An analogous conclusion was reached by S. T. Akin'yan [133], who stated that the frequency and time characteristics of radio bursts reflect the flare types corresponding to them.

The phenomena in the radio range verify the physical individuality of the A and C flares. The radio bursts generated by these two types of events indicate significant differences in the localization and propagation of A and C flares. We will now enumerate the arguments indicating that the altitude of C flares is greater than the altitude of A flares. The question here is the initial localization at the time of origin.

1. As we have verified above, the initial frequency of the radio emission indicates the high level of origin of C flares and the low level of origin of A flares [12, 13].

2. It is no less significant that, as has already been noted, radio bursts of C flares are shifted with time toward higher frequencies, and bursts of A flares, on the contrary, are shifted with time toward lower frequencies [12, 13].

3. The phenomena in the optical regions also reveal an analogous picture. For C flares, the process propagates from the corona into the chromosphere (stationary discharges of plasma); for A flares — from the chromosphere into the corona (ejections of plasma jets) [12, 13].

4. The pulsating nature of bursts of several emission points and centers of C flares is very similar to the nature of the radiation of points and jets of prominences formed in the corona above spots [7]. Thus, it is natural to assume that these specifics of the luminosity curves for C flares are explained by their coronal origin. /29

5. The interaction with the coronal medium can also explain the fact that, according to our calculations, 34 out of 49 flares, in which helium lines were observed in the emission according to the data of [21], i.e., 70%, belonged to type C [7].

6. This same interaction with the coronal medium can explain the appearance of the Balmer continuum in the emission indicating recombination processes, which were observed predominantly in C flares (in 6 out of 8 cases, according to our calculations [7] performed on the basis of the materials of [21]).

7. Judging from [134, 135], regenerative flares, i.e., type C flares, often build up along the neutral line of the transverse field of a region, in other words, at the tops of arches formed by the magnetic field lines. This indicates that C flares are localized in the corona above the group [7].

8. Finally, as statistical investigation has shown [136], the greatest altitude above the chromosphere is reached by weak flares,

i.e., mainly C flares (with a small H α width and, consequently, with low brightness [17]).

All these facts coordinate well with the hypothesis of the coronal origin of C flares, and indicate the high localization of their initial points.

TABLE 2

Initial frequency of radio emission of flare, MHz	3400—2000 (λ=3—15 cm)	2000—500 (λ=15—60 cm)	200—80 (λ=150—375 cm)
Total length of filament	15°.5	22°.5	35°.5
Altitude of flare, 10^3 km	17	24	65

Refinement of the question of altitude localization of flares is directly assisted by their relation to stationary filaments. We have shown in [10] that the average dimensions of stationary filaments depend on the frequency of the initial radio emission of flares associated with them. For the shortest filaments, flares are generated with initial bursts in the centimeter range, and for the longest filaments, are generated with initial bursts in the meter range. This conclusion is based on the data of Table 2, constructed with the division of flare bursts into centimeter, decimeter and meter ranges for 40 filaments.

The dependence between the total length of the filament and the level of the initial burst of the generated flare (following directly from comparison of the first two rows of Table 2) indicates in itself, there must exist a relation between the dimensions of the stationary filament and its altitude. We actually established, on the basis of the materials of [22], that the dimensions of new filaments (i.e., filaments which have not merged with neighboring filaments) are undoubtedly correlated with their altitude [10]. The relation based on 127 filaments is presented in Figure 14. It permits a rough estimate of the spatial localization of flares, more

/30

precisely, the level of their ignition. In our opinion, it also permits the simultaneous tracing of the original altitude of the source of centimeter, decimeter, and meter radio emission. The estimates obtained by this method (measured from the edge of the chromosphere) are given in the last line of Table 2. They reveal a clear relation between the altitude of a flare and the frequency of the burst generated by it. This relation also appears distinctly in the following two tables of this section.

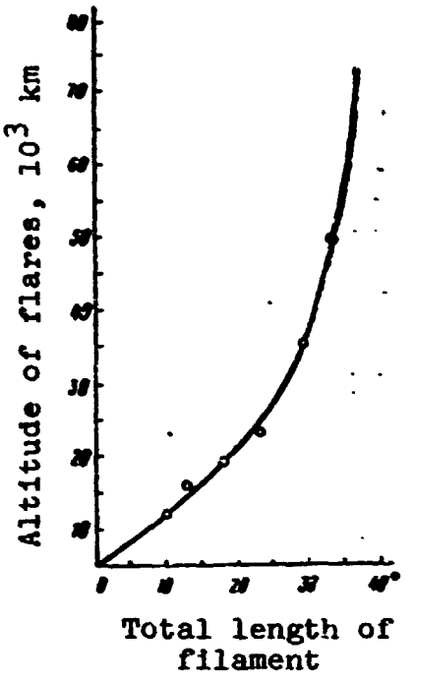

Figure 14. Relation between dimensions and altitudes of filaments

The dependence of Figure 14 leads to the average values of altitude indicated in Table 3 for the two specific types of flares A and C, whose dividing line lies

TABLE 3

Type of flare	A	C
Initial frequency of radio emission of flare, MHz	9400 - 2000	1000 - 80
Altitude of flare, 10^3 km	17	32

at the frequency of 1000 MHz. These values are obtained from intense complex flares with successively ignited centers, which actually could have been located at different levels. However, since the method being applied characterizes the altitude of the origin of these flares, i.e., the altitude of their initial points, which are localized either in the chromosphere or in the corona, we have the right to extend the obtained conclusions to the primary flares of types A and C.

But there also exists another more direct way of determining the altitude of emission of types A and C, which is based on the data of limb flares. We have also applied them in [20] to the verification of the results obtained by the preceding method. A number of attempts to find the true altitude distribution of flares on the basis of limb events is known [101, 137, 138]. However, the refined and complicated reduction processes used in these works are not always justified in practice, since they lead to very contradictory results. On the other hand, the statistics themselves on limb flares are selective just in view of the following two factors, which are difficult to take into account. Firstly, flares with the bottom lying in the visible hemisphere are recorded more often close to the edge of the Sun. They are more easily observed and more simply distinguished from bright prominences. Secondly, of the flares with longitude λ, close to /31
$\pm$ 90°, only those are recorded as limb, for which the ascending motions are directed beyond the edge of the Sun (positive radial velocity. It is clear from elementary geometric considerations that flares with motions directed toward the observer (negative radial velocity) do not usually emerge beyond the edge.

Being guided by these limitations imposed by the very nature of the observational material, we considered it advisable to use only those limb flares whose bases were located in the visible hemisphere, i.e., flares with $\lambda \leq \pm 90°$. Taking into account the contradiction of the results obtained in [101, 137, 138], we gave up complicated reduction procedures and approached the problem with an approximation method, using for the determination of the flare altitudes at the edge of the Sun the simple formula:

$$R_\odot + h = (R_\odot + H)\sec\lambda_e, \tag{11}$$

where h is the true altitude of the limb flare, H is its observed altitude at the time of the brightness maximum, and $\lambda_e = 90° - |\lambda|$ — is its longitude from the edge.

The obtained distribution of flares according to their true altitudes is shown in Figure 12c. This distribution based on 84

flares is very similar to that presented in [101], particularly if it is taken into account that in [101] the minimum values of the altitudes were taken, i.e., the bright structure crowning flares were rejected. Judging from the nature of the distribution shown in Figure 12c, the simplified method used by us for reduction to the edge is quite valid. Actually, according to this distribution, the altitudes of 88% of flares lie within the level of chromospheric bulges ($h_{max} \approx 30{,}000$ km), i.e., it is there that a majority of flares are actually ignited. These bulges, as was noted in the preceding section, are projections above the limb of low new filaments of active regions.

Several flares of the investigated distribution (cf. Figure 12c) were accompanied by radio bursts. This fact permitted the determination of the altitudes of A and C flares and a comparison of the results obtained by the first, indirect (I) and the second, direct (II) methods. They are summarized in Table 4. It should be taken into account that in case I, the altitude of the origin of flares is determined; and their altitude at the moment of maximum brightness is determined in case II. Thus, for rapidly ascending A flares, the altitudes estimated by method II must be greater than the altitudes found by method I. We emphasize that the results obtained by both methods agree well, although the first of them, based on the relation with filaments, operates only with very intense flares, and the second, based on limb events — with comparatively weak flares.

Table 4 indicates (cf. the last line) that the average altitude of all flares (without division by type) must be the order of 25,000 km. This estimate coincides completely with recent determinations of the altitudes of flares in the x-ray range [139].

Judging from the data obtained by method I, the average altitude of origin of A flares is the order of 17,000 km. The average level of their ignition practically corresponds to the average level of chromospheric bulges (14,000 km). Streams of ejections generated by

TABLE 4.

Type of flare	Method I		Method II	
	No.	Average altitude, 10^3 km	No.	Average altitude, 10^3km
A (9400 - 2000 MHz)	18	17	15	22
C (1000 - 80 MHz)	18	32	14	30
A and C	36	24	29	26

A flares frequently escape from such bulges. According to the distribution of Figure 12c, about 20% of the flares clearly related to type A originate at very low altitudes, from 2000 to 10,000 km. It is very probable that they are related to the type of low-lying filaments extending on the disk to the penumbra of a spot, the type which, in the opinion of Waldmeier [140], is located in deep layers at the H α_2 level, and is hardly reflected at the limb by prominences. On the other hand, observations on the disk indicate that A flares frequently (in 90% of the investigated cases) ignite in the immediate vicinity of spots, i.e., where the trajectories of filaments near spots descend downward into the chromosphere. All this indicates that A flares are localized close to the upper boundary of the chromosphere; they originate in low filaments and in the chromospheric "roots" of filaments. Taking into account all the facts and, also, that A flares are sometimes associated with changes of the shape of flocculi themselves, they should be called chromospheric flares. /32

C flares originate in high chromospheric bulges (new filaments of active regions) ascending up to the level of 32,000 km. They are also ignited above the bulges in large activated prominences (i.e., filaments). Thus, for example, Zirin recently described two flares originating close to the edge of the Sun in extended active filaments [141]; according to our classification, these flares belonged to the

type C. Zirin found that the altitude of the filament associated with one of them was no less than 140,000 km. According to our estimates (cf. Tables 3 and 4), the average altitude of C flares is 30,000 km, and the average level of origin of the highest of them related to initial meter bursts reaches 65,000 km (cf. Table 2). C flares are clearly ignited in the corona, and we have the right to call them coronal flares.

The combined representation of low, flat and static flares is based on the disregard of their relationship with prominences. The tendency has also risen from this to differentiate the nature of the flares on the disk and at the edge of the Sun, and also the uncertainty with which observers relate limb events to the discharge of flares. It should be remembered that for observations on the disk, we overlook the highest and most dynamic components of flares, and not only because of their Doppler shifts. While the contrast increases in proportion to the opening of the line wings for the absorbing components, it sharply decreases for the emission components with a brightness close to the continuum. Thus, the loops of flares are as difficult to observe on the disk even using a spectrohelioscope or an interference-polarization filter with shiftable pass band. We will see these loops in the red wing of lines only when they, having faded, are recorded in absorption, i.e., at the later stage of the flare. Meanwhile, the greater extent of the red wing of H α signals the discharge of material along the loops long in advance of that. Only for very intense flares are the loops visible in emission at the earlier stage of the process, thanks to their exceptional brightness (exceeding 150% of the continuum) and the line width.

In view of these reasons, we can obtain a complete presentation /33
of the flare event just at the edge of the Sun. That is why limb flares are so dissimilar to flares on the disk. Finally, it is this which explains the tendency for even experienced observers to consider the base of a flare and the prominence resulting from it as two independent, although related phenomena. Such an interpretation is artificial and contradicts the logic of the facts, since hardly

anyone has seen a plane flare at the limb, i.e., a flare which would seem to be a bright static band at the edge of the chromosphere.

The physical characteristics of flares are clearly related to their spatial localization. This conclusion follows directly from the fact that A flares, which are characterized by a swift pulsed development, bright emission and narrow spectral lines, originate high in the corona (cf. Table 4). This dependence of the physical characteristics of flares on the level of their generation is also traced in more complex events, in which A and C centers can be combined. It is easily recognized by differentiating such intense complex flares by their initial radio bursts. The conclusions based on them are even more convincing statistically, because they are always associated with phenomena in the radio range, whereas many ordinary flares, particularly type C, do not generally generate bursts (it is sufficient to compare the first two lines of the summary on page 41). We have used for these purposes a list of 174 particularly intense flares associated with type IV bursts [142]. As a result of their differentiation by the frequency of the initial radio emission, the average relative characteristics of low and high flares were obtained (Table 5).

TABLE 5

Initial frequency of radio emission of flare	9500 - 2000 MHz (λ = 3 - 15 cm)	100 - 80 MHz (λ = 30 - 375 cm)
Flare altitude, 10^3 km	17	32
Duration of flare, min	106	131
Rise time of flare brightness of maximum, min	17	25
H α width in flare, Å	7.3	4.7
Flare area, sq. deg.	11	15

Note: Altitude of flare determined by method I.

The subdivision of flares by ascending and descending bursts, equivalent in principle (Table 6), leads to practically the same results.

TABLE 6

Propagation of initial flare burst	Upward (frequency falls)	Downward (frequency rises)
Duration of flare, min	98	135
Rise time of flare brightness to maximum, min	18	26
Width of H α in flare, Å	7.0	4.8
Flare area, sq. deg.	11	15

Tables 5 and 6 verify the ...sical differences of flares with chromospheric and coronal origin. Flares originating in the chromosphere are undoubtedly characterized by a shorter duration of the process, a swifter rise of brightness to maximum, a significantly greater width of the line H α, and a smaller area. Thus, even in such complex persistent events, the features of the differences characteristic of the primary types A and C appear clearly. This conclusion broadens the framework of our original classification and permits extending it to all flares with chromospheric and coronal origin /34 irrespective of the dependence on their intensity and even on their complex nature.

Finally, on the basis of the same data [142], the flares were subdivided according to the nature of the initial radio emission into three categories, roughly corresponding to the centimeter, decimeter, and meter ranges. The results of this differentiation are presented in Table 7.

TABLE 7

Initial frequency of radio emission of flare	9500-2000 MHz (λ=3-15 cm)	2000-500 MHz (λ=15-60 cm)	200 - 80 MHz (λ=150-375 cm)
Flare altitude, 10^3 km	17	24	65
Duration of flare, min	106	128	132
Rise time of flare brightness to maximum, min	17	26	28
Width of H α in flare, Å	7.3	5.1	4.1
Flare area, sq. deg.	11	13	16

Note: Altitude of flare determined by method I.

Strictly speaking, the flares with coronal origin are subdivided here into two levels: lower (decimeter), and upper (meter). Table 7 reveals, even more clearly than the preceding two, the close dependence of the physical characteristics of flares on their spatial localization, i.e., on the level of their origin. The lower a flare occurs, the shorter it is, the shorter the rise to maximum brightness, and the greater the width of H α, the more compact its center; in other words, the closer all the characteristics of the flare are to the pulse type, based on our representations of this phenomena. And, on the contrary, the higher the flare is ignited, the more anomalous it is from the point of view of the component representations; the more gradual its evol ion, the smaller the width of H α, the more extended its boundaries, and the less determinate its configuration.

§9. Interrelation of processes of the upper layer of an active region. The results of §8 reveal the key role of the filament field in the flare event. But the field generating a stationary filament /35
plays a no less important role in the mechanism of fast processes. We will trace the chain of mutually conditional phenomena of the upper layer of an active region: flares, filaments, and fast processes;

and try to justify a physical classification of past processes based on the evolution of the field shell of a filament [11, 12, 13].

The short-term phenomena observed in the upper layer of an active region, called "fast processes", represent in essence either a transformation of prominences (filaments) previously existing, or the formation of new prominences. These processes, with all their external diversity, can be differentiated, first of all, into two categories, according to the features of the flares associated with them. The first of them related with the explosive A flares is characterized by a swift pulsed development. The second category related with the slowly developing C flares is charactarized by a relatively gradual evolution.

We will first consider the first category of processes. This includes the long-known and well-studied phenomena of re-entering ejections at the edge and on the disk (BSL, BSD, DSD) accompanying A flares. Up to now, it has been assumed that these phenomena are independent of stationary filaments, and are not related genetically with them. However, as was first shown in [11] and then verified with 15 processes as an example in [12], re-entering ejections always originate and are propagated (even if partially) along the trajectories of filaments previously existing in the region. They are emitted from "invisible" filaments. The conclusion that ejections are propagated along the route of stationary filaments, which have disappeared, is substantiated by the coincidence of their heliographic coordinates, as well as the evolution of specific physical processes. Examples of the latter are given in Figure 13 (VIIa - VIId, process 3; VIIIa - VIIIb). They indicate the replacement of a stable flare, which existed a day or sometimes an hour before them, by a formation undoubtedly identical to a re-entering ejection, and at the same time associated with the explosion of some loop structure. This reciprocity of filaments and re-entering ejections emphasizes their close genetic relationship.

We encounter a very similar process in the emission of plasma streams from filaments, discovered by us [12]. These ejections of

streams are also related to the pulsed A flares. Development of the process is characterized by a regeneration of the stationary filament, or part of it, into a loop structure, by the splitting of strands of this structure and by their flight up into the corona (Figure 13, IXa - IXc, Xa - Xe). The process is sometimes concluded by the almost complete disruption of the entire filament (cf. Figure 13, frames Xa - Xe, and frame Xf obtained the following day).

The jet strand broken loose from the filament evolves quite similarly to a re-entering ejection. It displays the same swift ascent, expansion, dissipation in the corona and subsequent precipitation into the chromosphere of its remaining part. From the physical point of view, both processes are quite identical; the difference between them lies only in the fact that an ejection stream is emitted not from an existing filament, but from one which has disappeared.

The emission process of jet strands from filaments can be regenerated; a case has been noted when it was repeated three times. We encounter an analogous regeneration of a phenomenon for the re-entering ejections, as if some trigger mechanism acts here and there, releasing the excess energy accumulated in the original field of the filament.

But in the best expressed and typical form, the phenomenon of /36
the disruption of a filament and the dissipation of its plasma in the corona is displayed in the third type of processes related to A flares; that is, in the spontaneous upward flight of filaments and prominences. Such a process on the solar limb is classified as an eruptive prominence (EPL), and on the disk — as a sudden decay of the filament (SDF). We stipulate at once that the topic is precisely sudden disappearances, i.e., the actual explosions of filaments and prominences. Unfortunately, the established term has become vague and imprecise, since, along with such actually catastrophic events, it includes gradual dissipations of filaments. These gradual disintegrations of filaments, their activation, their depletion by streams pouring into centers of attraction are characterized by a

relatively quiet evolution, and are related with the prolonged C flares. They belong to the second category of processes.

For actual sudden disappearances, the upward flying filament degenerates into a swiftly expanding loop system, which then explodes, disintegrating into individual rapidly ascending and uncoiling stream threads (cf. Figure 13, IXa - XIc, and also Diagram 18, based on an actually observed upward flight of a filament).

The conclusion about the unity of the nature of the three considered types of processes — that is, re-entering ejections (DSD, BSD, BSL), emission of jets from filaments and the upward flight of filaments (SDF, EPL) — is verified by the analysis of their dynamics [12]. The dependence of velocity and time was constructed for 21 such processes on the basis of measurements carried out on a spectrohelioscope with the help of a lineshifter. Nine re-entering ejections (Figure 15, A_1), seven emissions of jet strands from filaments (Figure 15, A_2), and five eruptive prominences (Figure 15, A_3) were investigated. In the first two cases, there were intentionally considered only those processes where all stages of development were tracked, i.e., where for the upward flight of an ejector or strand their observed complete dissipation in the corona did not occur so frequently. The motion of the basic core was considered in analyzing eruptive prominences, i.e., the dynamics of the points scattering in all directions of the EPL, which masks the essense of the phenomenon, were not taken into account*.

In all the studied cases, the dependence of velocity and time demonstrates the same pattern, well known for the evolution of

*The dynamics of the upward flight of filaments have been insufficiently studied. Our presentation is based on the tangential component (motions of the prominences in the image plane), where it is difficult to delimit the actual motions from the effects of the propagation of the distrubance. As Waldmeier correctly notes [140], neither the first nor even more so the second law of Pettit [143, 144] is satisfied for observing phenomena on the disk.

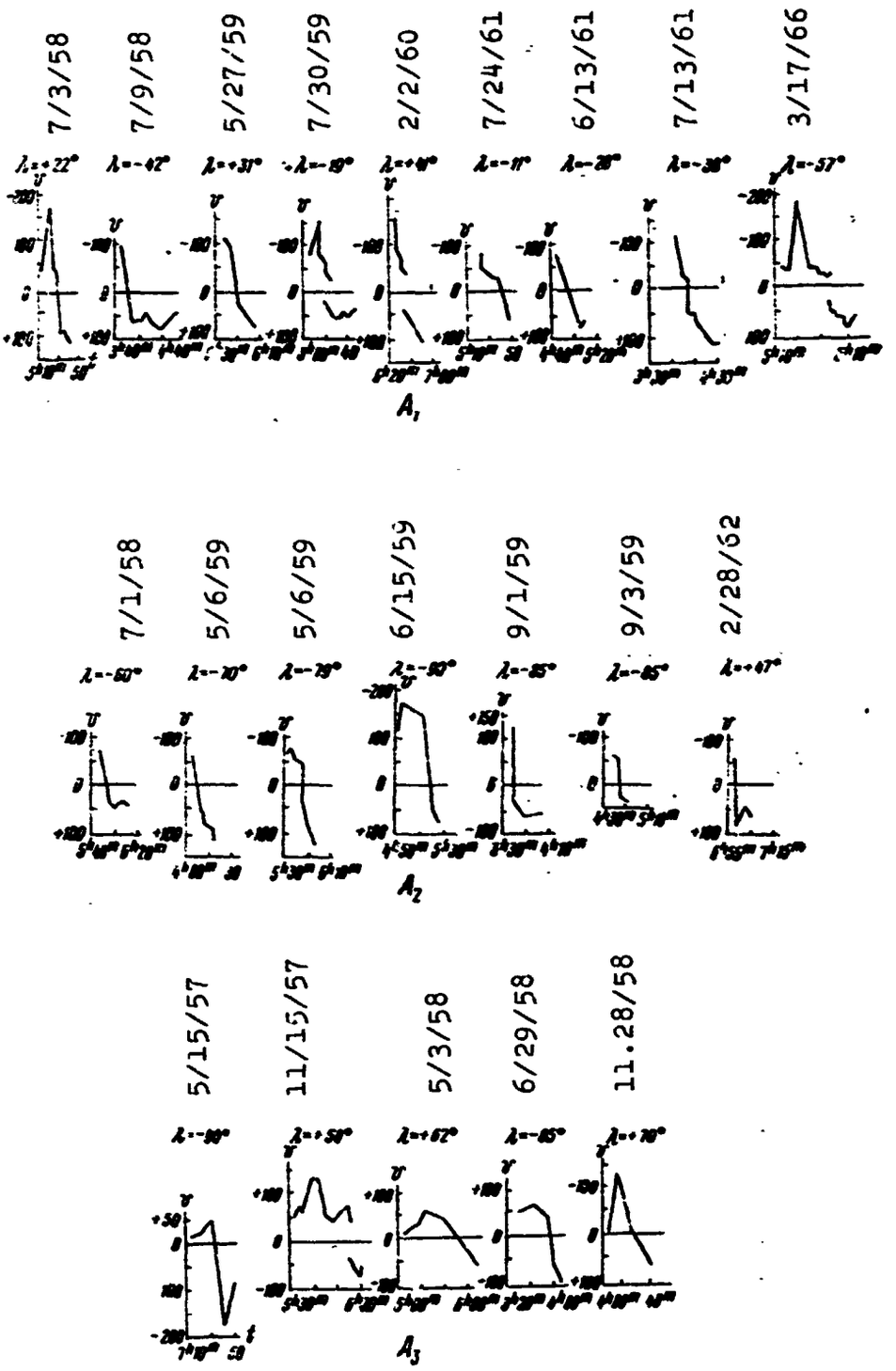

Figure 15. Dynamic pattern for A flares; t — universal time, v — radial velocity (km/sec)

re-entering ejections. For the upward flight of a filament as a whole or its individual jet strands, as well as for the upward flight of a re-entering ejection, the velocity of ascent rapidly increases, reaches a maximum ($\sim$ 150 - 200 km/sec); then the motion slows and finally reverses, i.e., the fragments of the jet settle into the chromosphere, attracted to it with increasing velocity. We consider this generality of the dynamic features of re-entering ejections, the emissions of jet strands, and the explosion of filaments as an important argument of the genetic unity of processes related to A flares.

The internal relationship of these processes and their explosive nature are also emphasized by their evolutionary features. There occurs for all the processes associated with A flares a swift expansion of the loop-type shell, its disruption and the ejection of jet strands from it. In the case of re-entering ejections [6 - 11] and the emission of strands from filaments [12], as well as in the case of the upward flights of filaments [145], the ejected streams have a characteristic coil structure, reminiscent of a tightly interwoven rope or "cable" of bright strands. This structure, in proportion to the ascent of plasma jets, decays, as if unwinding, into expanding spiral coils (Figure 16). The difference between the processes under consideration involves only the scale of the phenomena; for the upward flight of filaments and prominences (SDF, EPL), their entire loop structure explodes (cf. Figure 13, XIa - XIc and Figure 18), whereas for re-entering ejections (DSD, BSD, BSL) and the emissions of jets from filaments, the fast expansion of the loop structure is concluded with the explosion of only an individual component or the decay of an individual strand (Figure 13, IXa - IXc, Xa - Xe). /37

It is natural to relate the spontaneous explosions of filaments and the emissions of jet strands from them with the explosive disintegration of the fields forming them. The phenomena of re-entering ejections, firmly tied, as has always been shown, with the routes of previously existing filaments, can be interpreted analogously as the result of the disruption of those fields which formally generated these filaments. It is in this sense that one should interpret the

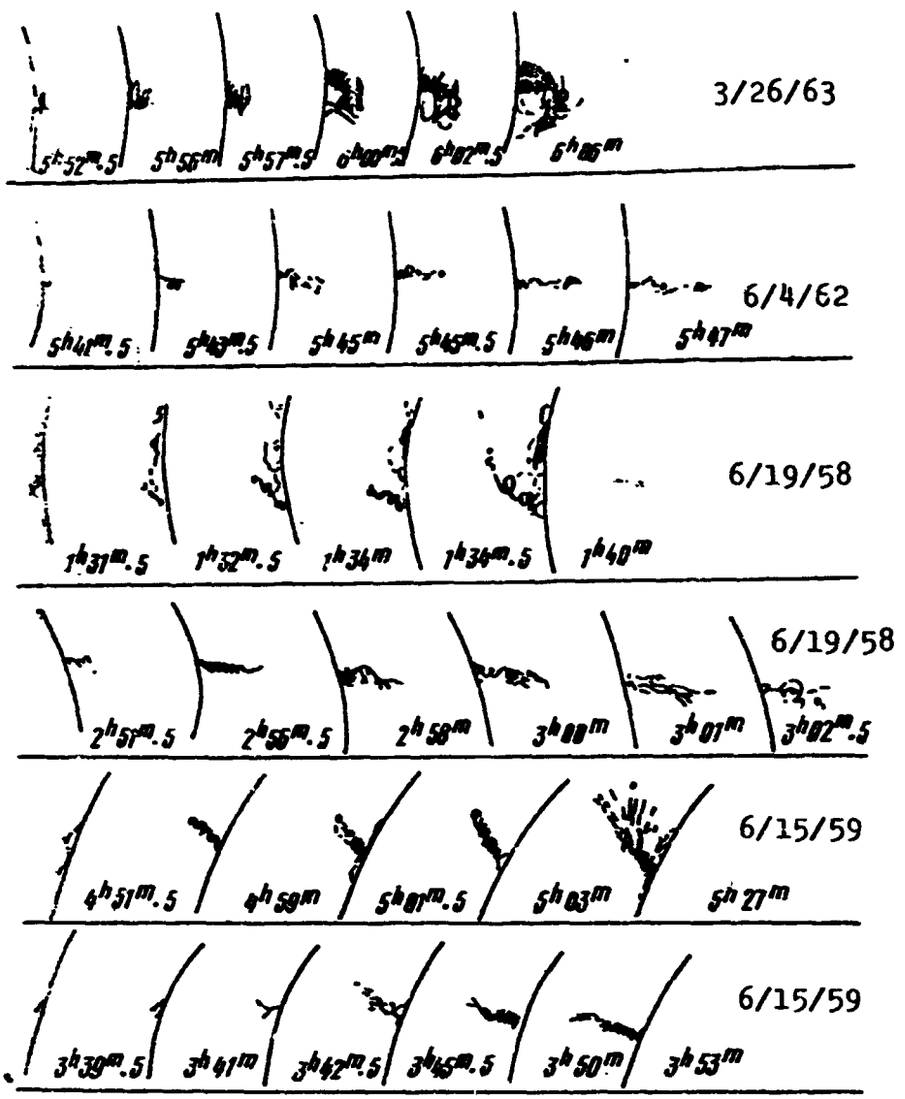

Figure 16. Spiral structure of plasma ejections

pattern of evolution of all fast processes associated with A flares. / 38
Actually, if loop systems appearing at the location of filaments, existing or having disappeared (in the case of re-entering ejections), are interpreted as systems of magnetic field lines forming shells around the filaments, then the entire observed combination of features of these phenomena are clear, logical and natural. The expansion of loop systems, the distruption of their components, the transformation of these components into spiral coils unwinding and untwisting into

threads — all this is completely contained within the framework of the representation of the catastrophic disintegration of the original filament fields and the release of the plasma contained by them.

The explosive nature of processes associated with A flares is completely verified by the features of these flares themselves, established in §6, by their swift pulsed development, the appearance /39 of hazy expanding shells around them (cf. Figure 13, VIIb, process 3), the large width of the H α line and their correlation with the flare area. The detected dependence between the width of the H α line and the velocity of the plasma ejection ascending from a flare (cf. Figure 9) is also contained within the framework of the explosive nature of the considered set of processes. Finally, the revealed statistical relation between A flares and the effects of the disintegration of the magnetic field (cf. Figure 11) is consistent with the phenomena of filament explosions actually observed with these flares, which indicate the actual disintegration of the fields forming them.

In summing up this discussion, we reach the conclusion that pulsed A flares are accompanied by swiftly developing fast processes characterized by plasma ejections. These flares are accompanied by explosions of filaments or their individual strands (SDF) and the upward flights of prominences paired with them at the edge (EPL), and also by all forms of re-entering ejections (DSD, BSD, BSL). All these processes undoubtedly have a common nature, which is indicated by their genetic origin, i.e., the direct relation with the magnetic field of the filament, the complete analogy of their evolution and the identity of their dynamic pattern. The entire set of these processes can be interpreted as the catastrophic disruption of the filament field, which is reflected by the disintegration of its loop shell.

Other fast processes are encountered with C flares. Here, a gradual expansion of the loop shell occurs, and not its swift expansion and explosion sometimes concluded by a complete disruption of the filament. This dilatation of the shell appears in the gradual emergence of systems of loop prominences into the corona (cf. Figure

13, IIIa - IIIc), and it involves the activation and dissipation of the filaments enclosed within them. Judging from the ascent of loop systems of intense C flares above the edge, the rate of shell expansion at the initial stage is the order of 15 - 20 km/sec; toward the final stage, it drops to 2 - 3 km/sec [8, 46]. These loop systems sometimes display not only a tangential velocity, but also a radial velocity close to it in value. The presence of a radial component indicates that the observed opening of the flare loops reflects their actual motion. A real dilatation of the loop shell occurs here, and not a successive formation of new higher loops caused by some effects of the propagation of the disturbance.

The process of the development of several limb C flares permits one to trace this gradual dilatation of the loop shell of a filament. Thus, the recurrent flare 1 on the filtergram IV of Figure 13 represented a bright opening loop, straddling the position of the filament under it on the disk of the Sun. The flare of VIa - VIc (in the same figure) was ignited at the crest of a large prominence, and was then transformed into an expanding loop arch; it would have clearly replaced the previously existing stationary filament with recording on the disk. We note that in both these examples, the flares originated close to the top of the filament. This conclusion is verified by the high level of generation of the C flares (§8) and by the phenomena accompanying them in the optical and radio range (§6 and §8), which indicate that the development of the process is from above downward, from the corona to the chromosphere. It is possible that the emission of the C flare actually propagates from its top to the base, but this effect is masked at the edge by the simultaneous growth of its entire loop.

The gradual expansion process of a loop shell of a filament is /40
well-traced not only on the edge, but on the disk of the Sun, particularly for intense C flares. At the initial stage of such a flare, the loop strands of the shell illuminated by it are compact, they completely screen the filament contained within them. But with the development of the flare, this arch of loops expands, its components

thin out and fade, uncovering the dark channel within which the previously hidden filament gradually protrudes (cf. Figure 13, V). It is still blanketed by a "cocoon" of weak threads, the last traces of the dimming and dispersing loop "braid". The effect of the temporary screening by the flare is particularly clearly perceptible for such processes of covering and uncovering a filament (cf., for example, Figure 13, VIIa - VIId, centers 1 and 2). Thus, we will describe them by the term "replacement of a filament by a flare". And here, the fact that a filament is screened on the disk by an intense flare indicates the external and higher localization of its loop arch.

Two bright emission ropes are formed at the base of the sides of the loop arch, i.e., one observes the well-known effect of the splitting of bands of an intense flare (type C), which is frequently accompanied by the exposure of the filament screened by it (cf. Figure 13, V). These ropes gradually separate with the dilatation of the loop arch. In recent models, the effect of the splitting of the initial band of a flare into two parallel bands is commonly explained by the disturbance of the chromosphere under the effect of descending streams of hot coronal plasma [146, 147, 148], or discharges of material from the filament itself (the "drop-shock" mechanism of Hyder [149, 150]). However, the actual pattern for intense C flares is more complicated. The great brightness of loop arches rising to altitudes of 50,000 km, and particularly of points at their tops, which reach $\approx$ 150% of the adjacent continuum [6], does not fit into Hyder's proposal. The emission of C flares clearly involves the corona, and not just the chromosphere.

Not all intense C flares, by far, display the effect of the splitting of the emission band, which follows from the models of [146, 147, 148 and 149, 150]. Thus, for example, those which develop in compact groups are characterized by only one band-shaped rope located along the route of a ring filament (cf. Figure 13, VIIa- VIId, XIIa - XIIb). The second flare center is a point here, and it occurs directly in the spot (cf. Figure 13, XIIa).

Weak C flares illuminate only individual components of the loop envelope (Figure 13, VI, process 1); the flare does not fill in the profile of the filament, and only an isolated bright sprinkling appears (the replacement effect does not occur). But for some weak flares, one can observe a negative image of the pattern recorded for more intense events. Here the filament itself splits into to parallel rope-dashes joined by a dark arched tunnel, i.e., the phenomenon is recorded not in emission, but in absorption (cf. Figure 13, XIIIa - XIIIb, and also IV, process 2, where the splitting of the filament is seen after the weak flare). The difference between intense and weak flares does not involve the nature of the phenomenon, but its scale.

Thus, for C flares we also encounter the appearance of typical loop formations at the location of filaments. However, in contrast to type A, these formations do not evolve by explosion, but by gradual expansion. By identifying, as previously, the observed loop systems with systems of magnetic field lines, we reach the conclusion /41 that C flares are associated with a gradual dilatation of the field shell of the filament, i.e., with a gradual disruption of its field. It is natural to extend this conclusion to C flares ignited along the channels of filaments previously existing or formed later in the region, since they are also clearly related with the magnetic fields generating these filaments.

C flares are associated not only with the appearance of loop systems, but also with other forms of fast processes. The dilatation of the field shell must affect the stability of the filament, i.e., disrupt its equilibrium state. Actually, it frequently stimulates activation of filaments. The effects of activation are observed for intense as well as for weak C flares, i.e., independently of whether the filament is replaced by a flare or not.

Activations of filaments occur not only in disturbed regions, but also beyond their limits, and are associated in these cases with sluggish anomalous flares [2, 3, 14, 15], which from their optical features and radio bursts also belong to type C [11]. In a number

of occurrences, the expansion of the field shell leads to a gradual dissipation of the entire filament. To be sure, some flares do not cause a visible reciprocal reaction in the filament. The reason probably involves the sensitivity of the instrument used. For very weak features of activation and correspondingly small velocities of the gas, a spectrograph is required, and not a spectrohelioscope.

The close relation of the effects of activation and disintegration of filaments with the expansion of their loop shell is obvious; it is traced even without obvious flares. Thus, the gradual dissipation of the large stationary filament XIV in Figure 13 is marked by the appearance around it of a translucent loop "braid", which is particularly well examined about the limb (frame XIVb). Thin weak threads of such loop shells are rather frequently detected around large activated prominences with the attentive examination of patrol films. Special fine-grain varieties of film are necessary for their reliable registration.

The nature of the gas motion for the replacement of filaments by intense C flares and for their activations and dissipations with weak C flares is absolutely identical. This indicates the generality of the mechanism generating the phenomena under consideration, as well as the generality of the nature of the flares related to them. Analysis of the radio component of the motions (measured with a line-shifter on a spectrohelioscope) indicates that prolonged stable discharges of plasma into the chromosphere are typical for the processes under consideration. The velocities of the discharges are constant and are relatively small: 40 - 60 km/sec.

Figure 17 presents 12 of 30 investigated cases. The symbol C_1 denotes filaments related to intense flares (replacements); the symbol C_2 — to weak flares. The discharges are sometimes accompanied by simultaneous and rather stable ascending motions with velocities of the same order (cf. for example, 7/24/61, 6/26/59, 9/19/59). Another type of motion appears less frequently; that is, an

accelerated influx of jets (7/24/61, 9/29/57: the western end of the filament with coordinates $\phi = -10°$, $\lambda = +2°$).

All these motions can be interpreted as an expansion of the field envelope and the disruption of the filament equilibrium; the plasma no longer contained by the magnetic shell slips along the field line downward to the solar surface, producing the observed effects of regular discharges. The dilatation of the field shell also leads to the expansion of the filament itself, which explains the appearance in them not only of descending, but also frequently ascending /42

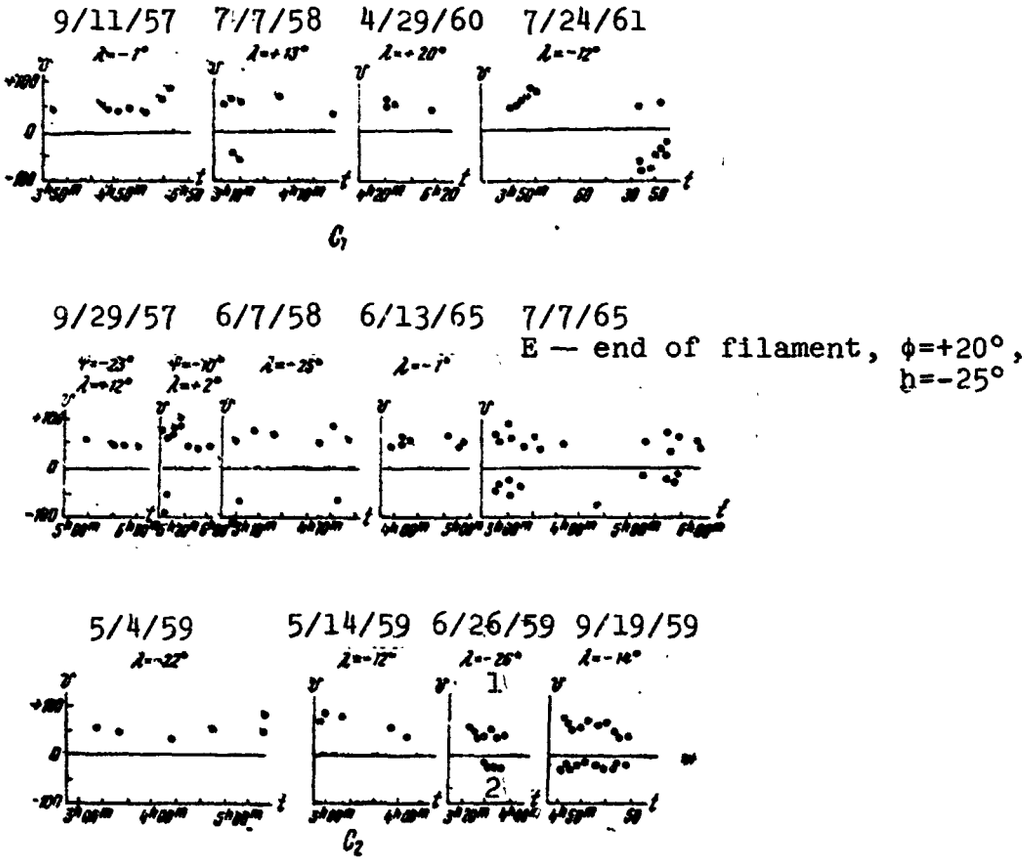

Figure 17. Dynamic pattern for A flares; t — universal time, v — radial velocity (km/sec):

1 — near flare; 2 — near spot

motions. Finally, the disruption of the filament equilibrium stimulates emissions of jets toward the centers of attraction and their accelerated influx into these centers.

As Figure 17 indicates, the dynamic pattern of phenomena accompanying C flares is quite different from the pattern observed for the explosive A flares.

Thus the gradual disintegration of filament fields, i.e., the dilatation of their field envelope, generates, firstly, activation of the filaments and, secondly, their gradual dissipation. The third type of fast process produced by the disintegration of the filament field is systems of loop prominences, directly reflecting by their development the expansion of its field shell. Loop systems are inherently prototypes of many, if not all, passively developing forms of prominences near spots. Actually, fan-shaped streams located on the stems of condensation heads, funnels, etc., are essentially underdeveloped forms of loop systems, in which the loops are traced only as "dashes" because of the effects of the disturbance. All three forms of processes enumerated above (activation of filaments, their disappearance, loop systems) characterized by relatively slow evolution are related to C flares.

In summing up the results discussed in this section, we are convinced that flares and filaments permit one to reduce all fast processes into a single genetic set and to trace the internal physical relation hidden behind the external variety of their forms (Figure 18). All these processes arise as a result of the transformation of the field shell of the filament, i.e., its magnetic field. The swift disintegration of the field reflected by a pulsed A flare and the explosion of the shell (or its individual strands) generates eruptions of plasma of the re-entering ejection type (DSD, BSD, BSL), and the sudden upward flights of filaments and prominences (SDF, EPL). The slow disintegration of a filament field reflected by the retarded expansion of its field shell and a prolonged regenerating C flare generates loop systems and related types of prominences (APR) and also activation and dissipation of stationary filaments. 43

Flares and past processes are directly related to phenomena occurring in the magnetic field producing the filament. The boundary between the flares themselves and these processes is relative, and

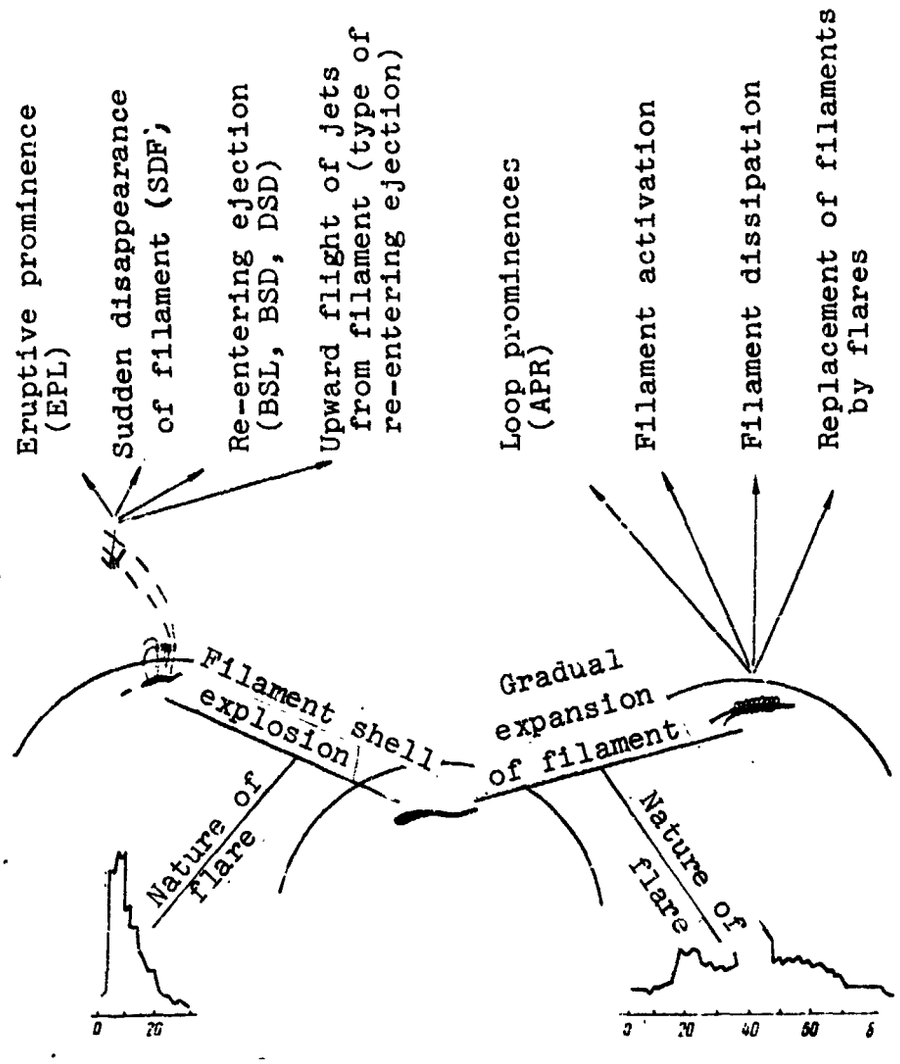

Figure 18. Diagram of filament shell transformations and the interrelation of fast processes

is sometimes practically imperceptible, which is indicated by the similarity of their forms, their motions, their spectra and, particularly, their interchangeability. The mutual conditionality of flares and fast processes, i.e., the consistence of their appearance, is evidently dictated only by the energy reserves of the event itself. Recording and studying the fields producing filaments should be considered as one of the immediate problems of the physics of active regions.

In conclusion, we present some additional arguments in favor of the proposed classification, which is generalized schematically in Figure 18.

1. Both specific types of the expansion of loop shells are traced not only by the evolution of fast processes in H α, but also by the development of coronal formations accompanying the appearance of flares. The upward flight and explosion of coronal arches according to the types of motions of eruptive prominences and ejections occur for A flares [109]; and for C flares, a gradual ascent and expansion of compact or open loop arches [9, 88, 109]. /44

The repetition typical for A and C flares of processes in coronal phenomena indicates, in our opinion, the physical soundness of the proposed classification. Moreover, the reflection of the processes generated by A and C flares in coronal phenomena verifies the close association of these processes with the structure of the magnetic field itself and with its transformations in time.

2. All the forms of the detailed morphological classification of Pettit [151] fit naturally into the framework of the proposed simple, purely physical scheme. Actually, the first type of phenomena (explosions of filament shells) include eruptive and quasi-eruptive prominences (IIb_1, IIb_2, IIa), ordinary and expanding re-entering ejections ($IIId_1$ and $IIId_2$), eruptions (IIIe), secondary prominences (IIIf), and, evidently, tornadoes (IVa, IVb) — at least at the stage of their disruption. The second type of phenomena (slow expansion of the field shell) includes ordinary and active prominences near spots (Ib, IIIc), loop prominences (IIIb), and their undeveloped form (IIIa), and also coronal band prominences and coronal clouds (VI, Ic, IIIg) with the expressed effects of their discharges. Finally, quiet prominences (V) and their rudimentary representatives, cap prominences, i.e., bulges (IIIo), should be considered as the initial stage of filaments, the basis of all subsequent transformations, i.e., all forms of fast processes.

3. The boundary between the two basic types of processes characterizing the activity of an active region is sometimes somewhat relative. The actual patterns, particularly in the case of intense

complex flares, can be more complicated and can combine both types of phenomena. For such a flare, one part of the field envelope of the filament can explode, and the other part can evolve into a loop system. By analogy, the explosion of an individual strand can stimulate further gradual expansion of the whole filament shell and lead to its gradual dissipation. But these hybrid phenomena only verify the value of the classification being introduced, by emphasizing the generality of the nature of all the processes under consideration and their genetic relationship with stationary filaments.

In concluding the discussion of the relation of flares to phenomena of the upper layer of an active region, we should emphasize that the differentiation of flares into two independent types, established and documented in §6 (the explosive A and the prolonged or pulsating C), is supported by additional arguments. The physical independence of the types A and C is verified by differences in the nature of the phenomena stimulated by them in the radio range, by differences in the level of their generation and, finally, by differences in the transformation of the original magnetic field.

§10. Role of filaments in the mechanism of flares and fast processes. We will now consider the role of filament fields in the mechanism of flares and fast processes [18, 19]. As previously, we will proceed from the identification of the loop envelope of a filament with its magnetic field shell. The sudden or gradual disintegration of this field shell partially or completely eliminates the heat shielding system of the filament [115, 116]. The disintegration of the shell disrupts the barricade between the filament and the hot coronal medium surrounding it, as a result of which there occur its heating and intensification of its emission, which is perceived as a replacement of the filament by a flare. Such a representation of the flare phenomenon is completely linked with the conclusions obtained from the analysis of the spectra themselves of this phenomenon at the edge and on the disk of the Sun [152]. As was shown in [152], the flare has a small effective thickness and must consist of a set of thread-like structural elements formed in the corona or in the upper chromosphere.

For a filament density $\rho = 10^{12}$ atom/cm^3 [51], heating depth $\Delta = 5 \times 10^7$ cm, flare temperature $T = 2 \times 10^{4\circ}$ K, and heat flux at the corona-filament boundary $F = 5 \times 10^5$ erg/cm^2·sec [115, 153], the heating of the filament requires the time:

$$t \approx \frac{3/2kT_p\lambda}{F} \approx 4 \times 10^2 \text{ sec} \approx 7^m.$$

This interval agrees well with the ignition time of flares. A flare related to the explosion of the field shell must flare up very rapidly and have a compact nature, since the entire heat shielding system is removed at once. C flares related to the gradual expansion of the shell must flare up more slowly and have a dispersed nature in the initial phase. Actually, the heating occurs here by the penetration of the coronal material between the diverging components of the shell. All of this agrees well with the actually observed pattern of the development of A and C flares.

However, the coronal heating of a filament, caused by the disintegration of its force shell, can explain only the ignition of the flare, but is not able to provide the energy for its emission. This energy cannot be borrowed from the corona, since, as is well known, the energy density in the flare is 4 - 5 orders higher than in the corona. The energy of flares must be derived from the magnetic field of the filament itself. We will consider this hypothesis from the point of view of its energy balance. The final results of these following calculations and estimates are summarized in Table 8.

The optical yield of flares has been determined many times [51, 91, 92, 154, 155, 156, 157, 158, 159, 160]. The obtained estimates, related mainly to very intense Class 3+ phenomena, are overestimated in many cases. Thus, Ellison [158, 159] takes the total optical yield of such a flare as $E_{op} = 10^{32}$ erg. Its monochromatic energy (E_M) is determined from the relation:

$$E_M = 0.5\, E_{op} \times 25 \times T = 5 \times 10^{31} \text{ erg}. \qquad (12)$$

Here, E_{H_α} is the optical yield in H α at the maximum, estimated as 1.1×10^{27} erg/sec, on the basis of measuring the equivalent width and areas of five intense flares; T is the duration of the flare (3600^s); and 25 is a factor taking into account the radiation in the other terms of the Balmer series ($\approx 15\ E_{H\alpha}$) and in the remaining lines ($\approx 10\ E_{H\alpha}$). Without going into a discussion of this rather arbitrary coefficient, we note that the first factor in (12), that is, the coefficient 0.5, is clearly overestimated. This implies that the flare emission over its whole duration is half the maximum value. Actually, the equivalent line width decreases extremely rapidly; even in Class 3+ flares, it contracts by about ten times over a period of $2 - 3^m$. This can be judged, in particular, from the profiles of a Class 3 flare 4^m after maximum (the flare of 5/18/51), which is presented in the work of Ellison himself [158]. Consequently, the conversion factor from the energy radiated at maximum should not be 0.5, /46 but the order of 0.1, i.e., the value of E_M is overestimated by about five times. Moreover, the flare energy in white light is esti-estimated as 8×10^{31} erg. It is assumed for this that the emission in the continuum continues for a period of 10^m, whereas the continuous spectrum of a flare is actually observed for no longer than $2 - 3^m$.

Taking these corrections into account, one can assume that the total optical energy of a Class 3+ flare should not in any way exceed the value:

$$E_*(3+) = 5 \times 10^{31} \text{ erg}, \qquad (13)$$

which agrees with the estimate obtained in [155].

The total optical energy of a Class 2 flare can be estimated by using the value of $E_{H\alpha}$ (1.7×10^{26} erg/sec) determined by Ellison [158] for one such flare. By taking $T \approx 30^m$ [161] and assuming that the

TABLE 8

Optical energy of flares, erg	Energy of fast processes, erg	Energy of filaments, erg
Class 3+ flare: $E \leq 5 \times 10^{31}$	Intense ejections: $E_{kin} = 10^{32}$	$E_{obs} = 10^{33}$ (actually contained during flares)
Class 2 flare: $E \leq 10^{29}$	Loop systems: $E_{mech} = 5 \times 10^{29}$ (from loop ascent)	$E_{theo} = 10^{33}$ (accumulated during action of field line twisting mechanism)
Class 1 flare: $E \leq 2 \times 10^{28}$	Loop systems: $E_{kin} = 10^{29}$ (from discharge of loop material into chromosphere)	

flare radiation is concentrated in three or four lines (Hα , H and K, Lα), we obtain:

$$E_{op}(2) = 10^{29} \text{ erg}. \tag{14}$$

We find analogously for Class 1 flares:

$$E_{op}(1) = 2 \times 10^{28} \text{ erg}. \tag{15}$$

under the assumption that $T \approx 20^{m}$ [161], and that its area is about 0.2 times the areas of Class 2 and 3 flares.

Since we are considering the flare as one of the effects of the disintegration of filament fields, it is important to compare the obtained estimates (13), (14), and (15) with the scales of the processes reflecting this disintegration, i.e., with the energies of intense ejections, filament-ejected streams and loop systems.

From five intense ejections, we obtained the following average value of their mass, assuming a density $\rho = 10^{12}$ atom/cm^3:

$$M = 2.4 \times 10^{17} \text{ gm.}$$

The average radial velocity of the ejection is $v = 2 \times 10^7$ cm/sec, from which:

$$E_{kin} = 5 \times 10^{31} \text{ erg.} \quad (16)$$

This is evidently only the lower limit of the energy realized for explosions of filament shells. If it is assumed that the eruptions of material observed by Athay and Moreton [162] are generated by the same explosion, then for their mass of about 0.1 times the mass of an ejection, and $v = 10^8$ cm/sec:

$$E_{kin} \gtrsim 10^{32} \text{ erg.} \quad (17)$$

The obtained energy values for the explosions of filament shells are comparable with the energy carried away by cosmic rays, which is the order of 5×10^{31} erg, according to [155, 163].

Let us now consider the energy realized for the ascent of loop systems, i.e., for gradual disintegrations of filament shells. It can be roughly estimated, based on the following considerations: For the mass $M = 10^{16}$ gm [164], the mechanical energy expended in raising the material from the level of the filament 5×10^9 cm [107] up to the altitudes reached by loop systems during their growth 10^{10} cm [46] is determined as:

$$E_{mech} = Mgh = 10^{16} \times 10^4 \times 5 \times 10^9 = 5 \times 10^{29} \text{ erg.} \quad (18a)$$

We arrive at the same value by estimating the total kinetic energy of stationary discharges of this material into the chromosphere, i.e., of the descending motions accompanying the development of loop systems. For $M = 10^{16}$ gm and $v = 5 \times 10^7$ cm/sec (cf. §9): /47

$$E_{kin} = 10^{29} \text{ erg.} \quad (18b)$$

Thus, the processes reflecting the disintegration of filament fields are at least equivalent in their energy scale to the flare processes accompanying this disintegration. The energy balance of the processes being considered clearly does not fit into the framework of coronal and chromospheric reserves.

The energy being realized for these processes must be accumulated in the filament itself. Let us consider its energy reserves. According to [122, 125], the field intensities in activated filaments reach 150 - 200 G. This corresponds to a magnetic energy density:

$$\frac{H^2}{8\pi} = 900 \div 1600 \ \frac{\text{erg}}{\text{cm}^3} \approx 10^3 \ \frac{\text{erg}}{\text{cm}^3},$$

quite comparable with the energy density in a flare ($0.5 - 5 \times 10^3$ erg/cm^3). It is even more indicative that, according to the same data [122] in bright loop systems, i.e., in the flare-illuminated field shells of filaments, fields were recorded up to 750 G. Fields as strong (800 G) were detected in re-entering ejections associated with flares [165], which can be interpreted as processes of the disintegration of these shells. Finally, recent determinations of the fields of active prominences, just published, have led to values of approximately 1500 [166] and even 1000 - 10,000 G [167], where these intense fields are related to precisely the upward flight phase of eruptive prominences [168], i.e., to the explosion phase of a filament shell. All these facts indicate that the fields of stationary filaments are extremely large during the flares. By assuming that the field of a filament is concentrated in its field shell, we approximate this loop system with a hollow cylinder. For r of the filament equaling 2.50×10^9 cm [107], R of the loop system equaling 2.65×10^9 cm, and its generatrix equaling the length of the filament 2×10^{10} cm [107], the volume of the shell $V = 5 \times 10^{28}$ cm^3, which agrees with the estimates of the volumes of loop systems obtained in

[113]. Then, for H =750G*, the total amount of magnetic energy contained in the filament shell at the time of the flare:

$$E_t = 10^{33} \text{ erg.} \qquad (19)$$

Such energy reserves are capable of providing their actually observed realization in all processes associated with the disintegration of the field shells of filaments, including flares.

However, the problem lies in how such intense energy reserves are accumulated in the filament. One might think that the filament field arises and intensifies because of certain effects leading to twisting of the field lines. Such a mechanism of field intensification was developed by Gold and Hoyle [157], to be sure, as applied to lower-lying points of arch structures, and not to filaments. However, in this case we should not lean on this abstract speculative model, but on specific observational facts indicating that filament fields are actually twisted. This is indicated, for example, by the nature of plasma motions with the disintegration of the filament field (cf. §9). The streams of ejections and eruptive prominences reflecting this disintegration have an expressed twisted structure, reminiscent of a tightly interwoven rope or "cable" of force lines. During ascent, the stream uncoils, decaying into expanding spiral coils [6, 11, 12]. The relation between the frequency of ejections and the rate of twisting of the spot field, developed in [169] is no less indicative in this sense. /48

The twisting mechanism itself for the filament field lines should be sought in the deeper layers. It was shown in §7 that the fields of stationary filaments must be related to the photospheric fields outlined by chains of calcium flocculi [118, 119, 120]. The proximity and directionality toward spots of filaments, which are formed in the active region itself, at the instant of their

*By taking into account the results of recent determinations of the fields of active filaments [166, 167], this value is underestimated, rather than overestimated.

appearance in it [117] are no less symptomatic. Thus, the cause of the twisting of filament fields should most likely be found in the rotational motions occurring in the photospheric or sub-photospheric layers. As follows from [170], there has actually been detected near spots the effects of the rapid rotation of the field vector $H_{\perp}$, with velocities of $\gtrsim 15°$ per hour, or one rotation per day.

The work performed by the twisting can be roughly estimated from the relation [157]:

$$W = 2\pi N \frac{H^{2*}}{8\pi} d^3, \tag{20}$$

where d is the diameter of the filament (5×10^9 cm [107]), and H is the initial field of the region in which it appeared (50 G). Stable filaments are formed in a region on the $14 - 30^{th}$ day of its existence. We will take the lower of these values, i.e., we will assume the age of the region at the time of the appearance of a filament as equaling 14 days. Then, for the observed angular velocity of twisting of a rotation per day, we can assume the number of rotations N = 14. Formula (20) indicates that even for this minimum value of N, the energy

$$W = 10^{33} \text{ erg}. \tag{21}$$

must be accumulated in the filament as a result of the effects of twisting. This value coincides with (19), i.e., with the energy reserves contained in the filament shell during a flare, which we estimated from field intensities actually recorded in bright loop systems. Consequently, the performed calculations indicate that the energy reserves of filaments can provide its observed realization in flares and fast processes (cf. Table 8, in which all the previously obtained estimates characterizing the energy reserves of phenomena of the upper layer of an active region are collected and compared).

The degree of twisting of the field lines must increase with the age of the filament. This can explain the smaller energy scale

*Translator's note. H^2 is inadvertently given in the original foreign text as H_2.

of C flares in comparison with A flares, since the first arise in the earlier stage of evolution in a region; and the second — in the later stage.

One can try to interpret the differences of the types A and C by the degree of twisting of the field lines, by considering schematically the C loop flares as phenomena associated with the expansion of weakly twisted components of the filament shell, and the A explosion flares as phenomena associated with the disintegration and uncoiling of these tightly twisted components.

Analysis of the relation of flares with the photospheric characteristics of a region confirms that the ultimate source of energy of the filaments themselves and the trigger mechanism, which leads to the distruption of their fields and to the release of their energy in flares and fast processes, must be localized in deeper layers.

Let us recall some results of this analysis obtained in the /49
first part of the work. A flare should be considered as a normal feature of the evolution of an active region, and groups — as a natural event in its development. Actual rearrangements of the photospheric field undoubtedly occur during a flare [28, 29, 30, 172]. Some flares (type A) are associated with phenomena of spot granulation, i.e., with processes of field tube splitting. The role of photospheric factors is indicated by the statistical dependence presented in the first part of the work, which indicates that the frequency of flares in a region is determined by the initial reserves of its magnetic energy, and is a function of the number of poles and the field intensity. A number of features indicate that many flares are accompanied by the emergence of field tubes on the solar surface, and by the propagation of the field into the external layers. These include the emergence of photospheric material into the chromosphere and corona [9], and also the appearance of photospheric loop structures [11, 86]. Flares are particularly frequent in groups, where spots or nuclei of opposite polarity are adjacent [3]. The close

coexistence of unlike poles can also be considered as a sign of the recent emergence of a field tube. Analysis of the features of particularly active centers, in which up to 100 flares per synodic half-rotation are ignited, leads to the same conclusion. The renewal of spot-processes, i.e., the generation of new "fresh" formations inside already existing groups, is typical for these centers. The real cause of the high flare activity of these centers evidently lies precisely in the fact that, as a result of their relapsing activity, there are created in the chromosphere and in the corona the conditions for the interaction between the previously existing system of field lines and the system of lines of the new field, which emerges from the sub-photospheric depths*. Finally, it is very indicative, from the point of view of the origin of flares, that the large-scale vortex motions, typical for active centers, derive their energy from the convective zone and can be the transmitters of energy into the external layers.

The enumerated observational arguments serve to confirm that /50
the sources of energy of filaments and mechanisms leading to the release of this energy in flares and fast processes are contained in the photospheric and even, more likely, in the sub-photospheric layers.

We note that after the publication of [17, 18, 19] by the author, summarized in this section, investigations appeared in which similar presentations were independently developed and substantiated. These investigations [173, 174, 175, 176] also accentuated the role of photospheric motions in the twisting of chromospheric and coronal fields and in the accumulation of energy realized in flares.

In concluding the second part of the work, we briefly summarize its basic conclusions.

---

*These interactions are most probable in filaments where the coronal magnetic fields are concentrated.

1. Flares are divided into two independent types, differing by the nature of development, physical and dynamic features, altitude of generation and time of appearance in the region.

2. The flare event develops in an analogous manner in the optical and radio ranges. The initial localization and direction of propagation of the optical phenomenon coincide with those of the radio burst.

3. Flares are genetically related with all the sporadic and stationary processes of the upper layer of an active region.

Conclusion

The picture discussed here of the interrelation of flares and the processes of an active region has appeared to the author as a result of thirty years of observing the combination of solar phenomena. This picture has been dictated by the classification of selected observational facts, the interpretation of the obtained empirical relationships, and the comparison of the related features of phenomena which show through the kaleidoscopic variety of their forms and transformations.

Let us summarize the obtained results.

I. It was established that flares should be considered as a natural symptom of the evolution of an active region [2, 3, 16].

II. The inherent relationship between flares and all the sporadic processes of the upper layer of an active region and, in particular, loop systems was traced [4, 6, 7, 8].

III. The close relation between flares and stable filaments of an active region was substantiated [10, 11, 12, 18, 20]. The mutual conditionality of these two phenomena is documented by the arguments enumerated below.

1. Flares are always ignited along the route of filaments which exist, have disappeared, or are formed later in the region.

2. Flares are identical in their spatial dimensions with filaments, i.e., they coincide with filaments not only in their location in an active region, but also in their altitude localization.

3. The interrelation of flares and filaments is also traced outside active centers. The effects of activation and disintegration of stable filaments, occurring far beyond floccular regions, are accompanied by flare-type processes, i.e., with the appearance of short-term emission components [2, 3, 14, 15].

4. Flares degenerate in the process of their development into loop formations [6, 7, 8, 11]. The axis of such a loop system is oriented along the route of existing filaments, or filaments which are visible previously or later. The flare loops straddle, i.e., encircle the filament itself or the route along which it is formed. This indicates that the flare originates in the external layers of /51
the flare, illuminating the structure covering it, the previously invisible loop shell [11, 18]. Weak flares display only individual emission speckles; the greater part of the loop envelope of the filament is not visible in emission, but in absorption.

IV. It was shown that the evolution of the loop shell of a filament can occur in two ways [12, 13]. The first of these is the sudden explosion. It generates the swiftly developing fast processes, characterized by plasma eruption into the corona. They include the upward flight of filaments or their individual strands (SDF), and the appearance of eruptive prominences (EPL) paired with them at the edge of the Sun. These processes also include all forms of re-entering ejections (DSD, BSD, BSL), since it was established in [12] that they all originate and are propagated (if only partially) along the trajectories of filaments previously existing in the region. Ejections are emitted from "invisible" filaments.

The second evolutionary path of the loop shell of a filament is its gradual dilatation. For such a gradual transformation of a shell, there arise passively developing processes; that is, systems of loop prominences (APR) appear, whose growth directly reflects the expansion of this loop structure. At the same time, the dilatation of the loop structure disrupts the equilibrium state of the stationary filaments themselves, and stimulates their activation and even their gradual dissipation [13].

Thus, all fast processes, with the external variety of their forms, have an internal physical relation and represent a single genetic set. They all arise as the result of the transformation of the loop shell covering the filament. On the basis of the assumed identification of loop systems with systems of magnetic field lines, one can consider the loop envelope of a filament as its magnetic field shell, and interpret all fast processes as the result of the disruption of this shell. Then one can assume that the first group of processes can be associated with the swift, and the second — with the gradual disruption of the field shell of the filament, i.e., its magnetic field.

V. It was revealed that the flare processes related to these two groups differ significantly in their nature and evolution [6, 7, 10, 11, 12, 13, 18, 20].

Flares of the pulse type A arise for processes of the first kind [6, 7]. They are compact in structure, are ignited almost instantaneously ($t_{ave} \approx 5^m$), and are very short-lived ($\tau_{ave} \approx 30^m$) [6, 7, 18]. These bursts of radiation have a clearly explosive nature. The explosive nature of type A is also emphasized by the large spectral line width, reaching 20 Å ($\Delta H \alpha_{ave} \approx 5.5$ Å), and its clear positive correlation with the flare area [6, 7, 12, 18]. A flares originate at low altitudes ($h_{ave} \approx 15{,}000$ km); they arise in very low-lying filaments (identified at the limb with low chromosphere "bulges") or in the chromospheric "roots" of filaments [10, 12, 18,

20]. The propagation of the process from below upwards, i.e., from the chromosphere into the corona, is typical for these chromospheric flares; they are accompanied by swift emissions of plasma jets, ejected with velocities of $\approx$ 200 km/sec [6, 12, 18]. Their initial radio bursts originate predominantly in the centimeter range, and /52
are also propagated from the chromosphere into the corona (the burst frequency decreases with time) [12, 18]. Finally, A flares appear predominantly at the decay phase of the group and, consequently, of the magnetic field of the region [7, 12].

For the processes of the second kind, on the contrary, there arise prolonged flares, frequently displaying repeated pulsations of brightness (repeated maxima or ignition of adjacent points) [4, 6, 7, 13, 18]. These flares (type C) are dispersed; they are generated in the form of individual spray points, which often do not appear at the same time. For extended flares, these points later merge into a continuous band [4, 6, 13, 18]. C flares ignite slowly ($t_{ave} \approx 15^m$); they are prolonged ($\tau_{ave} \approx 75^m$)[4, 6, 7, 13, 18]. Their spectral line width is small ($\Delta H \alpha_{ave} \approx 2.8$ Å), and a correlation with the area of the illuminated center is not detected [6, 7, 13, 18]. The C centers are weaker in brightness than the A centers [6, 7]. C flares originate at high altitudes, reaching 60,000 km ($h_{ave} \approx$ 30,000 km) [13, 18, 20]. Propagation of the process from above downward, i.e., from the corona into the chromosphere, is typical for these coronal flares. Thus, they are accompanied in the optical range by stable discharges of plasma with relatively small velocities $\approx$ 50 km/sec [13, 18]. The initial bursts of their radio emission are localized predominantly in the meter and decimeter ranges, and are also propagated from the corona into the chromosphere (the frequency of the burst increases with time) [13, 18]. Finally, C flares appear mainly at the growth phase of the group and, consequently, of the magnetic field of the region [7, 13, 18].

These features of the difference of the primary chromospheric (A) and coronal (C) flares also shows through in more intense and

complex events, since the relative characteristics of such events (the total duration, ignition time, spectral line width, area of the emission center) depend on the altitude of their origin.

VI. Observational reasons were presented which indicate the relation of the filament field with the photospheric fields. Specific observational facts were considered, which indicate that the magnetic fields of filaments intensify by twisting of the field lines. The energy reserves contained in the field shells of filaments were evaluated, and it was shown that these reserves are capable of providing the actually observed realization of energy for fast processes and flares [19].

VII. A sufficiently close correlation was substantiated between the frequency of flares and the group characteristics: its initial energy reserves, the number and arrangement of its poles, its magnetic field intensity, the spot formation and decay phenomena (the processes of emergence and disintegration of the field tubes [2, 3, 16]). Specific features of particularly active flare centers were revealed [10], which involve: a) their regenerative (frequently repeatedly) spot-formation activity, and b) large-scale vortex motions, hydrodynamic in nature. The energy reserves of these centers were evaluated from their work against the magnetic field forces. It was shown that the investigated motions can serve as energy transmitters from the convective zone into the external layers in which flares are ignited [17]. The combination of enumerated facts leads to the conclusion that the energy sources of the filament fields, as well as the mechanism stimulating the release of this energy in flares and fast processes, should be sought in the photospheric or, more likely, in the sub-photospheric layers.

References

/53

1. Slonim, Yu. M. Bull. Solnechnyye dannyye, No. 3, 1956, p. 138.
2. Slonim, Yu. M. Trudy Tashkentskoy atronomicheskoy observatorii, Ser. 2, Vol. 6, 1957, p. 61.
3. Slonim, Yu. M. Izvestiya AN UzSSR, Phys-math. ser., No. 1, 1957, p. 83.
4. Slonim, Yu. M. Tsirkulyar Tashkentskoy atronomicheskoy observatorii, No. 300, May, 1959.
5. Slonim, Yu. M. Astronomicheskiy zhurnal, Vol. 37, 1960, p. 347.
6. Slonim, Yu. M. Astron. zh., Vol. 39, 1962, p. 798.
7. Slonim, Yu. M. Bull. Solnechnyye dannyye, No. 4, 1963, p. 67.
8. Slonim, Yu. M. Bull. Solnechnyye dannyye, No. 12, 1964, p. 48.
9. Slonim, Yu. M. Bull. Solnechnyye dannyye, No. 1, 1965, p. 51.
10. Slonim, Yu. M. Astron. zh., Vol. 45, 1968, p. 286.
11. Slonim, Yu. M. Astron. zh., Vol. 45, 1968, p. 726.
12. Slonim, Yu. M. Astron. zh., Vol. 46, 1969, p. 570.
13. Slonim, Yu. M. Astron. zh., Vol. 46, 1969, p. 697.
14. Slonim, Yu. M. Trudy Tashkentskoy atronomicheskoy observatorii, Ser. 2, Vol. 3, 1953, p. 83.
15. Slonim, Yu. M. Trudy Tashkentskoy atronomicheskoy observatorii, Ser. 2, Vol. 3, 1953, p. 152.
16. Slonim, Yu. M. Bull. Solnechnyye dannyye, No. 4, 1968, p. 58.
17. Slonim, Yu. M. Bull. Solnechnyye dannyye, No. 5, 1968, p. 79.
18. Slonim, Yu. M. Bull. Solnechnyye dannyye, No. 2, 1968, p. 95.
19. Slonim, Yu. M. Bull. Solnechnyye dannyye, No. 3, 1968, p. 64.
20. Slonim, Yu. M. Bull. Solnechnyye dannyye, No. 10, 1970, p. 93.
21. Quarterly Bulletin on Solar Activity, No. 119 - 130, 1958 - 1960.
22. Cartes Synoptiques de la Chromosphere Solaire et Catalogues des Filaments et des Centres d'Activité, Ann. observ. Paris, Meudon, 1962.

23. Mouradian, Z, G. Oliveri and I. Soru. Annee Geophysique Interm., Participation francaise, Ser. 6, Fasc. 1, C.N.R., S., Paris, 1963.

24. Bull. Solnechnyye dannyye, Nos. 4 - 10, 1958.

25. Ellison, M. Monthly Notices Roy. Astron. Soc, Vol. 109, 1949, p. 3.

26. Smith, H. and E. P. Smith. Solar Flares. New York, 1963. Russian translation edited by A. B. Severnyy, Moscow, "Mir" Press, 1966.

27. Waldmeier, M. Z. Astrophys., Vol. 16, 1938, p. 276.

28. Severnyy, A. B. Izvestiya Krymskoy astrofizicheskoy observatorii (Izv. Krymskoy astrofiz. observ.), Vol. 20, 1958, p. 22.

29. Severnyy, A. B. Izv. Krymskoy astrofiz. observ., Vol. 22, 1960, p. 12.

30. Severnyy, A. B. Izv. Krymskoy astrofiz. observ., Vol. 31, 1964, p. 159.

31. Gopasyuk, S. I. Izv. Krymskoy astrofiz. observ., Vol. 27, 1962, p. 110.

32. Gopasyuk, S. I., M. B. Ogir', A. B. Severnyy and Ye. F. Shaposhnikova. Izv. Krymskoy astrofiz. observ., Vol. 29, 1963, p. 15.

33. Severnyy, A. B. Izv. Krymskoy astrofiz. observ., Vol. 9, 1952, p. 3.

34. Severnyy, A. G. and Ye. F. Shaposhnikova. Izv. Krymskoy astrofiz. observ., Vol. 13, 1955, p. 103.

35. Severnyy, A. G. and Ye. F. Shaposhnikova. Izv. Krymskoy astrofiz. observ., Vol. 24, 1960, p. 235.

36. Banin, V. G. Bull. Solnechnyye dannyye, No. 8, 1960, p. 80.

37. Roberts, W. Trans. I. A. U., Vol. 10, 1960, p. 648.

38. Menzel, D. Publ. Astron. Soc. Pacific, Vol. 73, 1961, p. 194.

39. Krat, V. A. Kurs astrofiziki i zvezdnoy astronomii (Course in Astrophysics and Stellar Astronomy). Ed. by A. A. Mikhaylov. Vol. 3. Mosocw, "Nauka" Press, 1965, p. 133.

40. Ellison, M. Monthly Notices Roy. Astron. Soc., Vol. 102, 1942, p. 11.

41. Newton, H. Monthly Notices Roy. Astron. Soc., Vol. 102, 1942, p. 2.

42. Bruzek, A. Z. Astrophys., Vol. 31, 1952, p. 99.

43. Bruzek, A. Observatory, Vol. 72, 1954, p. 225.

44. Bruzek, A. Z. Astrophys., Vol. 54, 1962, p. 225.

45. Bruzek, A. AAS-NASA Symp. Physics of Solar Flares. Washington, 1964, p. 301.

46. Bruzek, A. Astrophys. J., Vol. 140, 1964, p. 764.

47. Zirin, H., K. Watson and G. Curtis. Publ. astron. Soc. Pacific, Vol. 70, 1958, p. 406.

48. Tandberg-Hanssen, E. and H. Zirin. Astrophys. J., Vol. 129, 1959, p. 408.

49. Zirin, H. Astrophys. J., Vol. 129, 1959, p. 414.

50. Zirin, H. and E. Tandberg-Hanssen. Astrophys. J., Vol. 131, 1960, p. 717.

51. Kiepenheuer, K. AAS-NASA Symp. Physics of Solar Flares, Washington, 1964, p. 323.

52. Krat, V. A. and V. M. Sobolev, V. M. Izvestiya Glavnoy astronomicheskoy observatorii v Pulkove (Izv. Gl. astron. observ. v Pulkove), No. 170, 1962, p. 10.

53. Zirin, H. I.A.U. Symp. No. 22, Stellar and Solar Magnetic Fields, Amsterdam, 1965, p. 339.

54. Gordon, I. M. Doklady AN SSSR (DAN SSSR), Vol. 94, 1954, p. 813.

55. Krat, V. A. and L. M. Pravdyuk. Bull. Solnechnyye dannyye, No. 11, 1961, p. 47.

56. Gopasyuk, S. I., M. B. Ogir' and T. T. Tsap. Izv. Krymskoy astrofiz. observ., Vol. 30, 1963, p. 148. /54

57. Michard, R. Ann. Astrophys., Vol. 22, 1959, p. 887.

58. Stepanyan, N. N. Izv. Krymskoy astrofiz. observ., Vol. 29, 1963, p. 68.

59. Banin, V. G. Izv. Krymskoy astrofiz. observ., Vol. 33, 1965, p. 118.

60. Ellison, M. Monthly Notices Roy. Astron. Soc, Vol. 103, 1943, p. 3.

61. Krat, V. A. DAN SSSR, Vol. 106, 1956, p. 619.

62. Krat, V. A., T. V. Krat and L. M. Pravdyuk. Izv. Gl. astron. observ. v Pulkove, No. 156, 1956, p. 60.

63 Krat, V. A. and V. M. Sobolev. Izv. Gl. astron. observ. v Pulkove, No. 160, 1957, p. 116.

64. Mustel', E. R. and T. T. Tsap. Izv. Krymskoy astrofiz. observ., Vol. 17, 1957, p. 162.

65. D'Azambuja, L. Bull. Soc. Astron. France, Mars., 1939, p. 3.

66. Trans. I. A. U., Vol. 6, 1938, p. 48.

67. Vitinskiy, U. I. Izv. Gl. astron. observ. v Pulkove, No. 178, 1965, p. 49.

68. Stepanov, V. Ye., Ye. F. Shaposhnikova and N. N. Petrova. Strengths and Polarities of Magnetic Fields of Sunspots for the Period of the International Geophysical Year (July 1, 1957 - December 31, 1958), Ann. I.G.Y., Vol. 23, 1962.

69. Steshenko, N. V. Izv. Krymskoy astrofiz. observ., Vol. 37, 1967, p. 21..

70. Giovanelli, R. Astrophys. J., Vol. 89, 1939, p. 555.

71. Nicholson, S. Publ. Astron. Soc. Pacific., Vol. 45, 1933, p. 51.

72. Houtgast, J. and A. van Sluiters. Astron. Inst. Netherl., Vol. 10, 1948, p. 325.

73. Summary of Mount Wilson Magnetic Observations of Sun-Spots. Publ. Astron. Soc. Pacific, Vols. 49 - 60, Nos. 287 - 357, 1937 - 1948.

74. Romanovskiy, V. N. Primeneniye matematicheskoy statistiki v opytnom dele (Application of Mathematical Statistics in Experimental Work). Moscow - Leningrad, State Technical and Theoretical Press, 1947, p. 185.

75. Avignon, Y., M. Martres and M. Pick. Ann. Astrophys., Vol. 27, 1964, p. 23.

76. Sturrok, P. and B. Coppi. Astrophys. J., Vol. 143, 1966, p. 3.

77. Avignon, Y., C. Caroubalos, M. Martres and M. Pick. AAS-NASA Symp. Physics of Solar Flares, Washington, 1964, p. p. 25.

78. Avignon, Y., C. Caroubalos, M. Martres and M. Pick. I.A.U. Sump. No. 22, Stellar and Solar Magnetic Fields, Amsterdam, 1965, p. 373.

79. Ellison, M., S. McKenna and J. Reid. Dunsink Observ. Publ., Vol. 1, 1961, p. 53.

80. Svestka, Z. I.A.U. Draft Reports, 1955, p. 69.

81. Gnevysheva, R. S. Astron. zh., Vol. 18 1941, p. 27.

82. Gnevyshev, M. N. and R. S. Gnevysheva. Bull. Solnechnyye dannyye, No. 8, 1960, p. 66.

83. Waldmeier, M. Z. Astrophys., Vol. 52, 1961, p. 1.

84. Babcock, H. W. Astrophys. J., Vol. 133, 1961, p. 572.

85. Gopasyuk, S. I. and M. B. Ogir'. Izv. Krymskoy astrofiz. ovserv., Vol. 30, 1963, p. 185.

86. McIntosh, P. Astron. J., Vol. 70, 1965, p. 683.

87. Krivsky, L. I.A.U. Symp. No. 35, Structure and Development of Solar Active Regions, Dordrecht-Holland, 1968, p. 465.

88. Krivsky, L. Bull. astron. Inst. Dzechslovakia, Vol. 20, 1969, p. 139

89. Fokker, A. Bull. astron. Inst. Czechslovakia, Vol. 15, 1964, p. 119.

90. Chapman, S. Monthly Notices Roy. Astron. Soc., Vol. 103, 1943, p. 117.

91. Parker, E. Phys. Rev. Vol. 107, 1957, p. 830.

92. Wild, J. Solar Corona. Proc. I.A.U. Symp., No. 16, New York and London, 1963, p. 115.

93. Dodson, H. Astrophys. J., Vol. 110, 1949, p. 382.

94. Dodson, H. Proc. IRE, Vol. 46, 1958, p. 149.

95. Martres, M. and M. Pick. Ann. Astrophys., Vol. 25, 1962, p. 293.

96. Moreton, G. I.A.U. Symp., No. 22, Stellar and Solar Magnetic Fields, Amsterdam, 1965, p. 371.

97. Kiepenheuer, K. Solar Spectrum. Proc. Symp. University Utrecht, edited by C. De Jager, Dordrecht-Holland, 1965, p. 240.

98. Dodson, H. Solar Phys., Vol. 13, 1970, p. 401.

99. I.G.Y. Solar Activity Maps D 1, Ann. I.G.Y., Vol. 21, Oxford - London - New York - Paris, 1961.

100. I.G.Y. Solar Activity Maps D 2, Ann. I.G.Y., Vol. 22, Oxford - London - New York - Paris, 1961.

101. Banin, V. G. Bull. Solnechnyye dannyye, No. 6, 1960, p. 62.

102. Koeckelenbergh, A. Com. Observ. Roy. Belgique, Nos. 173, 189, 197, 219.

103. Shaposhnikova, Ye. F. Izv. Krymskoy astrofiz. observ., Vol. 25, 1961, p. 122.

104. D'Azambuja, L. Bull. Soc. Astr. France, June, 1942, p. 97. /55

105. Sivaram, K and L. Punetha. Kodaikanal Observ. Bull., No. 179, 1967.

106. Bumba, V. and J. Kleczek. Observatory, Vol. 81, 1961, p. 141.

107. Pettit, E. Astroph. J., Vol. 76, 1932, p. 9.

108. Dolfus, A. I.A.U. Symp. No. 22, Stellar and Solar Magnetic Fields, Amsterdam, 1965, p. 355.

109. Bruzek, A. and H. Demastus. Solar Phys., Vol. 12, 1970, p. 447.

110. Roberts, W. I.A.U. Symp., No. 4, 1955, p. 336.

111. Correll, M. and W. Roberts. Astrophys. J., Vol. 127, 1958, p. 726.

112. Jaeger, F. Proc. of the Meeting on Solar Magnetic Fields and High Resolution Spectroscopy, Florence, 1966, p. 166.

113. Kleczek, J. AAS-NASA Symp. Physics of Solar Flares, Washington, 1964, p. 71.

114. Rust, D. Measurement of the Magnetic Fields in Quiescent Solar Prominences, NCAR Cooperative Thesis No. 6. University of Colorado and High Altitude Observatory, 1966.

115. Shklovskiy, I. S. Fizika solnechnoy korony (Physics of the Solar Corona). Moscow, State Physics and Mathematics Press, 1962.

116. Rosseland, S., E. Jenssen and E. Tandberg-Hanssen. I.A.U. Symp. No. 6, Electromagnetic Phenomena in Cosmic Physics, Cambridge, 1958, p. 150.

117. D'Azambuja, L. and M. D'Azambuja. Ann. Observ. Paris, Meudon, Vol. 6, Fasc. 7, 1948.

118. Spepanov, V. Ye. and N. N. Petrova. Izb. Krymskoy astrofiz. observ., Vol. 21, 1959, p. 152.

119. Howard, R. Astrophys. J., Vol. 130, 1959, p. 193.

120. Leiton, R. Astrophys. J., Vol. 130, 1959, p. 366.

121. Zirin, H. and A. Severny. Observatory, Vol. 81, 1961, p. 55.

122. Zirin, G. Astron. zh., Vol. 38, 1961, p. 861.

123. Ioshpa, B. A. Geomagnetizm i aeronomiya, Vol. 2, 1962, p. 172.

124. Kyznetsov, D. A. and V. Ye. Stepanov. In the collection: Reports of SibIZMIR on the theme "Fizika Solntsa" (Solar Physics). Irkutsk, 1965, p. 15.

125. Ioshpa, B. A. In the collection: Solnechnaya aktivnost' (Solar Activity), No. 3. Moscow, "Nauka" Press, 1968, p. 44.

126. Harwey, J. Ph.D. Diss., Univ. of Colorado, 1969.

127. Kiepenheuer, K. Convergo Volta, Vol. 11, Rome, 1953, p. 105.

128. Mogilevskiy, E. I. Solar Corona, Proc. I. A. U. Symp., No. 16, New York, 1963, p. 281.

129. Severnyy, A. B. Uspekhi fizicheskikh nauk, Vol. 88, Issue 1, 1966, p. 3.

130. Mogilevskiy, E. I. Space Research, Vol. 4, Amsterdam, 1964, p. 789.

131. Mogilevskiy, E. I. and B. D. Shel'ting. Proc. of the Meeting on Solar Magnetic Fields and High Resolution Spectroscopy, Florence, 1966, p. 222.

132. Shklovskiy, I. S. Astron. zh., Vol. 23, 1946, p. 333.

133. Akin'yan, S. T. Bull. Solnechnyye dannyye No. 10, 1965, p. 58.

134. Bruzek, A. Z. Astrophys., Vol. 50, 1960, p. 110.

135 Michard, R., Z. Mouradian and M. Semel. Ann Astrophys., Vol. 24, 1961, p. 55.

136. Warwick, J. Astrophys. J., Vol. 121, 1955, p. 376.

137. Warwick, C. Astrophys. J., Vol. 129, 1959, p. 801.

138. Giovanelli, R. and M. McCabe. Australian J. Phys., Vol. 11, 1958, p. 350.

139. Beygman, I. L., Yu. I. Grineva, S. L. Mandel'shtem and I. A. Zhitnik. Solar Phys., Vol. 9, 1969, p. 160.

140. Waldmeier, M. Ergebnisse und Probleme der Sonnenforschung (Results of Problems of Solar Research) 2nd Edition. Leipzig, 1955, p. 273.

141. Zirin, H. Solar Physics, Vol. 7. 1969, p. 243.

142. Svestka, Z. and J. Olmr. Bull Astron. Inst. Czechoslovakia, Vol. 17, 1966, p. 4.

143. Pettit, E. Publ. Yerkes Observ., Vol. 3, 1925, p. 205.

144. Pettit, E. Astrophys. J., Vol. 84, 1936, p. 319.

145. Severnyy, A. G. and V. L. Khokhlova. Izv. Krymskoy astrofiz. observ., Vol. 10, 1953, p. 9.

146. Banin, V. G. Izv. Krymskoy astrofiz. observ., Vol. 35, 1966, p. 190.

147. Banin, V. G. Izvestiya SibIZMIR (Izv. SibIZMIR), Issue 2. Irkutsk, 1967.

148. Banin, V. G. In the collection: "Issledovaniya po geomagnetizmy, aeronomii i fizike Solntsa" (Research in Geomagnetism, Aeronomy and Solar Physics), Issue 6. Irkutsk, 1970, p. 91.

149. Hyder, C. Solar Physics, Vol. 2, 1967, p. 49.

150. Hyder, C. Solar Physics, Vol. 2, 1967, p. 267.

151. Pettit, E. Astrophys. J., Vol. 98, 1943, p. 6.

152. Suemoto, Z., E. Hiei and T. Hirayma. J. Phys. Soc., Japan, Vol. 17, Suppl. A-2, 1962, p. 231.

153. De Jager, C. Stroyeniye i dinamika atmosfery Solntsa (Structure and Dynamics of the Solar Atmosphere). Russian translation edited by E. R. Mustel'. Moscow, Foreign Literature Press, 1962, p. 207.

154. Severnyy, A. B. Izv. Krymskoy astrofiz. observ., Vol. 9, 1952, p. 3.

155. Severnyy, A. B. Solar Flares. Ann. Rev. Astron. and Astrophys., Vol. 2, 1964, p. 365. /56

156. Gurtovenko, E. A. Nablyudeniya Solntsa, Mezhdynarodnyy geofizicheskiy god (Solar Observations, International Geo-Physical Year). Moscow, AN SSSR Press, 1959, p. 25.

157. Gold, T. and F. Hoyle. Monthly Notices Roy. Astron. Soc., Vol. 120, 1960, p. 89.

158. Ellison, M. Publ. Roy. Observ. Edinburgh, Vol. 1, 1952, p. 5.

159. Ellison, M. Dunsink Observ. Reprint, 1963, p. 24.

160. Billings, D. and W. Roberts. Astrophys. J., Vol. 118, 1953, p. 429.

161. Ellison, M. Trans. I.A.U., Vol. 9, 1955, p. 146.

162. Athay, R. and G. Moreton. Astrophys. J., Vol. 133, 1961, p. 935.

163. Stepanyan, A. A. and B. M. Vladimirskiy. Astron. zh., Vol. 38, 1961, p. 439.

164. Jefferies, J. and F. Orrall. AAS-NASA Symp. Physics of Solar Flares, Washington, 1964, p. 71.

165. Ioshpa, B. A. Geomagnetizm i aeronomiya, Vol. 3, 1963, p. 1125.

166. Smol'kov, G. Ya. and V. S. Bashkirtsev. Bull. Solnechnyye dannyye, No. 11, 1970, p. 97.

167. Shpital'naya, A. A. and G. F. Vyal'shin. Bull. Solenchnyye dannyye, No. 4, 1970, p. 100.

168. Kuznetsov, D. A. and A. A. Shpital'naya. Bull. Solnechnyye dannyye, No. 9, 1970, p. 98.

169. Gopasyuk, S. I. Izv. Krymskoy astrofiz. observ., Vol. 33, 1965, p. 100.

170. Severnyy, A. B. Izv. Krymskoy astrofiz. observ., Vol. 33, 1965, p. 3.

171. Brey, R. and R. Loukhed. Solnechnyye pyatna (Sunspots). Russian translation edited by V. Ye. Stepanov. Moscow, "Mir" Press, 1967, p. 324.

172. Severnyy, A. G. Trans. I.A.U. Vol. 12A, 1965, p. 755.

173. Anzer, U. Solar Phys., Vol. 3, 1968, p. 298.

174. Sturrok, P. Astron. J., Vol. 73 No. 5, Pt. 2, 1968, p. 79.

175. Stenflo, J. Solar Phys., Vol. 8, 1969, p. 114.

176. Anzer, U. and E. Tandberg-Hanssen. Solar Phys., Vol 11, 1970, p. 61.

PROPER MOTIONS OF SPOTS IN MULTICENTER GROUPS

Z. B. Korobova, V. M. Tishchenko, A. A. Tshkay
and V. V. Baturin

ABSTRACT. The proper motions of spots in 25 multicenter groups (10 typical bipolar centers, 10 irregular multipolar spots, and 5 complex groups, which were formed as the result of a new formation joining an already existing active center) are investigated. It is shown that vortex motions predominate in developed groups of any magnetic class. The direction of rotation of the vortices is not related to the hemisphere in which they are generated. It is established that the directions of translational motions of intermediate spots of bipolar groups are closely linked with their magnetic polarity; independently of their point of origin, spots with the leading polarity move toward the group leader, and spots with the trailing polarity move toward its eastern component. It was discovered that in complex groups the new, less stable spots changed their trajectories, being repulsed from the old, larger, more stable components. The linear velocities of the translational and the vortex motions are 100 m/sec; the angular velocities of the vortex motions increase with decreasing vortex radius, varying from 20° to 120° per day.

Investigations of the proper motions of sunspots are related /57
to a wide circle of problems of solar physics; from large-scale motions on the Sun as a whole to fast changes in its active regions.

The study of the motions of individual spots was begun in the generally-known works of the end of the last and the first quarter of the present century. A list of them is presented in the detailed review of G. V. Kuklin [1].

Contemporary researchers study the motions of sunspots within groups by two methods. Part of the work is statistical in nature, where one uses the data on the spot coordinates, published in such long-term catalogs as the Greenwich Photoheliographic Results. These works are based, as a rule, on a large amount of data encompassing several solar cycles. On the other hand, without original data the authors are limited to the study of the motions of only the main spots of a group, the leading and the trailing. Nonetheless, a number of fundamental investigations have been based on the data of the Greenwich catalogs. Thus, for example, V. Ye. Stepanov and M. A. Klyakotko [2] obtained the characteristics of the motions of sub-photospheric elements by analyzing the complex pattern of motions of the main spots in groups. They showed that the sub-photospheric kinematic elements have a marked influence on the general pattern of motions of spots in groups. Yu. I. Vitinskiy and R. N. Ikhsanov [3, 4, 5] developed the basic relationships of the emergence of the magnetic field of a group onto the surface of the Sun. They also showed that the dispersion of the main spots in longitude at the growth stage of the group occurs according to a single law within the errors. At the disintegration stage of a group, the motions of the main spots are more varied, but in a majority of cases the distance between the main components is either practically unchanged or increases.

The other method for investigating the motions of sunspots in groups is based on direct measurements of their coordinates from original photoheliograms, and permits one to construct a detailed picture of the motion of all stable nuclei. We will limit the survey of works in this direction to those investigations in which questions close to the content of this article are considered.

The first detailed study of the proper motions of a large number of spots inside six complex groups permitted R. S. Gnevyshev [6] to observe vortex motions encompassing the whole active region. /58 Vortex motions are certainly very typical for sunspots. Brunner-Hagger [7] later recognized them in a large group of spots. L. A. Nikitenko [8] studied the spiral structure in the arrangement of pores near leaders of fifteen groups. Waldmeier [9] considered an interesting case of the splitting of a spot into two components. After splitting, one of the generated spots began to rotate about the other. These examples of cases of rotational motions detected by various observers are far from the limit. Descriptions of vortex motions encompassing an active region as a whole and rotational motions of individual spots about the axis can also be found in works where these questions are involved only indirectly, for example, in the investigations of flares by Yu. M. Slonim [10].

G. V. Kuklin and A. Ye. Syklen [11] studied the motion of subphotospheric currents displacing individual parts of a group as a single whole, using as an example multicenter spot groups exceptional in their extent and complexity of structure. They showed that a group can be arranged simultaneously in several kinematic elements, within which the spot trajectories have a similar [illegible]e. The kinematic elements, according to [11], have dimensions [illegible]he order of $(5 - 10) \cdot 10^4$ km.

In recent years, the relation between the proper [illegible] of spots and the structure of the group magnetic field has been studied in some detail. Thus, Bumba [12], in comparing maps of magnetic fields with photoheliograms of eight bipolar groups, established that small spots move predominantly along isogauss of the longitudinal field. G. B. Kuklin [13] refined this relation by indicating data from two groups that close satellites of the principal spots move independently of the magnetic field, whereas, far from the principal spots, their trajectories strictly follow the field lines. While moving, the principal spots drag the field lines behind them,

deforming the field. S. I. Gopasyuk and Moreton [14] arrived at this conclusion somewhat earlier.

It follows from a very incomplete survey of works based on direct measurements of spot coordinates from original photoheliograms (for more details, cf. [1]), that numerous problems formulated in them are considered, as a rule, on limited material. The reason for this, as is correctly indicated in [1], is the time consumption of the spot coordinate determination process itself.

The main goal of this work is the study of the most typical characteristics of the proper motions of spots in multicenter groups during the maximum development of their area on the basis of a rather large amount of original material.

Observational material. Data for the investigation were obtained from photoheliograms of the Tashkent Solar Service, taken with the meniscus photoheliograph FG-1 of the system of D. D. Maksutov [15] during 1957 - 1969, on Agfa Printon film (in recent years — ORWO FU-5). The diameter of the solar image on the photoheliograms is about 8 cm.

The basic relationships of the proper motions of spots in a group are undoubtedly related to its structure. Thus, we have considered the motion of spots in 25 groups, by dividing them by structural features into three forms:

1. ten groups with a clearly expressed bipolar configuration of spots (types β, βp and βf of the Mount Wilson magnetic classification);

2. ten groups, being irregular multipolar spots (types δ, γ, βγ, infrequently α);

3. five groups, infrequently encountered, which have been formed as the result of the combination of two active centers, /5

having originated at different times during the same or in two successive rotations. It is interesting to examine the interaction of the old and new centers in them. We will call such groups complex.

Problems of technique. In order to construct the trajectory of a spot, it is necessary to determine its coordinates at least once a day.

The technique for determining the coordinates of spots (the geometric centers of their nuclei) involved the following. We rejected the use of precision measuring instruments, since because of the blurred edge of the disk their operation under high magnification does not give a significant gain in accuracy in comparison with the simpler (which is very valuable for the large volume of material to be processes) technique of the Solar Service.

Photoheliograms of excellent and good quality, with an interval of the observations of one day, were selected to determine the heliographic coordinates of spots. Photoheliograms, obtained daily, were not included in the processing when the distance of the groups selected for investigation exceeded 60° from the central meridian. Each photoheliogram was projected onto a circle of diameter 200 mm drawn on a sheet of white paper. The circle with marks plotted on it, indication the orientation of the reference thread, was superimposed on the solar image, and the groups were sketched with maximum care. Then a coordinate lattice was used to determine the positions of all spots which could be reliably identified on three or more successive photoheliograms. The correction for the position angle of the thread, specially determined from the Solar Service program, was taken into account for the superposition of the coordinate lattice onto the circle.

The described method is not free of systematic errors. The principal ones depend on how accurately the projection of the image coincides with the prepared circle, and the circle with the coordinate lattice. There is still a number of systematic errors,

difficult to take into account, which are characteristic of any method for determining heliographic coordinates [1]. The selection of the center of irregular nuclei is also somewhat arbitrary. Multiple repeated determinations of the coordinates of the same spots by different participants in the processing indicated that the errors of these determinations do not exceed 0.°2 - 0.°3. This value can be decreased with relative measurements, where one of the spots of the group is taken as fixed. Such a method is widely used [6, 12, 14]; however, we did not make use of it, since preliminary analysis of the processed material indicate that there are no spots which do not move more than 1° over 7 or 8 days and, thus, relative measurements introduce significant distortions in the general pattern of motions in the group. The accuracy of the method selected by us seems sufficient to reveal the most typical characteristics of the proper motions of spots.

Another technical problem arises in constructing the maps of the proper motions of spots. The general pattern of motions in a group is usually examined according to the trajectories of spots in the Carrington coordinate system. However, it is well known that this system is burdened with the systematic error caused by the differential rotation of the Sun. While the daily correction for differential rotation is small at mid-latitudes, it is 0.°3 -0.°5 at latitudes of 25° - 30°. As a result, distortion of the trajectories of high-latitude spots, constructed with Carrington coordinates, are so large that it becomes impossible to judge any of the typical characteristics in their motions. /61

In considering the problems of our work, we gave up the construction of maps of spot motions in the Carrington system. Corrections for the differential rotation of the Sun were introduced in the values of the Carrington longitudes of spots in the form $(n-1)\xi$, where $\xi = 0^{\circ}.196 - 2^{\circ}.77\sin^{4}\varphi$ (assuming the law of solar rotation obtained in [16]), n is the serial number of the day of observation of the spot, beginning from the first day of appearance in the coordinate analysis.

Thus, the proper motions of spots in bipolar groups, free of components related to the differential rotation of the Sun are shown in the maps presented below.

Proper motions of spots in bipolar groups.

The principal information on ten investigated bipolar groups is contained in Table 1. Here and in the following similar tables, the group numeration is given according to the bulletin "Solnechnyye dannyye" (Solar Statistics). The date of transit of the group through the central meridian of the Sun and its average coordinates are presented in the second, third, and fourth columns. The sketches of these groups, made from the photoheliograms with a diameter of the solar image of 30 cm, are presented in Figure 1. Nuclei with investigated proper motions are indicated by arrows with digits. The sketch of each group was made on the day with the maximum number of such nuclei.

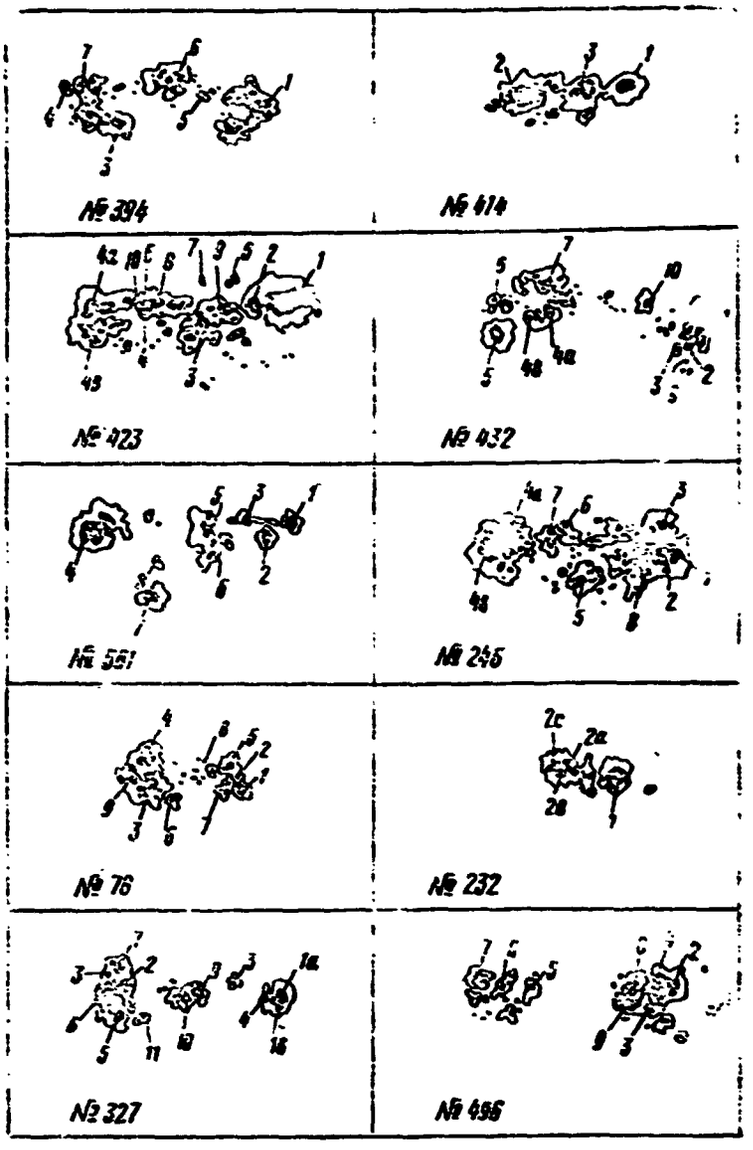

Figure 1. Bipolar groups of spots:
No. 394 — 9/2/1957; No. 414 — 9/13/1957; No. 423 — 9/19/1957; No. 432 — 9/28/1957; No. 561 — 10/21/1958; No. 246 — 7/3/1960; No. 78 — 3/4/1967; No. 232 — 6/15/1968; No. 327 — 8/20/1968; No. 496 — 12/26/1968

TABLE 1.

Group no.	Central meridian	ϕ	l	Interval of investigated proper motions*	Evolutionary and structural characteristics of group
394	8/31/1957	+16°	327°	8/28 - 9/4 (9/3)	Group of first rotation. Developed gradually up to 8/31. Vigorous renewal of activity and appearance of new, rapidly developing spots from 8/31.
414	9/11/1957	-16	186	9/11 - 9/16	Regeneration of previously existing group. One of the nuclei of eastern spot separated from its penumbra and entered penumbra of leader. Little change in the principal spots of group.
423	9/19/1957	+24	84	9/16 - 9/23	Group of first rotation. Stable leader, eastern spot rapidly separates in longitude. Interval between nuclei are filled with gright facular bridges [17].
432	9/27/1957	+14	340	9/23 - 10/1	Group of second rotation, consisting of a large number of dispersed spots. Eastern region dominates both in area and in rate of development.
561	10/22/1958	-10	231	10/18 - 10/23	Rapidly developing group of second rotation. Region of leader consists of a cluster of fine spots, elongated in longitude. Region of eastern spot, elongated in latitude, includes a large stable spot.

(Table continued on following page)

TABLE 1. (continued)

Group no.	Central meridian	ϕ	l	Interval of investigated proper motions*	Evolutionary and structural characteristics of group
246	7/3/1960	+9°	324°	7/1 - 7/7	Complex, compact group of second rotation with bright facular bridges. Eastern part decays significantly.
78	3/5/1967	-22	222	3/1 - 3/8	Slowly developing and rapidly decaying (after 3/5) group of first rotation. Eastern spot dominates.
232	6/13/1968	-14	180	6/11 - 6/18 (6/13)	Two close stable spots in group of first rotation.
327	8/20/68	-10	12	8/16 - 8/23	Rapidly developing group of third rotation. Gradual decay after 8/21. Structure similar to No. 561; region of leader elongated in longitude region of eastern spot elongated in latitude.
496	12/27/1968	+20	100	12/24 - 12/28	Group of first rotation. Leader is a complicated but stable spot. Eastern part is dispersed spots decaying after 12/27.

*Days of lapses in observations are indicated in parentheses. The same in Table 2 and 3.

Maps of the proper motions of spots in bipolar groups are presented in Figure 2. Here, and on the remaining maps, the circled numbers of nuclei correspond to the numbering on the sketches of the groups; the digits at the ends of the trajectories denote the dates of the first and the last measurement of the coordinates of the given nucleus. The black circles indicate the positions of nuclei of the leading polarity; the open circles — of the trailing polarity. To

determine the polarity of spots, we made use of the "Catalog of the Strengths and Polarities of Magnetic Fields of Sunspots for the Period of the International Geophysical Year" of V. Ye. Stepanov, Ye. F. Shaposhnikova and N. N. Petrova, the bulletins "Solnechnyye dannyye" and their appendices, and also the monthly bulletins "Solar Phenomena" [18].

The maps of the proper motions of spots permit one to recognize the regularities of the motions of the principal spots, as well as of their satellites.

Two types of motions are typical for the leading spots of bipolar groups during the maximum development of the group area: a gradual westward motion with small curvatures of the trajectory — the groups No. 394 (1957), 423 (1957), 432 (1957), 561 (1958), 78 (1967), 327 (1968);

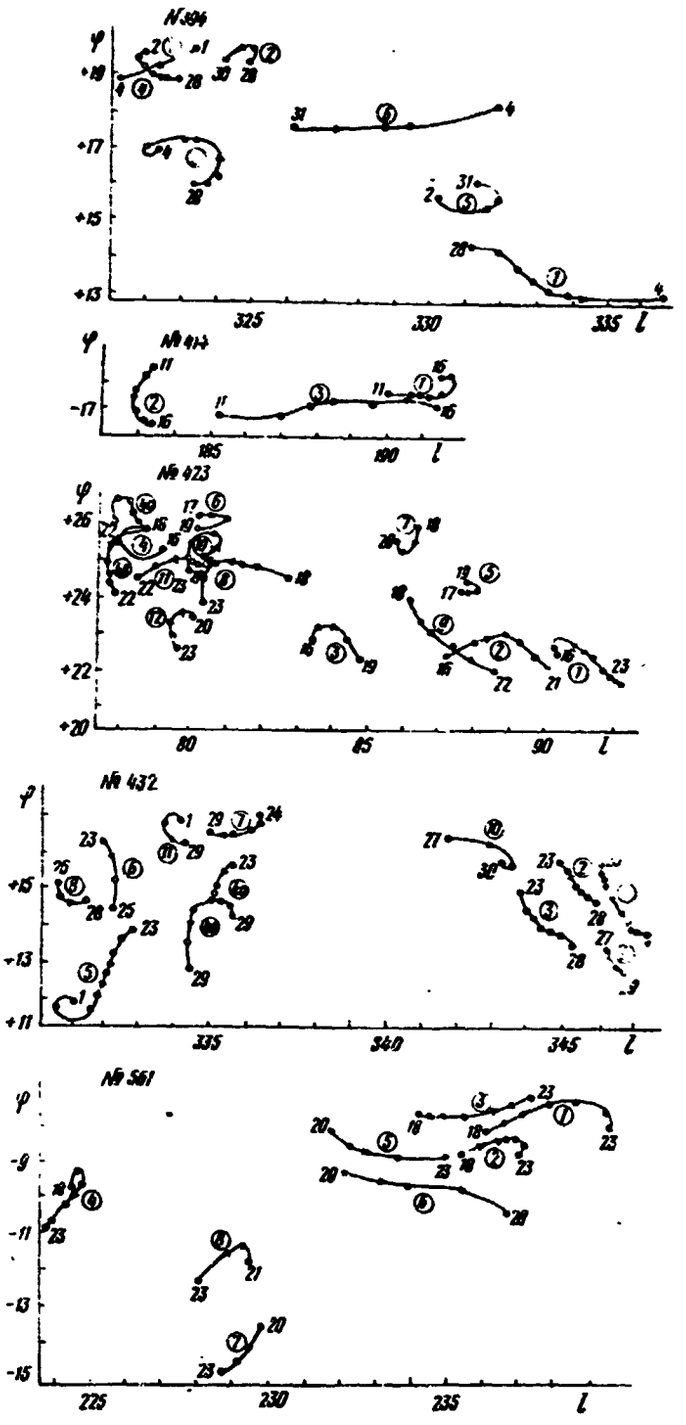

Figure 2. Proper motions of spots in bipolar stars

(Figure continued on following page)

/62

a vortex motion without a significant shift in longitude — the remaining groups. It is important to note that if the leader is a multinuclear spot or a close cluster of spots, then for the translational and for the vortex motions, all trajectories have similar coordinated directions. The directions of the vortex motions of a few spots, the satellites of the leader, more frequently coincide with the directions of motions of the leader itself. The order and directionality of the motion are generally characteristic of the whole region of the leading spot. This is easily seen for spots arising not only simultaneously, but sequentially, as in the groups Nos. 423 (1957), 432 (1957), 561 (1958), 78 (1967).

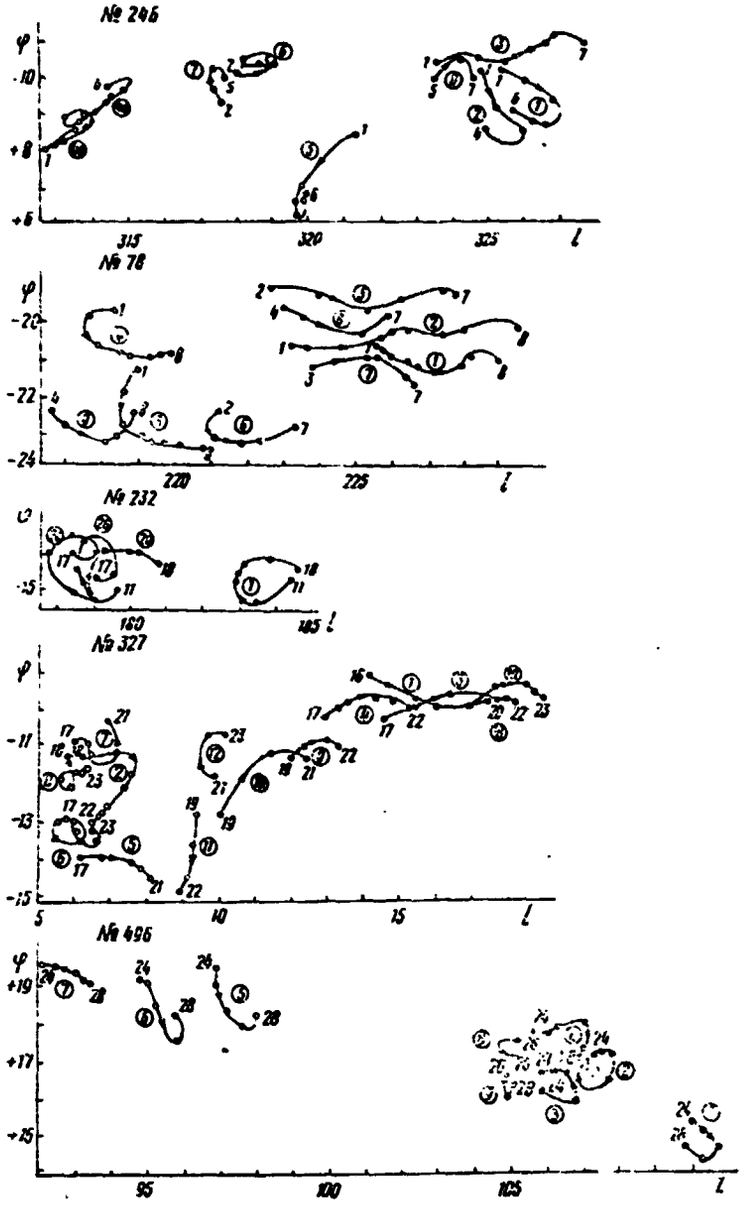

(Figure 2. (continued)

/64

It is impossible to relate the structure of leading spots and the degree of their stability to any one of the two forms of motion. The impression is created that translational and vortex motions are equally probable for long-lived regular spots whereas translational motions are more characteristic for dispersed clusters of spots, /65

such as the region of the leaders of the groups Nos. 432 (1957) and 561 (1958), and vortex — for close clusters [groups Nos. 246 (1960), 496 (1968)].

Let us proceed to the trailing spots. In all ten groups they are distinguished by complex structure and rapid development. The pattern of motions in this part of the group is more complicated than in the western, and it is more difficult to study, since the spots here are extremely unstable. Nonetheless, the general regularities of motions in the region of the eastern spot is completely obvious; only vortex motions are observed in all groups. But in contrast to the region of the leader, where rotational motions of the spots are coordinated, the trailing part of the group (both the principal spots and their satellites) is characterized by disordered intricate motions, directed to the east, toward the equator and toward the pole. The exceptions are the groups Nos. 414 (1957), 78 (1967), 232 (1968), which have the smallest extent in longitude. One can assume that each of these groups is situated in one kinematic element, which also determines the nature of its motion as a whole. This easily explains the similarity of the trajectories of spots in the western and eastern parts of these groups.

An interesting result is given by analyzing the proper motions of spots located between the principal components of the group. As was already mentioned, in comparing the proper motions of spots with the structure of the magnetic field of the group, a relation between them was established [12, 13, 14]. The trajectories of the intermediate spots in our maps indicate that the effect of this relation can be detected even without having the magnetic field maps available, but by knowing only the polarity of the spots and the direction of their motion. It was found that, in whatever part of the group the spot originated, the direction and nature of its motion are stipulated by the sign of the field; the intermediate spots of the leading polarity more predominantly to the west; the trailing polarity — in the opposite direction. We will discuss the most interesting examples.

In group No. 414 (1957), nucleus 3 of leading polarity, having been located in the penumbra of the eastern spot 2 on September 12-13, separated from it and, moving toward the west, entered the penumbra of the leader on September 14.

In group No. 78 (1967), nucleus 6 of leading polarity originated on March 2 in the eastern spot, where all the remaining nuclei had the opposite polarity. In repeating the vortex motion of the whole eastern spot, nucleus 6 separated from it on March 5, and turned westward toward the region of the leading spot.

In the slowly developing group No. 394 (1957), vigorously growing intermediate spots with anomalous distribution of polarities appeared on August 31. Thus, the spot with nucleus 5 arising near the leader had the polarity of the trailing spot; the spot with nucleus 6 in the region of the eastern component had the polarity of the leading spot. However, the trajectories of these spots were found in complete accordance with their polarity; nucleus 5 had a vortex motion; nucleus 6 had a translational motion toward the west.

In group No. 246 (1960), the spot with nucleus 5 was attracted in structure and localization in the group toward the leader, but, having the trailing polarity, moved away from it. In group No. 327 (1968), on the other hand, the intermediate spot with nuclei 9 and 10, appearing in the eastern part of the group but having the leading polarity, moved toward the west.

Proper motions of multipolar spots. The ten multipolar spots selected for the study of proper motions are described in Table 2. They all have a complex structure (Figure 3). In group No. 295 (1960), all the nuclei have only the leading polarity; the groups No. 250 /67
(1967) and No. 207 (1969) belong to the blass $\beta\gamma$ of the magnetic classification; the remaining seven — to classes γ and δ.

All the groups of classes γ and δ, and the unipolar group No. 295 (1960) evolved gradually. Their principal nuclei are preserved with significant deformations of the whole spot. The decay of such spots takes place by a gradual splitting or a slow separation of the peripheral parts.

The evolution of the two groups of class $\beta\gamma$ is identical to the evolution of the bipolar group; the region of the leader is stable, whereas in the eastern part, rapid changes take place. It is seen from the maps of the proper motions of the nuclei in these groups / 68
(Figure 4) that vortex motions take place in all the multipolar

TABLE 2.

Group no.	Central meridian	ϕ	l	Interval of investigated proper motions	Evolutionary and structural characteristics of group
295	7/5/1957	-30°	8°	7/1 - 7/9 (7/25)	Group of first rotation. Spot is deformed, but principal nuclei are stable.
343	8/1/1957	-30	6	7/30 - 8/5	Group of first rotation. Slightly changing principal spot with unstable satellites.
509	11/1/1957	-22	240	10/31 - 11/4	Group of first rotation. Region of spot filled with facular bridges, but nucle are stable.
316	6/17/59	+17	329	6/14 - 6/21	Group of second rotation. From 6/18 to 6/21, spot slowly divided into two parts.
379	7/14/1959	+16	330	7/13 - 7/18*	Group of third rotation. Spot stretches along the parallel, but nuclei remain.
295	7/30/1960	+9	330	7/26 - 8/3	Group of third rotation. Principal spot is deformed, but nuclei remain. Peripheral parts separate into stable satellites.
101	9/20/1963	+13	310	9/16 - 9/24	Regeneration of a previously existing region. Central part of spot moves toward the west, the eastern part slowly decays.
250	7/28/1967	+27	100	7/26-7/31	Regeneration of an active region which had existed six rotations with temporary fadings of activity. Region of leader is very stable. Eastern part of spot decays rapidly after 8/27, filling with bright faculae.

(Table continued on following page)

TABLE 2. (continued)

Group no.	Central meridian	ϕ	l	Interval of investigated proper motions	Evolutionary and structural characteristics of group
118	4/2/1969	+10°	278°	4/1 - 4/6	Group of first rotation. Spot is deformed, but nuclei are stable.
207	6/10/1969	-16	89	6/7 - 6/12	Regeneration of a previously existing region. Little change in region of leader. Eastern part grows significantly.

*V. F. Chistyakov kindly sent us the photoheliograms for 7/14 and 7/15/1959.

spots under consideration. However, the structure of the vortices is rarely uniform. A common vortex motion, for which all the nuclei have similar trajectories, is traced only in two groups, Nos. 295 (1960) and 118 (1969). A main vortex is distinguished in six groups out of the ten — Nos. 295 (1957), 343 (1957), 509 (1957), 316 (1959), 379 (1959), 101 (1963) — but other directions of rotation also exist. The close spots, with the rare exception of the groups Nos. 343 (1957) and 379 (1959), rotate in one direction.

We note that in multipolar groups, in contrast to bipolar, the nature of the motion is the same for nuclei of different polarity. The vortices encompassing the whole spot, or part of it, join spots with different field poles, neighboring spots of the same polarity can have opposite directions of motion.

In the groups No. 295 (1957) and 343 (1957), class $\beta\gamma$ on the other hand, the characteristics of motion of spots in bipolar groups are repeated. These are coordinated vortex motions in the western part; vortex, but irregular,— in the eastern.

Some cases are observed of the translational motion of one of the nuclei "through a spot" from east to west, independently of polarity. These are nucleus 4 in group No. 295 (1957), 3 in group No. 379 (1959), 3 in group No. 101 (1963). Nucleus 2 in the leading spot of the bipolar group No. 78 (1967) had an analogous motion. These nuclei do not participate in the vortex motion encompassing the whole spot or its individual parts. We have not been able to find whatever additional factors distinguish them from the remaining nuclei of the group.

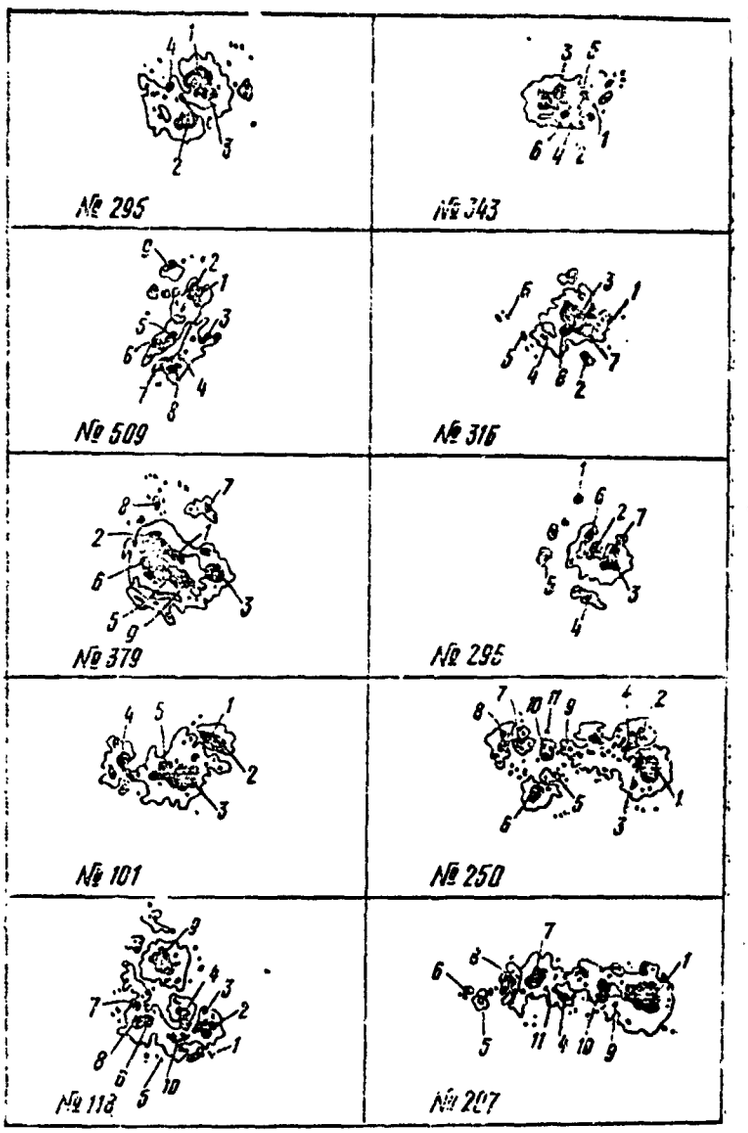

Figure 3. Multipolar spots:

No. 295 — 7/4/1957; No. 343 — 8/1/1957; No. 509 — 11/2/1957; No. 316 — 6/16/1959; No. 379 — 7/16/1959; No. 295 — 7/29/1960; No. 101 — 9/20/1963; No. 250 / — 7/27/1967; No. 118 — 4/2/1969; No. 207 — 6/10/1969

Proper motions of spots in complex groups. The complex groups selected for investigation of proper motions are described in Table 3, and their sketches are presented in Figure 5. One number is assigned to these groups in the publications, of which we made use to establish the polarities of the nuclei (appendix to the bulletin "Solnechnyye dannyye" and "Solar Phenomena"

[18]). But the evolution and distribution of polarity in them serve as a sufficient basis to consider each group as a result of the combination of two active centers. One such case is described in [19].

The principal characteristics of the motion of spots in these groups (Figure 6) are the same as in the bipolar. Either translational or coordinated vortex motions occur in the region of the leading spot; vortex, but irregular motions — in the eastern part. The intermediate spots with leading polarity move predominantly toward the west; with trailing polarity — toward the east. Thus, these groups could not give significantly new results for studying the general regularities in spot motions in comparison with bipolar.

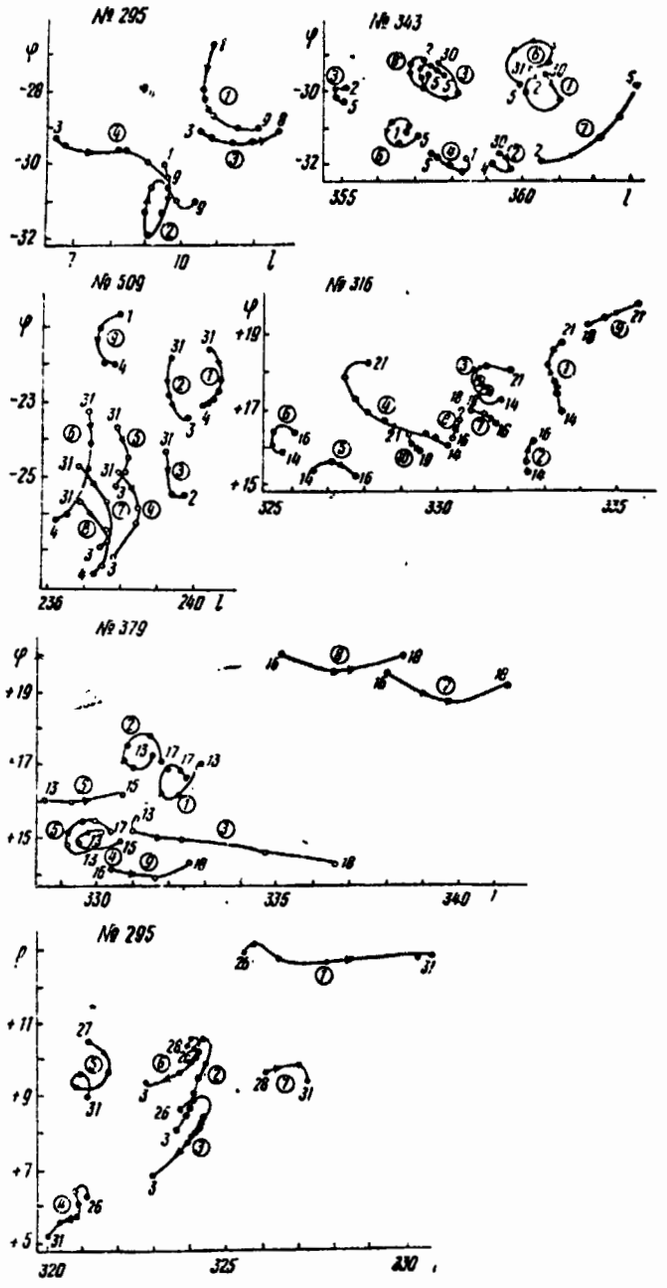

Figure 4. Proper motions of spots in multipolar groups

(Figure continued on following page)

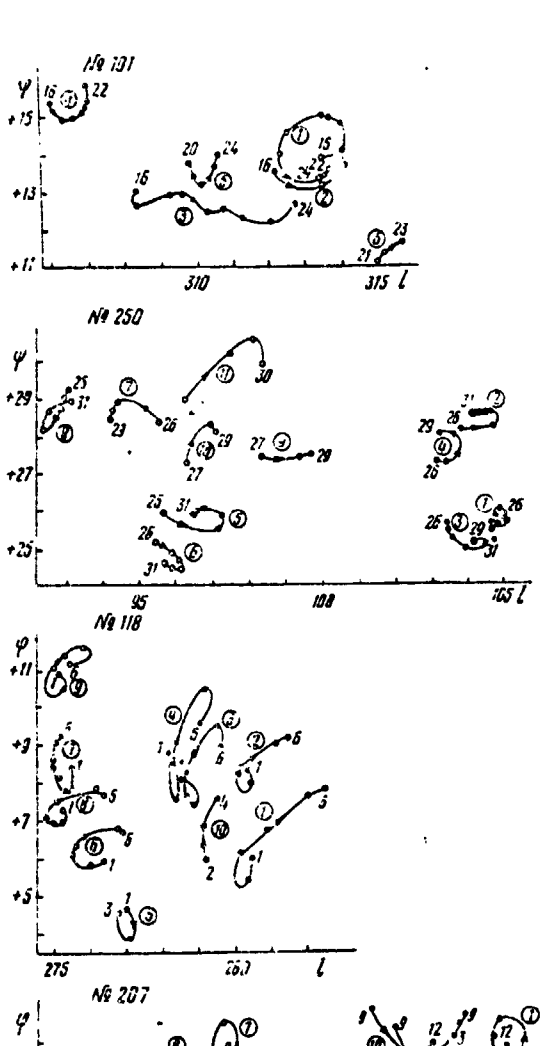

Figure 4. (continued)

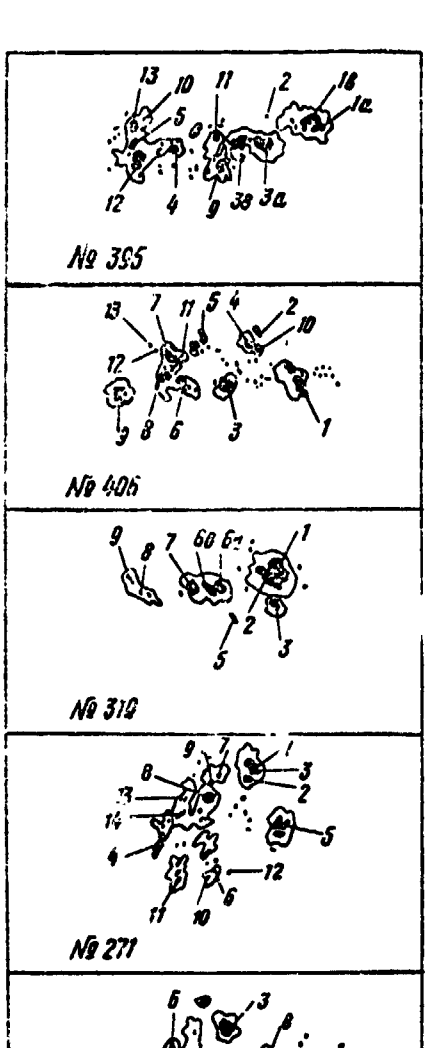

Figure 5. Complex groups: No. 395 — 8/31/1957; No. 406 — 9/10/1957; No. 319 — 8/15/1968; No. 271 — 8/3/1969; No. 301 — 8/26/1969

TABLE 3.

Group no.	Central meridian	ϕ	l	Interval of investigated proper motions	Evolutionary and structural characteristics of group
395	8/31/1957	+26°	330°	8/28 - 9/4	Complex, rapidly expanding group. Trailing spot, elongated in latitude, is the result of combination of eastern part of new group with group leader of preceding rotation.
406	9/10/1957	+12	196	9/7 - 9/13	Group of first rotation. Consists of a large number of spots dispersed in longitude. Distribution of polarities indicates combination of two active centers. Largest spot unites eastern component of preceding group and leader of following.
319	8/18/1968	-15	34	8/15 - 8/22	Spots of group of first rotation are concentrated in three centers. Leader is a regular stable spot. Middle spot consists of eastern part of preceding group and leader of following, which enters its penumbra 8/15. Spot splits after 8/18, and disappears by 8/21. Trailing spot is eastern component of following group. Disappears after 8/19.

(Table continued on following page)

TABLE 3. (continued)

Group no.	Central meridian	ϕ	l	Interval of investigated proper motions	Evolutionary and structural characteristics of group
271	8/1/1969	-8°	124	7/29 - 8/4	Region of first rotation consists of two groups, arranged one under the other. Northern group of class βγ emerged from behind eastern edge and slowly stretches in longitude. Southern bipolar group originated on disk 8/18, and develops rapidly. Intermediate spots of southern group begin to disappear by 8/21.
301	8/28/1969	+11	128	8/24 - 8/30	Region of first rotation, in which two groups, shifted in latitude, were combined. Leader is a close pair of regular stable spots. Spots of both groups are united in eastern part. Until 8/27, eastern part has complex multi-nuclear structure. Later, it rapidly disintegrates. Principal spot with satellites remains.

The main purpose in studying the proper motions of spots in complex groups is the study of the interaction of two combined active centers. Such an interaction must undoubtedly appear in the behavior of spots located "at the junction" of these centers. However, analysis of the motions of spots in complex groups is made difficult by the fact that the combination of two centers of activity is a rather rare and, probably, random phenomenon, in which it is difficult to detect any sort of typical features. Thus, the groups selected by

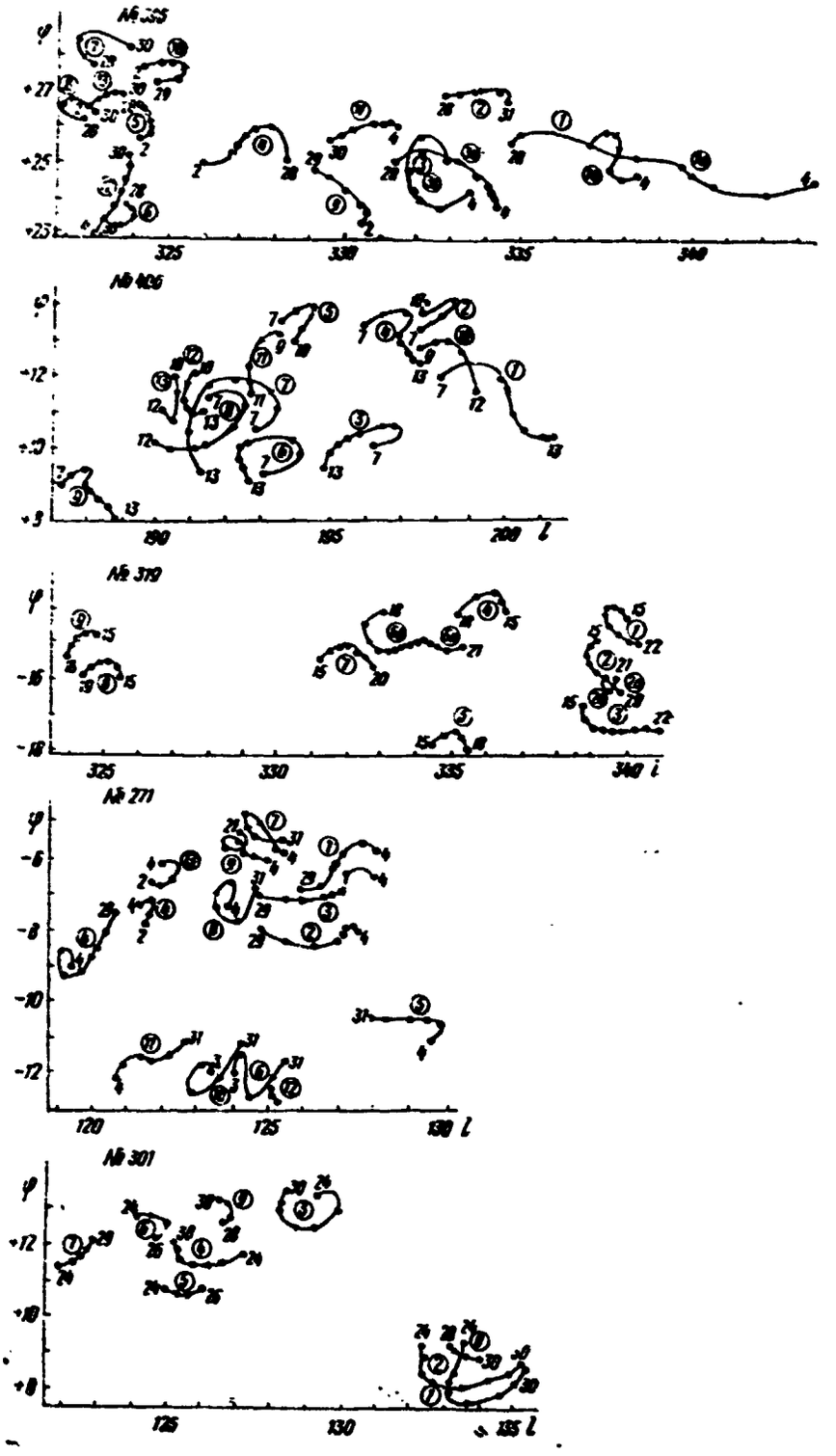

Figure 6. Proper motions of spots in complex groups

us are diversified in evolutionary characteristics. Thus, it follows from Table 3 that the interaction of old and new centers of activity can be judged only in two groups, Nos. 395 (1957) and 271 (1969), since only in these cases is it known which spots originated /69
in the given and preceding rotations. In the remaining groups, the interval of time between the generation of the two merged centers of activity is less than half a solar rotation, but the order of their origination is unknown.

The groups Nos. 406 (1957) and 301 (1969) are interesting in that one of the active centers combined in it has developed much more energetically than the other.

Let us consider each group. /70

In group No. 395 (1957), nuclei 5, 6, and 12 of the new expanding center of activity are ejected toward the equator from the spot whose northern part is the stable leader of the group, which existed in the preceding rotation.

In group No. 271 (1969), the eastern part of the new center of activity moves from the first day not to the east, but toward the equator, as if repelled from the already existing group.

In the irregular intermediate spot of group No. 406 (1957), nuclei 6, 7, and 11 of the preceding group and nucleus 8 of the following rotate in different directions, while the whole spot moves toward the east. Nucleus 8 does not separate from this spot, but the impression is created that the rapidly developing forward group /72
compresses the following group and inhibits its development. The area of nucleus 8 rapidly shrinks.

The trailing spot of the southern part of group No. 301 (1969), nucleus 4, rapidly moves toward the east. The intermediate nuclei 6 and 9 of the disintegrating southern group, located in the same penumbra with nucleus 4, perform vortex motions, and not the translational typical for them, and quickly disappear.

In group No. 319 (1968), the leader of the following group (nucleus 7), in moving toward the west, entered the penumbra of the eastern spot (nucleus 6). Nucleus 6 broke up into two parts, which began to separate quickly. Spot 6b, in moving toward the east, was obviously repelled from spot 7 and turned toward the equator.

Thus, in groups Nos. 395 (1957) and 271 (1969), the old and new centers of activity interact in a similar fashion. A shift of the new spots in latitude occurs, instead of the diverging motion in longitude typical for young groups. They are repelled from the previously existing group and recede from it. The trajectories of the old spots do not change.

In the remaining three groups, in which combined centers of activity were formed with some relative delay, the rapidly disintegrating nuclei with small area changed their trajectories under the effect of the more stable nuclei with larger area.

Velocity of proper motions of spots. We have calculated the linear velocity v, averaged over the interval of observations, along the trajectories of the proper motions of spots. The spots were grouped according to the nature of the motion:

	$\bar{v}$, m/sec	n
Translational motion in region of leader of bipolar group	85 ± 32	16
Vortex motion in region of leader of bipolar group	93 ± 29	17
Vortex motion in eastern part of bipolar group	88 ± 33	29
Vortex motion in multipolar spots	91 ± 47	34
Westward translational motion of new intermediate spots and spot satellites	188 ± 62	9
Motion of nucleus "through a spot"	120 ± 41	4
Motion of spots before splitting	118 ± 50	6
Motion of spots after splitting	90 ± 35	13

/74

It is seen from the presented data that during the maximum development of the area of the group, the average linear velocity of spots performing vortex motions does not depend either on their localization in the group or on the structure of the group, and practically equals the velocity of the translation motion of these spots.

The velocity of the translational motion of intermediate spots and spot satellites of the principal components of the group during the first days of their existence (spots arising during the investigation of proper motions are grouped) is comparable with the velocity of motion of the main spots of the group at the beginning of their development [20, 21].

The velocity of a nucleus passing "through a spot" from east to west exceeds the average velocity of the neighboring spots participating in the general motion of the spot.

The motion of splitting spots verifies the results of V. F. Chistyakov [22]: a spot before splitting moves more rapidly than its fragments.

The angular velocity of rotational motion was also calculated for individual spots with a clearly expressed vortex. Only those parts of the trajectories where the shape of the vortex is closest to a circle were used for this. In bipolar groups, 22 trajectories were selected, and 21 — in multipolar spots. As follows from Figure 7, the smaller the radius of the vortex, the higher the angular velocity of the nucleus. The values of angular velocities presented in Figure 7 agree well with results of [23, 24]. The linear velocity of spots on these same segments of rotations does not depend on the distance from the center of the vortex, and takes values from 60 to 140 m/sec, with an average value of 92 m/sec.

Directions of vortex motions of spots. The question of the direction of vortex motions of spots in the two hemispheres of the

Sun has been discussed repeatedly in the literature. R. S. Gnevysheva [6] showed from six groups of 1937 - 1938 (solar cycle No. 17) that vortices located in the northern hemisphere are directed counterclockwise, and clockwise in the southern hemisphere. Brunner-Hagger [7] observed a vortex in a group in 1941, located in the northern hemisphere, also directed counterclockwise. Finally, in a group of 1951 (cycle No. 18), located in the northern hemisphere, a vortex motion was directed clockwise.

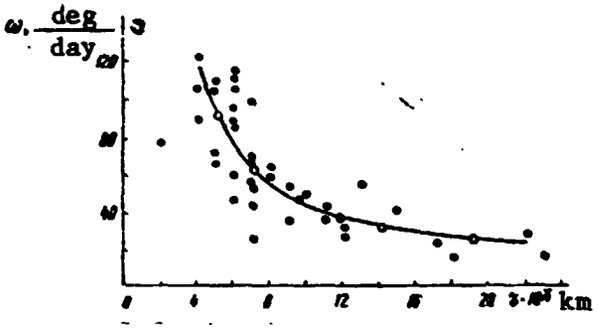

Figure 7. Dependence of the angular velocity of the vortex motion of a nucleus on the vortex radius

/75

The first two results served as a basis for the conclusion that the direction of rotation of active regions on the Sun corresponds to the effect of the Coriolus forces, and the last result suggested a shift of the directions of vortex motions from cycle to cycle. However, these deductions were contradicted by the conclusion of L. A. Nikitenko [8], that the twisting of the spiral structure of pores during 1955 - 1962 was clockwise in both hemispheres. We have examined the question of the direction of vortex motions of spots by using the trajectories of their proper motions (cf. Figures 2, 4, 6). The statistics included all clearly expressed vortices, encompassing the group as a whole, or part of it, without taking into account the vortex motions of spots in the regions of interaction between two active centers in complex groups. We present the results of the statistics:

Hemisphere	Direction of rotation	No. of vortices
	Cycle No. 19	
Northern	Clockwise	4
	Counterclockwise	2
Southern	Clockwise	5
	Counterclockwise	4
	Cycle No. 20	
Northern	Clockwise	3
	Counterclockwise	4
Southern	Clockwise	4
	Counterclockwise	3

It follows from them that in the groups considered by us, any sort of predominating directions of vortex motions is not observed either in the northern or in the southern hemisphere of the Sun.

* *
*

The basic results of the investigation of proper motions of spots in 25 multicenter groups reduce to the following.

1. Vortex motions of spots predominate in developed groups of any magnetic class.

2. During the maximum development of the area of bipolar groups, the proper motions of spots located in their leading and trailing parts differ significantly. Either translational motions directed toward the west or vortex motions without a significant shift in longitude occur in the region of the leader. Both forms of motion have a coordinated ordered nature. Only vortex motions, but complicated and irregular, directed toward the east, toward the equator and pole, are observed in the trailing region of the group.

3. The direction of motion of the intermediate spots of bipolar groups is related to the sign of their field. Independently of the point of origin, spots with leading polarity move toward the leader of the group; spots with trailing polarity move toward the trailing spot.

4. The nuclei of multipole, single and multipolar spots have only vortex motions, while in the multipolar spots, the nuclei of different polarity do not differ in the nature of the motion.

5. With the combination of spots of two centers of activity /76 into one group, the new, less stable spots change their trajectories, being repelled from the more stable, larger spots.

6. In bipolar and multipolar groups, the linear velocity of translational and vortex motions is about 100 m/sec, on the average. The linear velocity of intermediate spots and spot satellites during the first days of their existence is comparable with the velocity of the principal spots of the group at the beginning of their development (about 200 m/sec). The angular velocity of the vortex motions of individual spots increases with decreasing vortex radius, varying from 120° to 20° per day.

7. A predominating direction of vortex motions is not observed in the investigated groups in either hemisphere of the Sun.

References

1. Kuklin, G. B. In the collection: "Issledovaniya po geomagnetizmy, astronomii i fizike Solntsa" (Research in Geomagnetism Astronomy and Solar Physics), Part 10. Moscow, "Nauka" Press, 1970, p. 161.

2. Stepanov, V. Ye. and M. A. Klyakotko. Izv. Krymsk. astrofiz. observ., Vol. 16, 1956, p. 80.

3. Vitinskiy, Yu. I. and R. N. Ikhsanov. Bull. Solnechnyye dannyye, No. 10, 1964, p. 57.

4. Vitinskiy, Yu. I. and R. N. Ikhsanov. Bull. Solnechnyye dannyye, No. 12, 1964, p. 63.

5. Vitinskiy, Yu. I. and R. N. Ikhsanov. Izvestiya Glavnoy astronomicheskoy observatorii (Izv. GAO), No. 180, 1966, p. 40.

6. Gnevysheva, R. S. Astron. zh., Vol. 18, 1941, p. 26.

7. Brunner-Hagger, W. Astron. Nach., Vol. 272, 1942, p. 153.

8. Nikitenko, L. A. Bull. Solnechnyye dannyye, No. 7, 1963, p. 60.

9. Waldmeier, M. Z. Astrophys., Vol. 57, 1963, p. 207.

10. Slonim, Yu. M. Bull. Solnechnyye dannyye, No. 5, 1968, p. 79.

11. Kuklin, G.V. and A. Ye. Syklen. In the collection: "Resultaty nablyudeniy i issledovaniy v period MGSS" (Results of Observations and Research during IQSY), Part 1, 1966, p. 64.

12. Bumba, V. Prace Wracl. Nauk, Ser. B, No. 112, 1964, p. 31.

13. Kuklin, G. V. Proc. IAU Symp., No. 35, 1968.

14. Gopasyuk, S. I. and G. E. Moreton. Proc. Astron. Soc. Austr., Vol. 1, 1967, p. 8.

15. Dobychin, P. V. Bull. Komissiya po issledovaniyu Solntsa (Bull. Kom. po issl.) No. 2 (16), 1949, p. 1.

16. Newton, U. W. and M. Nunn. Z. M. N., Vol. 111, 1951, p. 413.

17. Korobova, Z. B. Astron. zh., Vol. 43, No. 3, 1966, p. 480.

18. Solar Phenomena. Oss. astron. Di Roma, Monthly Bulletins, 1968 - 1969.

19. Künzel, H., W. Mattig and E. H. Schtröter. Die Sterne, Vol. 37, 1961, p. 198.

20. Waldmeier, M. Ergebnisse und Probleme der Sonnenforschung. (Results and Problems of Solar Research). Leipzig, 1955.

21. Dezsö, L., O. Gerlei and V. Sipos. Publ. Debrecen heliophys. obs., Vol. 1, No. 2 - No. 4, 1964, p. 27.

22. Chistyakov, V. F. Bull. Solnechnyye dannyye, No. 4, 1968, p. 87.

23. Chistyakov, V. F. Bull. Solnechnnye dannyye, No. 2, 1964, p. 56.

24. Gopasyuk, S. I. Izv. Krymsk. astrofiz. observ., Vol. 33, 1965, p. 100.

RELATION BETWEEN SPORADIC CHROMOSPHERIC PROCESSES AND THE EVOLUTION OF SUNSPOT GROUPS

K. F. Kuleshova

ABSTRACT. An attempt is made to differentiate sporadic chromospheric processes according to the phases of the evolutionary curve of a spot group. It is shown that swiftly developing processes of the surge type arise during the decay phase of the group, and are evidently related to the disintegration of the magnetic field of the region. Processes of the loop prominence type characterized by slow evolution, on the contrary, arise during the growth phase of the group, and are possibly associated with the penetration of the field into the chromosphere and corona.

Material obtained from observations of the Astronomical Institute of the AN UzSSR from 1957 up to the present has given us the opportunity to examine the question of the relation between sporadic chromospheric processes and the evolution of sunspot groups. The observations of these so-called fast processes were carried out simultaneously on two instruments: a chromosphere-photosphere telescope (AFR-2), and a spectrohelioscope. The combination of these instruments permitted not only the observation of the development of a majority of processes on the Sun in the image plane, but also the simultaneous determination of the radial component of their motion. /77

We have investigated the distribution of several fast processes according to the phases of development of the spot groups. Surges at the edge and on the disk of the Sun (BSL, DSD), and also active prominences of loop structures at the edge and on the disk, were considered (APR, AFR).

Only those surges which arose in groups with confidently recorded maximum of area, i.e., in groups for which the phase of their growth and decay was traced — even if partially — on the visible side of the sun, were considered on the disk. Since the spot areas were extracted from the Greenwich Catalogs [1], the time interval was limited from 1957 to 1961. In all, there were selected 62 spot groups and 76 surges related to them. The groups were combined by superimposing the time of the maximum development of their area. The time in days is plotted along the abscissa in Figure 1. The origin is taken at the time of the spot area maximum. The solid line represents the change of the total area of all the spot groups; the dashed line — the number of surges (DSD). As is seen, the curve of the surge frequency is shifted significantly toward the branch of spot area decline. Of the total number of surges, 64% occur during spot decay, 24% during growth, and 12% during maximum, which amounts to one day in this case.

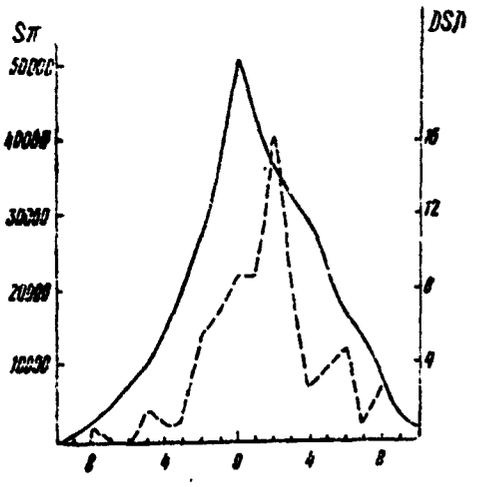

Figure 1.

From 1957 to 1969, 84 surges at the edge of the disk (BSL) were confidently recorded. Judging from our recordings of spots, 85% arose during the decline stage of group area, and only 15% during the growth stage.

In order to link more accurately the appearance of fast processes with the phase of development of spot groups, we used a curve

characterizing the typical evolution of spot groups which had existed 1.25 synodic rotations [2]. The lifetime T of these groups is close to one rotation. According to this feature, 30 groups achieving area maximum in the visible hemisphere, in which there arose 29 surges on the disk and 7 surges at the edge of the Sun, were selected over the priod from 1957 to 1961. The groups in this case were also combined by superimposing the time of maximum development of their area, and the distribution of surges by days of the group life was entered relative to this reference date of area maximum. The time in days is plotted along the abscissa in Figure 2a, and the origin is taken at the time of area maximum. The solid line represents the typical evolutionary change of area of a group with T = 1.25 synodic rotations; the dashed line — the smoothed curve of the surge frequency at the edge and on the disk. As is seen in Figure 2a, the maximum and main part of the surge frequency curve occurs on the decay branch of spot groups. Quantitatively, it appears that the average daily frequency of the appearance of surges during the growth phase of group area is 1.1, and 2.3 — during the decline phase.

/78

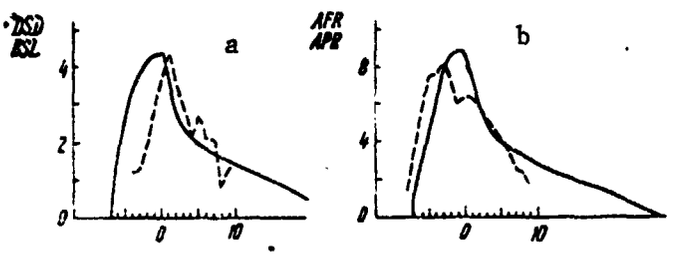

Figure 2.

From 1957 to 1961, 51 spot groups were observed with a lifetime close to one synodic rotation and maximum area development in the visible hemisphere. There were 86 active prominences of loop structure, 56 AFR and 30 APR, related to these groups. The evolutionary curve of spot area with T = 1.25 synodic rotations (solid line) and the number of prominences (dashed line) are presented in Figure 2b. The maximum of the frequency of appearance of active prominences is shifted toward the growth branch of spot area. The average daily frequency during the growth phase of area is 5.9, and during the decline phase — 3.9.

Thus, surges arise mainly during the decay stage of spot groups and are evidently caused by the disintegration of the magnetic field of the region. Active prominences of loop structure are formed predominantly during the growth stage of a spot group, and are evidently associated with the emergence of the magnetic field into the external layers of the Sun, and its slow expansion [3, 4].

References

1. Greenwich Photo-heliographic Results, 1957 - 1961. /79
2. Kuleshova, K. F. Bull. Solnechnyye dannyye, No. 10, 1963, p. 57.
3. Slonim, Yu. M. Astron. zh., Vol. 45, 1968, pp. 286, 726.
4. Slonim, Yu. M. Astron. zh., Vol. 46, 1969, pp. 570, 697.

ON A MODEL OF THE SOLAR CHROMOSPHERE

A. Sadikov

ABSTRACT. Recent representation of the structural and physical features of the chromosphere are summarized and a model is proposed, according to which the chromosphere consists, as it were, of cold and hot spicules having photospheric and coro.al origin, respectively. Their interface is localized at an altitude of the order of 3000 km. The model is based on some results previously obtained by the author, that is, the discovered variation of the Doppler widths of the lines of Ca, H and He with altitude, and the established dependence of the physical parameters of the chromosphere on the heliographic latitude.

The first structural models of the chromosphere were proposed /80
by Ye. Ya. Perepelkin [1] and Menzel [2]. Ye. Ya. Perepelkin explained the form of the solar chromosphere at the edge of the solar disk as being composed of a set of prominences with different altitudes, the small and medium predominating over the tall and forming a continuous array in the lower and middle chromosphere. Thus, we are not able to resolve it into individual elements. We will consider recent models of the chromosphere based on its physical and structural characteristics.

According to [3, 4], the temperature in the lower and upper chromosphere is approximately the same. In the model of Jeffries [5, 6], the chromosphere is an isothermal sphere with an electron temperature of 7500 - 100,000°, and electron density from 10^8 to 10^{13} cm^{-3}, this medium being located in a radiation field with a temperature of 5000°.

Van de Hulst [7] assumes that the temperature in the lower chromosphere at an altitude of 2000 km is 5850°, and 10% of the hydrogen is ionized. Pagel [8] and Pecker [9], on the basis of a study of the infrared Fe I lines and proceeding from local thermodynamic equilibrium, have proposed models in which the simultaneous emission of atoms with low excitation potentials and atoms of neutral and ionized helium is explained either by the presence at altitudes below 1100 km of regions with a temperature 18,000°, or by the presence of an external field of hard radiation. Miyamoto [10, 11] and E. V. Kononovich [12] assume that the helium in the chromosphere is excited by the ultraviolet radiation in the corona.

According to the calculations of Athay and Thomas [13], based on the data of [14], the optical thickness τ_{500A} must be the order of 100 at altitudes $\gtrsim$ 1100 km, so that, in a spherically summetric chromosphere, the coronal radiation cannot play any sort of role because of such a large optical thickness. Moreover, radiation in the chromosphere of the lines of neutral and ionized helium would require 100 times more quanta that is radiated by the corona. Giovanelli [5], Hoyle [15], Hagen [16], Woltjer [17], Athay and Menzel [18], Thomas and Athay [19] have proposed spherically asymmetric models with intermittent columns of "hot" and "cold" gas (spicules).

Many investigators explain the structure of the chromosphere with a two-component model. In these models, the spicule is considered as the principal hot element in the lower chromosphere, and the medium between spicules is assumed as cold [20]. In the upper chromosphere, on the contrary, the spicules are the cold elements, /81

and the space between spicules is filled with the hot coronal material.

In other works [21], on the contrary, it is assumed that the spicules are the cold component in the lower chromosphere, to which the temperature of 6300° is attributed. The hot component fills the space between spicules [22, 23], and has a temperature of 19,000°. In the upper chromosphere, the spicules (19,000°) are also the cold component, and the hot material surrounding them has a temperature of 100,000°.

Thus, in this model, the temperature in spicules increases with altitude from 6300° to 100,000°. According to Woltjer [17], the temperature of spicules is 21,000° at an altitude of 4000 - 6000 km. E. V. Kononovich [12] suggests that the spicule consists of a hot nucleus (with a temperature $\approx$ 12,000°), surrounded by several shells. The outermost layers give radiation principally in metallic lines. The radiation in the deeper layers is concentrated in the lines of hydrogen. In the center of spicules, the helium line is excited by the effect of the natural ultraviolet radiation. The space between spicules has a small volume, and its density is orders smaller than in the neighboring regions. However, it was shown in [19, 20, 24, 25] that the images of spicules coincide in the various lines.

According to the calculations of Athay [13], the observed width of D_3 corresponds to a temperature $\approx$ 50,000°, and non-thermal velocities v_t = 8 km/sec. G. M. Nikol'skiy [26] found that the temperature is 25,000°, and v_t = 4 km/sec.

Athay and Thomas [13] assume that the chromosphere at any altitude above the photosphere consists of regions of two types, with areas a and b, respectively. The radiation of helium originates only in regions a. The fraction of the radiation in the Balmar continuum is calculated respectively for the a-regions and b-regions; below the level of 3000 km, hydrogen is supplied principally by regions b, and above 4000 km, it almost completely originates in

areas a. Hence, it follows that the radiation of hydrogen and helium in the lower chromosphere (below 3000 km) arises in different locations, and in the upper (above 4000 km) — at the same locations. In the lower chromosphere, hydrogen, as a rule, is radiated in regions b, and helium — in regions a. Thus, a region a is hotter here than a region b. This point of view is also verified in [24, 25], where it is shown that above 4000 km, spicules with identical components are seen in the first lines of the Balmer series and in the helium lines.

Thus, above 5000 km, the region a can be identified with spicules. Chromospheric spicules are observed only at high altitudes. Some authors assume that the whole chromosphere consists of spicules, but in its lower part the set of superimposed short spicules screen each other, forming a continuous array, because of which we cannot observe them individually.

Spectral observations of spicules indicate that their line widths are large. Thus, the investigations of Smith [23] and Athay [25] showed that the line width of H α is confined within 1.1 - 1.9 Å. This corresponds to values of the Doppler width ($\Delta \lambda_D$) from 0.72 to 1.14 Å. G. M. Nikol'skiy and A. A. Sazanov found, from observations performed on an outside-eclipse coronograph, that the width of H α in spicules is 0.6 - 1.2 Å (0.8 Å on the average) at an altitude of 5000 - 6000 km. Such large values of line width can be explained by the great optical thickness and line broadening because of self-absorption, or by the high temperature in the region of hydrogen emission ($\approx$ 30,000°), or by nonthermal motions with v_t = 20 km/sec [26]. When observed at the limb, spicules are optically thin in the line of H α [27]. In other words, at 30,000°, hydrogen must be almost completely ionized, and its weak radiation must be recombination in nature. V. A. Krat [28] has shown that in a region of hydrogen emission in spicules, T $\leq$ 10,000°. G. M. Nikol'skiy also proceeds from T $\approx$ 6000° in constructing a model of the chromosphere. One can assume that the temperature in spicules should not reach 30,000°. For a qualitative explanation of the line width in spicules, G. M.

/82

Nikol'skiy [27] interprets their profile as the sum of two Gaussian profiles. The width of the total profile depends, of course, on the width of each of the original profiles and their relative shift. By using this technique as applied to lines of hydrogen and helium, he found that $v_t \approx 20$ km/sec inside spicules. The authors of [24] arrive at an analogous explanation of line profiles in spicules.

There is also another explanation of the large width of line profiles in spicules. V. A. Krat and T. V. Krat [28] have drawn the conclusion that spicules arise above the chromosphere and are not components of it; for the macro-structural components of the chromosphere, usually assumed as groups of spicules, the Doppler width ($\Delta \lambda_D$) must be no less than in the individual spicules. However, the macro-structural elements correspond to formations having $\Delta \lambda_D < 0.5$ Å in the line of H α. V. A. Krat and T. V. Krat [28], on the basis of these reasons, and proceeding from the fact that spicules appear only at high altitudes, arrive at the conclusion that spicules are formed from coronal material which has condensed and cooled. The observed rates of ascent are not the actual ascent of material, but the growth rate of the upper end of spicules. In addition, it should be taken into account that the line profiles of spicules are sometimes like the line profiles of chromospheric flares. It is possible that a portion of the spicules in the upper chromosphere are microflares.

Spicules in H α are sharply outlined formations, and in D_3 they are more diffused and have a background of uniformly weak emission. The width of the spicule in D_3 is almost twice as great as in H α. This difference [28] is explained by the clustering of a large number of helium filaments in the spicule. They border a colder cluster of hydrogen filaments, which compose the spicule center.

A structural model of the chromosphere is also proposed in [28 - 31]. According to this model, the chromosphere consists of filaments of various temperatures T_e and densities n_e: the so-called

metallic ($T_e \approx 5000°$, $n_e \approx 10^{12}$), hydrogen ($T_e \approx 6000°$, $n_2 \approx 10^{12}$), helium ($T_e \approx 15{,}000°$ and $n_e \approx 10^{11}$, and in the lower chromosphere $T_e \approx 15{,}000°$ and $n_e \approx 10^{12}$), and sub-coronal, existing only in the upper chromosphere ($T_e \approx 100{,}000°$ and $n_e \approx 10^{10}$). Only the relative number of filaments of the different types changes with altitude. The metallic and hydrogen ("cold") flares predominate in the lower and middle chromosphere, the helium ("hot) and sub-coronal ("very hot") — in the upper chromosphere. The filaments are in a state of continuous formation and disintegration, since they are moving and evolving all the time. The simultaneous existence of both "hot" and "cold" filaments in the chromosphere is explained [32] by the presence of a complicated magnetic field, whose magnitude is estimated from the condition of equilibrium of kinetic and magnetic energies. It is shown in [32] that one can also explain the significant extent in altitude of chromospheric filaments by the presence of a turbulent magnetic field.

An original model of the chromosphere was proposed by H. Zirin [33]. In it, the temperature at the edge of the photosphere equals 4500°. The temperature then increases somewhat with altitude, and the density rapidly decreases, and at an altitude of about 1500 km, the density of the chromosphere corresponds to the coronal values. The spicules are ejected from flocculi. The temperature of spicules ranges from 30,000° to 100,000°. The corona is directly above the flocculi. It is impossible within the framework of this model to explain the existence of the chromosphere outside the floccular regions, the emission of spicules in the polar regions of the sun and at high altitudes. /83

A systematic study of the spectroheliograms of the lower chromosphere (mainly in the metallic lines) was performed by d'Azambuja [34]; later it was repeated with his data by Reichel [35].

The nuclei of almost all metallic lines display dark structural elements on a brighter background in the undisturbed regions of the

Sun. The diameters of the elements lie in the range of 2000 - 6000 km, and the distance between them is 10,000 and 20,000 km. A chromospheric network is highly visible in the nuclei of metallic lines. The presence of structural components is also detected in photographs obtained with a filter having a wide pass band in the wings of the H α line [36]. Dark filaments (spots) of width 2 - 3" and length 5 - 15' are visible. These dark objects form the chromospheric network. Pairs of filaments (they are joined by weak fibrillar filaments) are reminiscent of loops in the nature of the motions; gas flows out of one such speck, flows toward the other, and exits downward into the photosphere. The fibrils are visible mainly in the center of H α. Observations at the limb, performed with a filter in H α $\pm$ 0.75 Å, have shown that spicules, bright in one wing of the line, are not visible or are very weakly visible in the other. At a distance 0.5 Å from the center of H α, the chromosphere decays into a set of individual radial structures.

Leighton [37] identifies spicules on the disk with small ejections, located near regions with descending motions in the cells of the chromospheric network. A change in the direction of motion of the ejection is sometimes noted several minutes after its beginning.

The so-called fine and coarse nodules are visible in the lines of Hβ , Hγ , in the wings of H α ($\Delta \lambda > 0.5$ Å), and in the lines of helium and Ca II; the chromospheric network being formed by them evidently reflects the motions of ascending and descending masses of chromospheric gas. The ascending motions appear from the level of the photosphere up to altitudes of $\approx$ 5000 km. V. Ye. Stepanov [38] and de Jager [39] recognized ascending motions with a velocity of - 0.96 km/sec, and descending — with a velocity of + 1.25 km/sec in nodules, visible in the light of CA II.

E. Ye. Dubov [40 - 42] suggests a model of the chromosphere based on observational material obtained by him. E. Ye Dubov observed the solar chromosphere in different parts of the line H α with the help of an interference-polarization filter reconstructed

by him, which permits separation of the nucleus and wings of this line. It is known from [39] that the different parts of the H α line appear at different altitudes from the edge of the photosphere, which is evident from the following data:

Δλ, Å:	0.0	0.2	0.4	0.6	0.8;
h, km:	5000	5000	4000	3000	1000.

The bottom part of the chromosphere, according to the model of E. Ye. Dubov [42], is esse ially in local thermodynamic equilibrium, /84 and T_e gradually increases to 7000°. Above 3000 - 3500 km, the temperature gradually increases to the value 20,000°. Hot (20,000°) and cold (7000°) regions coexist in the interval of altitudes 2000 - 3000 km. The upper chromosphere, where the temperature is 20,000°, the same as the bottom (from the edge to an altitude of 2000 km), is essentially uniform and is in a state close to thermodynamic equilibrium. A balance is achieved in each layer between the energy released as the result of dissipation of shock waves and the energy carried away by radiation. Such a balance is provided in the bottom layers by hydrogen emission, and in the upper — by emission of ionized helium. This model is based on observations of the chromosphere in the H α line of hydrogen, i.e., one can say that it is a model of the hydrogen chromosphere.

Van de Hulst [7] also arrives at roughly the same picture on the basis of analysis of numerous observations. He assumes that below 4000 km, the chromosphere consists of comparatively cold gas. Above 6000 km, it is hot gas, intensely ionized hydrogen. Complete ionization of hydrogen, an increase of temperature, etc., occur in the intermediate layer between the upper and lower chromosphere. The authors of [43] also assume that the chromosphere is divided into several layers: in the region 0 - 1500 km, T_e increases from 5000° to 6000°, and ionization of hydrogen begins; in the region from 1000 to 3500 km, the ionization of hydrogen increases from 5 to 99%, and T_e gradually increases; in the interval 2400 - 6400 km,

T_e reaches $\approx 7 \times 10^4$. Above 5500 km, it is necessary to take into account the inhomogeneity of the chromosphere.

The relation between the chromosphere and the corona should be discussed. During the eclipses of 1936 and 1941 in the Soviet Union, among many others, a special expedition to the edge of the eclipse path was organized in order to observe the polar regions of the Sun. On the basis of the obtained materials, S. K. Vsekhsvyatskiy and Ye. Ya. Bugoslavskaya [44] established a relation between many coronal and chromospheric formations. It was revealed that in the northern and scuthern ray systems, a majority of coronal rays is a continuation of chromospheric projections, i.e., spicules.

A physical relation between the polar rays of the corona and chromospheric spicules is also communicated in [45 - 47]. Good agreement between chromospheric spicules and polar rays, both in inclinations and in the position of segments of high density, was found in [47].

The formation of prominences from coronal material by its condensation has been considered and substantiated for a long time [48]. It is possible that chromospheric spicules, localized at the boundary between the chromosphere and corona, the same as prominences, are formed from coronal material, which was first indicated by V. A. Krat and T. V. Krat [28].

"As is well known, the corona can radiate energy only as the result of free-free and free-bound transitions of protons and free electrons. The first of these processes are more frequent than the second. The source function for continuous radiation of coronal material increases proportionally to the square of the density, and also increases with decreasing temperature. If any segment in the lower part of the corona has a low temperature or high density, it will cool and increase its density only under the condition that heat can be radiated. Heat transfer from the corona into the chromosphere is noted in the theoretical model of Wooley and Allen

[49]. The heat flux transmitted downward in CGS units is:

$$\varepsilon = \eta T^{5/2} \frac{dT}{dh},$$

where $\eta = 0.5 \times 10^{-6}$, according to [49], or $\eta = 2.0 \times 10^{-6}$, according to [50]. /85
In accordance with Wooley and Allen [49], the heat flux is $\varepsilon = 1.7 \times 10^4$ erg/cm^2/sec at the assumed upper boundary of the chromosphere h = 46,000 km, $\varepsilon = 0.85 \times 10^4$ erg/cm^2/sec at an altitude of h = 13,000 km, and ε = 0 at an altitude of h = 6000 km. The variation of ε with altitude occurs because of radiation. Giovanelli [50] found that $\varepsilon = 60 \times 10^4$ erg/cm^2/sec." [7]. Such a large value of ε, i.e., such a high yield is not compensated by radiation; part of the energy must be transferred further downward into the chromosphere by some mechanism. According to Van de Hulst [7], heat from the corona is transmitted downward by free electrons.

We established [51] that values of the parameter $\frac{\Delta\lambda_D}{\lambda} 4000\,\text{Å}$ vary with a change in distance from the edge of the photosphere somewhat differently for the different lines. The variation is very large in the hydrogen lines, the value of $\frac{\Delta\lambda_D}{\lambda} 4000\,\text{Å}$ increases with distance from the edge, particularly rapidly, beginning with altitudes of $\sim$ 3500 km. In the H and K Ca II lines, this parameter first decreases with altitude up to 3000 km, and then gradually increases. But the increase in Ca II is less than in hydrogen. For the helium D_3 lines close to the photosphere, $\frac{\Delta\lambda_D}{\lambda} \cdot 4000\,\text{Å}$ has relatively larger values than at other altitudes. At an altitude $\sim$ 2500 km, they drop to a minimum. However, at an altitude the order of 3600 km, their rise again begins to show.

Thus, judging from our investigations [51], the Doppler line widths clearly increase beginning with altitudes of 3000 - 3500 km above the photosphere. We take this level as the interface between the upper and lower chromosphere. We also assume this same interface

in [52], in which the optical thicknesses in the H and K lines were studied, and it was shown that the upper layer of the calcium chromosphere, responsible for the appearance of the components H_3 and K_3, scatter radiation of the lower-lying chromosphere and photosphere, i.e., it plays the role of a monochromatic "reversing" layer.

We assume that spicules observed above and below this interface have a different origin. Spicules visible in the upper chromosphere (i.e., the serrated structure of the chromosphere) is, in our opinion, none other than the condensed coronal material, and this material flows downward into the chromosphere. An analogy with the formation and motion of several types of prominences is observed here, only the process occurs on a small scale, smaller than in prominences. The descending material rapidly cools to 6000 - 7000° because of radiation. The cooling process itself is limited by a small scale time of $\approx$ 2 minutes (the time of ascent and descent of spicules) and by the length of spicules; they are small with respect to prominences.

A spicule descends to the level of 3000 - 4000 above the photosphere. But it is possible that some individual spicules descend to lower altitudes and even to the edge of the photosphere. The observed velocities of spicule ascent are also the velocities of the condensation process of coronal material (the formation of spicules).

We assume that the increase of density and decrease of temperatureture in the lower corona must probably occurs because of the presence of weak magnetic fields with intensity $\geq$ 1 G in the external shells of the Sun, since the shape and inclination of spicules and coronal rays assume the presence of magnetic field lines. The condensed coronal material quickly discharges along field lines downward, where the recombination emission of hydrogen begins. This process begins at the lower end of a jet (spicule), and then propagates upward. Such an altitude distribution of the radiation front (visibility) is perceived as the ascent of a spicule. This fictitious ascent process, from the determination of Dizer [53], lasts all of two minutes, and the velocity of "ascent" is $\approx$ 20 km/sec, on the average. /86

As we know from observations, the space between spicules is filled mainly by coronal material. The processes described above can also occur in these regions. The temperature is rather great in the region of the chromosphere, consisting of "coronal" spicules (upper chromosphere). The emission lines have small optical thicknesses. The profiles of the observed lines have a single peak.

However, we cannot be certain that the chromosphere consists completely of condensed coronal material. It can be supplemented with photospheric material and, in turn, transmit part of this material to the corona. Without such an exchange, it is impossible to explain the existence of the corona itself, since its losses are not compensated by the mechanism of accretion of interstellar gas [7]. We assume that part of the spicules ascend from the photosphere. These spicules ("photospheric") are colder than the "coronal", their temperature is $\approx$ 6000°. In ascending up to altitudes of 3000 - 4000 km, the "photospheric" spicules (it is possible that there are higher and lower among them) mix with the "coronal" spicules somewhere at an altitude of 3000 - 4000 km. Finally, there are cases of the penetration of the "photospheric" spicules into the region of "coronal" and, conversely, "coronal" into the region of "photospheric" (cf. diagram).

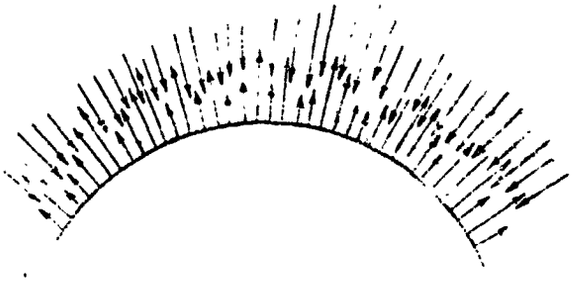

The velocity field in H α, obtained by the method of Leighton [54], can serve as a verification of the existence of "photospheric" and "coronal" spicules. This method permits the recognition of fine structural components with motions of descent and ascent, which can be explained as "coronal" and "photospheric" spicules, respectively.

If the magnetic field intensity is weak, then the condensation of coronal material is limited by the region surrounding it; when the material is condensed at a relatively close distance, the process stops for awhile, and the descent of material ends. However, after a lapse of some time, the coronal ions and electrons fall into a free region and the process of condensation begins once again /87 (a dark space must be formed about spicules because of condensation, which is similar to the dark shells which surround prominences in coronal lines).

The duration of the condensation and descent of material of spicules is defined as the lifetime of the spicules, which ranges from 2 to 5 minutes [53, 55, 56]. Since the chromosphere is at least partially condensed and cooled corona, then it must vary with heliographic latitude. This is well noted by the values of the gradient of chromospheric lines β [57] and the parameter $\frac{\Delta\lambda_D}{\lambda}$ 4000 Å [51]. It is possible that during the maximum of solar activity, the course of these parameters depending on heliographic latitude will be different than during the activity minimum [51, 57].

References

1. Perepelkin, Ye. Ya. Bull. Komissiya po issledovaniyu Solntsa (Bull. KISO), Vol. 4, 1933, p. 1.
2. Menzel, D. Publ. Lick. Obs., Vol. 17, 1931, p. 1.
3. Severnyy, A. B. Astron. zh., Vol. 31, No. 2, 1954, p. 131.
4. Morozhenko, N. N. In the collection: "Spektrofotometricheskiye issledovaniya aktivnykh obraxovaniy Solntsa" (Spectrophotometric Investigations of Active Formations of the Sun). Kiev, "Naukova dumka" Press, 1964.
5. Giovanelli, R. B. Australian Journ. Sci., Vol. 1, 1948, pp. 275, 305, 360.
6. Jeffreis, J. and R. G. Giovanelli. Australian J. Phys., Vol. 7, 1954, p. 574.

7. Van de Hulst, H. C. In the collection: "Solntse" (The Sun). Edited by D. P. Kuiper. Moscow, Foreign Literature Press 1955.

8. Pagel, B. E. J. Astrophys. J., Vol. 125, 1957, p. 298.

9. Pecker, J. C. C.R., Vol. 245, 1957, p. 639.

10. Miyamoto, S. Astrophys. J., Vol. 105, 1947, p. 1.

11. Miyamoto, S. Mem. College Sci., Kyoto Univ., Vol. 25, 1947, p. 31.

12. Kononovich, E. V. Model' solnechnoy khromosfery po materialam vnezatmennykh nablyudeniy (Model of the Solar Chromosphere from Data of Non-Eclipse Observations). Auth. abst. Doct. diss., Moscow, 1958.

13. Thomas, R. and R. Athay. Fizika solnechnoy khromosfery (Physics of the Solar Chromosphere). Moscow, Foreign Literature Press, 1965.

14. Huang, S. S. Astrophys. J., Vol. 108, 1948, p. 354.

15. Hoyle, T. Recent Researches in Solar Physics. London, Cambridge University Press, 1949.

16. Hagen, J. P. J. Geophys Research., Vol. 59, 1954, p. 158.

17. Woltjer, L. Bull. Astron. Inst. Netherlands, Vol. 12, 1954, p. 165.

18. Athay, R. G. and D. Menzel. Astrophys. J., Vol. 123, No. 2, 1956, p. 285.

19. Thomas, R. N. and R. G. Athay. I.A.U. Symposium No. 4, Radio Astronomy, Ed. H. C. Van de Hulst. Cambridge Univ. Press, 1956.

20. Thomas, R. N., R. W. Noyes and J. M. Pasachoff. New Observations of Solar Chromospheric Spicules. Paper given at the 120th meeting of the AAS, Berkeley, California, December 28, 1965.

21. Athay, R. G. and W. O. Roberts. Astrophys. J., Vol. 121, 1955, p. 231.

22. Zirin, H. NCAR Quart, No. 4, 1963, p. 24.

23. Smith, E. P. Astrophys. J., Vol. 126, 1957, p. 529.

24. Giovanelli, R. G., R Michard and Z. Mouradian. Ann. Astroph., Vol. 28, No. 5, 1965, p. 871.

25. Athay, R. G. Ann. Astroph., Vol. 21, No. 2, 1968, p. 98.

26. Livshits, M. A. Astronomiya, 1967. Fizika Solntsa, VINITI (Astronomy, 1967. Solar Physics, All-Union Institute of Scientific and Technical Information). Moscow, 1970.

27. Nikol'siky, G. M. and A. A. Sazanov. Atron. zh., Vol. 43, No. 5, 1966, p. 928.

28. Krat, V. A. and T. V. Krat. Izv. GAO, Vol. 167, 1961, p. 6.

29. Krat, V. A. Solar Physics, Vol. 1, No. 2, 1967, p. 191.

30. Krat, V. A., T. V. Krat and L. M. Pravdyuk. Izv. GAO, Vol. 156, 1956, p. 60.

31. Krat, V. A. DAN SSSR, Vol. 106, No. 4, 1956.

32. Krat, V. A. and V. M. Sobolev. Maryzalar Azerb. SSR Elmlar Akad., DAN Azerb. SSR (Doklady AN AzSSR), Vol. 12, No. 9, 1956, p. 617.

33. Zirin, H. Solnechnaya atmosfera (The Solar Atmosphere). Moscow, "Mir" Press, 1969.

34. D'Azambuja, M. Ann. Obs. Meudon, Vol. 8, Fasc. 11, 1930, p. 281.

35. Reichel, M. Zs. Astroph., Vol. 33, 1953, p. 79.

36. Bhavilai, Rowi. M.N., Vol. 130, No. 5-6, 1965, p. 411.

37. Leighton, R. B. Introduct. vept., Stellar and Solar Magnet. Fields. Amsterdam, 1965, p. 158.

38. Stepanov, V. Ye. Izv. Krymskoy astrofiz. observ., Vol. 11, 1954, p. 102. /88

39. Jager, C de. Bull. Astron. Inst. Netherl., Vol. 13, No. 476, 1957, p. 133.

40. Dubov, E. Ye. Izv. Krymskoy astrofiz. observ., Vol. 24, 1960, p. 301.

41. Dubov, E. Ye. Astron. zh., Vol. 44, No. 2, 1967, p. 342.

42. Dubov, E. Ye. Izv. Krymskoy astrofiz. observ., Vol. 22, 1960, p. 101.

43. Athay, R. G., J. C. Pecker, R. N. Thomas and D. H. Menzel. Astron. J., Vol. 59, No. 9, 1954, p. 314.

44. Vsekhsvyatskiy, S. K. and Ye. Ya. Bugoslavskaya. Trudy ekspeditsii po nablyudeniyu solnechnovo zatmeniya 21.IX.1941 g. (Works of the Expedition for the Observation of the Solar Eclipse of September 21, 1941). Moscow - Leningrad, AN SSSR Press, 1949, p. 266.

45. Zel'tser, M. S. and A. V. Markov. Trudy ekspeditsii po nablyudeniyu solnechnovo zatmeniya 21.IX.1941 g. (Works of the Expedition for the Observation of the Solar Eclipse of September 21, 1941). Moscow - Leningrad, AN SSSR Press, 1949, p. 154.

46. Roberts, W. O. Astrophys. J., Vol. 101, No. 2, 1945, p. 136.

47. Bugoslavskaya, Ye. Ya., M. S. Zel'tser and A. V. Markov. Trudy ekspeditsii po nablyudeniyu solnechnovo zatmeniya 21.IX.1941 g. (Works of the Expedition for the Observation of the Solar Eclipse of September 21, 1941). Moscow - Leningrad, AN SSSR Press, 1949.

48. Kiepenheuer, K. O. In the collection: "Solntse" (The Sun). Edited by D. P. Kuiper. Moscow, Foreign Literature Press, 1957, p. 283.

49. Wolley, R. v. d. and C. W. Allen. M.N., Vol. 110, 1950, p. 358.

50. Giovanelli, R. G. M.N., Vol. 109, 1949, p. 372.

51. Sadikov, A. Bul. Solnechnyye dannyye, No. 11, 1970, p. 100.

52. Sadikov, A. Tsirkulyar Astronomicheskovo instituta AN UzSSR, No. 28, 1971.

53. Dizer, M. C.R., Vol. 235, 1952, p. 1016.

54. Leighton, R. H. Astroph. J., Vol. 130, No. 2, 1959, p. 366.

55. Rush, J. H. and W. O. Roberts. Austral. Journ. Phys., Vol. 1, 1954, p. 230.

56. Lippinicott, S. L. Smithsonian Contributions to Astrophys., 1957, p. ..

57. Sadikov, A. Bull. Solnechnyye dannyye, No. 12, 1970, p. 102.

LASER TESTING OF THE ASP-20 SPECTROGRAPH

I. Sattarov

ABSTRACT. The results of a detailed investigation of the spectrograph ASP-20, installed on the horizontal solar telescope of the Astronomical Institute of the AN UzSSR, are presented. The quality of the instrument slit was analyzed with the diffraction method, its taper was eliminated and the method of its control is described. The diffraction grating is investigated, its practical resolving power is determined by two methods, the ghosts of the grating and line satellites were studied in three orders of the spectrum. The instrumental profile of the spectrograph was obtained; its parameters were determined by Voigt's method. The methods for converting from the observed line profiles to the true profiles are described. It is established that the spectrograph has a sufficiently high resolving power, and can be successfully applied to the study of Frauenhofer line profiles.

The quality of an instrument and its correct operation in experiment are the determining factors of the level of scientific research work. Without knowing the practical potentialities of an instrument, we cannot plan work on it. Thus, the laboratory testing of an instrument has an important value for its further application. /89

Soviet optics has achieved great successes in fabricating reflection diffraction gratings. The diffraction spectrographs APS-20, which are widely used for solar investigations, have been produced. Such a spectrograph has been installed on the horizontal solar telescope ATsU-5 of the Astronomical Institute of the AN UzSSR. An account of the results of testing this spectrograph is given.

Analysis of the slits. Since the spectrum is a set of monochromatic images of the slit, then any irregularity of its form leads to distortions in the spectrum. Irregularities of the edges affect the slit width, and their relative inclination specifies its taper. Thus, part of the spectrum where the slit is wider will be brighter than the neighboring part. The slit must be bounded by two rigorously straight edges, parallel to a high degree of accuracy and free of notches. The jaws of the slit must be movable, in order that it can be opened and closed in a measurable fashion without disturbing the parallelism of the edges. One should establish for observations the optimum slit width which, first, would provide the necessary amount of light, and, second, would permit obtaining sufficiently narrow spectral lines.

Thus, the slit of the spectrograph is an extremely important and delicate element, and its analysis is of definite interest.

The slit of the ASP-20 spectrograph of the ATsU-5 horizontal solar telescope had a significant taper when it was delivered from the supplier. But the edges of the slit jaws were straight, without defects or notches. To eliminate the slit taper, we had to remove the jaws. The slit itself was placed in the field of view of the measuring instrument UIM-23. By releasing the set screws and slightly opening the slit, we exposed the jaws so that the gap between them on the screen of the measuring device was the same at all heights of the slit. The optics of the UIM-23 measuring instrument permit projecting the image of a part onto a frosted screen with $30^{\times}$ magnification. This magnification is sufficient to detect taper

$\approx$ 3%. The analysis showed that the instrument was not able to reveal any deviation from coplanarity of the jaw edges at all heights of the slit. After the jaw set screts were fastened, we had to /90 determine the scale value of the drum controlling the slit opening, to establish the zero point of this scale and to construct the dependence between the scale readings of the drum, on the one hand, and the actual slit width, on the other. To solve these problems, we used the diffraction method [1], which is based on observing the diffraction pattern from the slit being investigated.

If the slit is illuminated by a parallel beam of light, then we will see a diffraction pattern on a screen placed parallel to the wave front at a sufficiently great distance from the slit. The phase difference for rays traveling from the two jaws of the slit is expressed by the formula:

$$\varphi = \frac{\pi}{\lambda} d \sin \alpha,$$

where λ is the wavelength of the light incident on the slit; d is the slit width; α is the angle between the normal to the incident wave front and the direction of the beams traveling to a given point N on the diffraction pattern. The amplitude of the diffracted wave A_N at point N is expressed in terms of the amplitude at the center of the zeroth maximum A_0 by the formula:

$$A_N = A_0 \frac{\sin \varphi}{\varphi}.$$

Obviously, the brightness minima of the diffracted image of the slit on the screen will correspond to the following values of ϕ:

$$\varphi_1^m = \pi, \quad \varphi_2^m = 2\pi, \quad \varphi_3^m = 3\pi \ldots\ldots$$

and the maxima: $\varphi_0^M = 0; \quad \varphi_1^M = 1.43\pi; \quad \varphi_2^M = 2.46\pi \ldots\ldots$

By knowing the distance between the slit and the film on which the diffraction pattern is photographed, and by measuring the distance between the corresponding maxima and minima of the image brightness, one can determine the value of the angle α. Then it is easy to

calculate the slit width from the formula:

$$a = \frac{\lambda\varphi}{\pi \sin \alpha}$$

The apparatus for photographing the diffraction pattern from the slit was assembled on an optical bench (Figure 1). The ribbon-filament lamp 1 was the light source, the light beam from which was focused with the lens L_1 onto the diaphragm D with an aperture diameter $\approx$ 0.5 mm. The lens L_2 was mounted so that its focal plane coincided with the position of the diaphragm D.

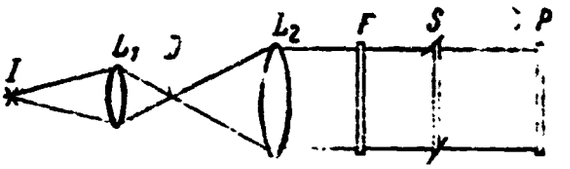

Figure 1. Optical diagram of installation for photographing the diffraction pattern from the spectrograph slit

Thus, the beam traveling from the diaphragm D exits parallel from the lens L_2. The slit S to be analyzed was placed in the parallel beam. A red filter was mounted in front of the slit. Panchromatic film was used. The jaws of the slit and the film plate P were mounted rigorously perpendicular to the optical axis of the whole system. We achieved this by superimposing the reflected image onto the object.

The diffraction pattern from the slit was photographed for various slit widths. The slit width readings were taken from the drum scale.

As the photographs of the diffraction pattern of the slit (Figure 2) indicate, the jaws do not have noticeable defects. The photographs also indicate that after adjustment, the slit did not have a noticeable taper.

The distance between the brightness maxima of the diffraction pattern were measured directly from the photographs on the UIM-23. They were also determined from recordings of these photographs, obtained on the microphotometer MF-4, with an automatic recorder. To verify the absence of taper, the measurements were carried out in three different sections of the diffraction pattern: at the upper, middle, and lower parts. /91

The measured widths d of the upper, middle, and lower parts of the entrance slit, depending on the reading n of the drum scale, are presented in Table 1. The dependence between the slit width, on the

one hand, and the readings of the drum scale, on the other, is almost linear. The scale value of the drum scale is 0.001 mm. The actual zero point is located close to the zero reading. After the reading 30, the slit width changes abruptly; its further opening occur more rapidly than is required by the linear dependence between d and n, obtained for the readings from 0 to 30.

Figure 2. Diffraction pattern from entrance slit of spectrograph for a width of 0.04 mm

TABLE 1

Reading of slit head scale	Slit width a, mm		
	Upper part	Middle part	Lower part
10	0.0105 ± 9*	0.0107 ± 5	0.0108 ± 9
20	0.0202 ± 4	0.0202 ± 4	0.0206 ± 6
30	0.0302 ± 5	0.030 ± 3	0.031 ± 1
40	0.0412 ± 1	0.0412 ± 1	0.042 ± 2
50	0.0513 ± 2	0.0514 ± 4	0.0519 ± 8
60	0.0616 ± 4	0.0618 ± 2	0.0624 ± 3
50	0.0718 ± 3	0.0717 ± 4	0.0724 ± 4

*Here and below — the mean square error of measurement.

As is indicated in Table 1, the lower part of the slit is approximately 0.0007 mm wider than its middle and upper parts. It is seen from the photographs of the diffraction pattern that the slight taper occurs only in the lower part of the slit up to a distance of 15 mm from the lower edge. If one takes into account that the total height of the slit is 50 mm, the remaining 35 mm is quite sufficient for performing spectral observations. We note that the detected taper of the lower part of the slit is less than 5% of its width, which is quite acceptable for a majority of problems. An exit slit, which can be added to the ASP-20 spectrograph and permits its use as a mono-

chromator, was investigated in an analogous manner. We will not present the results of these investigations here; we note only that after adjustment the slit was found to be quite suitable for operation.

Determination of resolving power. The practical resolving power of the spectrograph is one of the basic indices of the quality of the instrument. According to the Rayleigh criterion, it is defined as the ratio of the smallest distance ($\Delta\lambda$) between two spectral lines, which are still seen separately, to the average wavelength of these lines $R_p = \frac{\lambda}{\Delta\lambda}$. /92

The theoretical resolving power for diffraction spectrographs is given as the product of the number of the spectral order m and the total number of lines of the grating N: $R_T = mN$. But R_T is not always attainable. The practical resolving power depends on the shape of the intensity curves of the diffraction bands, the relative intensity of the diffraction maxima, the emulsion grain in photographic observation, the sensitivity of the light sensor and defects of the optical system. To achieve the maximum resolving power, the following factors are also significant: the entrance slit must be very narrow, the aperture of the dispersing element must be filled with radiation in the plane perpendicular to the slit. Finally, the intensity, actual shape of the profile, and the half-width of the spectral lines used for determining the resolving power are important. One value of R_p can be obtained from weak lines, and another from intense lines [2]. It is difficult to find double spectral lines of the same intensity. A special device with a birefringent prism is usually used to determine R_p. But we solved this problem by another method.

In the spectrum of a mercury discharge tube, which was a part of a set of comparison sources, we separated out molecular systems consisting of doublets of equal intensity. There appeared among them two series in which the distance between the components of the doublet varied with distance from the head of the series. The first series begins with λ=4300 Å, and consists of seven gradually weakening doublets, located on the short-wavelength side of the spectrum. It was found that each component of the doublet, in turn, consists of two lines. The distance between these lines also varies from one doublet to the next; more precisely, it decreases toward the beginning of the series. When we observe in the first order of the

grating, we resolve into two lines only the components of the remote doublets of the series, beginning with the fourth. In going to higher orders of the grating, we successively resolve into lines the components of the third, second, and, finally, the first doublets of the series.

The first line in the second analyzed series has $\lambda = 4314.2$ Å. The remaining components of the series are located on the violet side. We also have doublets here, the distance between which varies from doublet to doublet.

Other gases are probably present in the mercury tube. The presense of hydrogen, in any case, is certain, since the lines of the Balmer series are observed. The molecular series being recorded evidently belongs to the compounds HgH, CH, etc. /93

The cptical bench of the comparison source served as the supply optics of the spectrograph when the mercury discharge tube was used. It is represented schematically in the upper part of Figure 3. Here, L is the light source; O_1, O_2 are lenses; M_1, M_2 are plane mirrors; O_3 is a cylindrical lens. The optical bench projects an image of the comparison source with 85× magnification onto the spectrograph slit, and thereby permits filling the aperture of the diffraction grating with light. The spectrograph slit S and diffraction grating G are shown in the diagram. The concave mirror O serves both as a collimator and as the camera objective. The beam path in the spectrograph is reproduced in the lower part of Figure 3 (side view); the same designations are maintained, P corresponds to a cassette with a photographic plate or film.

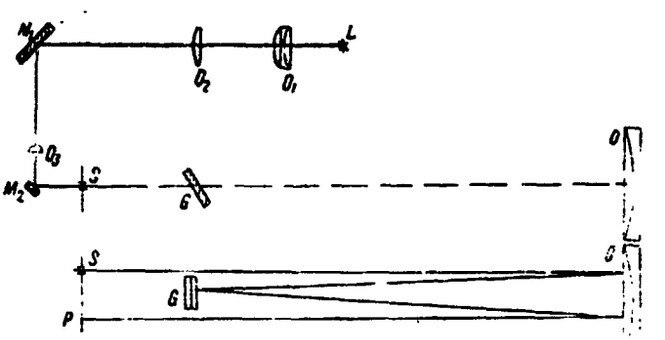

Figure 3. Optical diagram of ASP-20 spectrograph with the comparison source bench

The observations were carried out photographically. The photographic plates WP-1 of the firm ORWO were used. The exposure time was 1 - 10 minutes. The developer A-44 was used; the developing time was 7 minutes at a temperature of + 20° C. Very fine-grained negatives were thus obtained.

The limiting distance of $\Delta\lambda$ for still resolvable doublets of these series was measured on the UIM-23; $\Delta\lambda$ were also determined from recordings obtained on the MF-4 microphotometer with an automatic recorder. $R_p = \frac{\lambda}{\Delta\lambda}$, characterizing the practical resolving power of the spectrograph, were calculated from the measured $\Delta\lambda$. The results of these calculations (method I) are presented in Table 2, the ratio of the practical resolving power R_p and the theoretical R_T, expressed in percent, is shown in the fourth column. As is seen from Table 2, the practical resolving power is close to the theoretical in the first and second orders of the grating. In the third order, R_p is 2/3 of R_T. Several authors [6, 7] determine R_p from the width of the instrumental profile at the 0.41 intensity level. Using this method based on the instrumental profile, we arrive at the results presented in the right part of Table 2 (method II). Both methods give similar values of R_p for the first and second order of the grating; for the third order, the estimate of R_p by method II is somewhat greater.

TABLE 2

Order of Spectrum	Method I			Method II	
	R_T	R_{p_I}	$R_p/R_T \cdot 100$	R'_p	$R'_p/R_T \cdot 100$
1	90000	80000 ±2000*	90±2%	80000 ±1000	90±1%
2	180000	140000 ±10000	78±6%	136000 ±5000	76±4%
3	270000	175000 ±15000	64±6%	230000 ±10000	85±1%

*Here and below — measurement error.

Instrumental profile of the spectrograph. The observed profile /94
of spectral lines is a result of the superposition of two profiles: the true line profile and the instrumental profile of the spectrograph. If the instrumental profile is wider than the true line profile, then the observed profile would have the shape of the instrumental. Conversely, if the line is wider, its observed profile will be close to the true in shape.

We denote by S (x) the observed, and by W (x) the true distributions of intensity within a given line, and by A (x) — the instrumental profile, i.e., the curve of the intensity distribution obtained as the result of distortion of an ideal monochromatic line by the spectrograph optics. The relation between these three functions is represented mathematically in the form:

$$S(x) = \int_{-\infty}^{+\infty} W(\xi) A(x-\xi) d\xi.$$

Here, the coordinates x and ξ are measured from the center of the line in the direction of the dispersion or along the spectrum. In order to calculate the true profile of a spectral line W (x) from the observed S (x) with this formula, it is necessary to know the instrumental profile of the given spectrograph A (x). To determine it, the entrance slit of the spectrograph is illuminated by a light source, deliberately having narrow spectral lines in its spectrum. The observed profile of such lines is taken as the instrumental profile. Gas discharge tubes at low pressure with heavy elements (mercury, krypton, or xenon) are usually used for determining the instrumental profile. There are lines with a half-width of ≈ 7—10 mÅ in the spectra of these elements. Ordinary spectrographs have an instrumental profile with a half-width of the same order or wider. However, for better spectrographs, the instrumental profile is narrower than 5 mÅ. Moreover, the radiation power of a gas discharge tube in one emission line does not exceed several tens of microwatts, which is insufficient to record the profile wings which extend several Ångstroms from the line center.

The application of gas lasers to study the instrumental profile has a number of advantages from the point of view of the monochromaticity of the radiation, and also in the sense of the light source power [3]. The radiation of these coherent light sources is concentrated in a few narrow lines, and is characterized by a power from several milliwatts to several tens of milliwatts. The line half-width of a laser in the visible region of the spectrum is the order /95
of 1 mÅ and can be reduced a million times with the use of a single-stage operation. In spite of these obvious advantages, lasers also have a number of disadvantages [4]. First, the laser beam is a thin, approximately parallel beam; second, the distribution of light intensity is not uniform in the cross section of the beam. Here, one requires an optical system providing the condition for complete illumination of the diffraction grating by the laser beam.

To investigate the instrumental profile of the ASP-20 spectrograph, we used the helium-neon gas laser LG-75. It emits radiation with a power of 25 mW in one spectral line with a wavelength λ 6328 Å. The optical bench of the comparison sources (cf. Figure 3) served as the supply system, directing the laser radiation onto the spectrograph slit. In this case, a milk glass diffuser replaced the source L, and the laser beam entered the optical system through it. The optical bench of the comparison source provided complete illumination of the ruled portion of the diffraction grating. We controlled this visually by placing our eye in the focal plane of the camera mirror at the point where the image of the laser emission line was produced. The optical system of the comparison bench, when all the lenses were mounted correctly, does not shift the focal planes of the collimator-camera mirror. We verified this by photographing the spectral line of the laser for different positions of the collimator-camera mirror.

The panchromatic photographic plates WP-1 of the firm ORWO were used for the investigations. The exposure was varied from 0.2 seconds to 5 minutes. The plates were processed in the A-44 developer. The developing time was 5 - 7 minutes at a temperature of + 20° C. The laser line was taken in the first, second, and third orders of

the diffraction grating for different (from 0.01 to 0.07 mm) widths of the entrance slit of the spectrograph. The normal slit width in the spectral region of λ=6300 Å equals 0.035 mm.

The optical system of the comparison source bench permits photographing the spectra of the Sun and laser simultaneously. Three spectra are obtained simultaneously on the photograph; the middle spectrum belongs to the Sun, and the two side spectra belong to the laser. The spectrograms indicate that sharp spectral lines of the laser are obtained for normal exposure of the solar spectrum. Thus, the conditions for observing the laser are close to the conditions for observing the Sun. In order to investigate the wings of the instrumental profile, we overexposed the laser photographs. The solar spectrum was not taken then.

It is seen from the spectrograms taken with a normal exposure time that the laser line is rather thin, and is composed in height of individual elements resembling beads. The cross section of the laser beam has a granular structure. The beam consists of individual rays. This disadvantage of laser light (which has already been indicated in [3, 4]) is not completely eliminated even with milk glass placed in the beam path. However, it does not depreciate the value of the laser for investigating the instrumental profile and its advantages over gas discharge tubes [3].

Calibration photographs of a ten-stage attenuator were obtained with sunlight on the same photograph on which the laser line was taken.

The obtained material was processed on the MF-2 and MF-4 microphotometers. The latter, as was already indicated, is significantly modified (the photocell is replaced by a photomultiplier, an electronic potentiometer EPP-60M is introduced in the circuit), which /96
permits one to obtain recordings with a large scale. The profile of the spectral line of the laser, assumed as the instrumental profile of the spectrograph, was constructed as the result of the

corresponding measurements and calculations. This profile is presented in Figures 4 - 6 for the different orders of the diffraction grating. The instrumental profile of the spectrograph, obtained in the first order of the grating for an entrance slit width of 0.03 mm, is represented in Figure 4. The central portion of the profile is symmetric. The half-width, i.e., the width of the profile at the relative intensity level of 0.5, h = 90 mÅ. Several side satellites, arranged symmetrically, are traced below the level of intensity of 0.23.

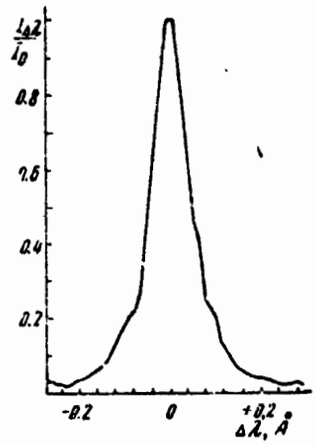

Figure 4. Instrumental profile in first order of diffraction grating

The instrumental profile of the spectrograph, obtained in the second order of the diffraction gratings, is reproduced in Figure 5. Only the central portion of the profile is presented in Figure 5a. The intensities, expressed in units of the central intensity

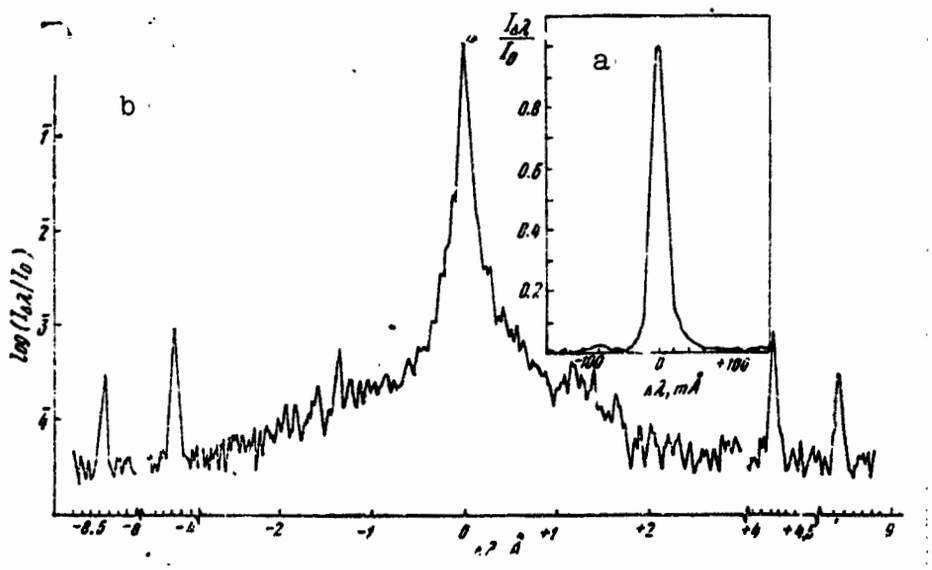

Figure 5. Instrumental profile in second order of grating:

a — nucleus of profile; b — nucleus of profile with remote wings and Rowland ghosts

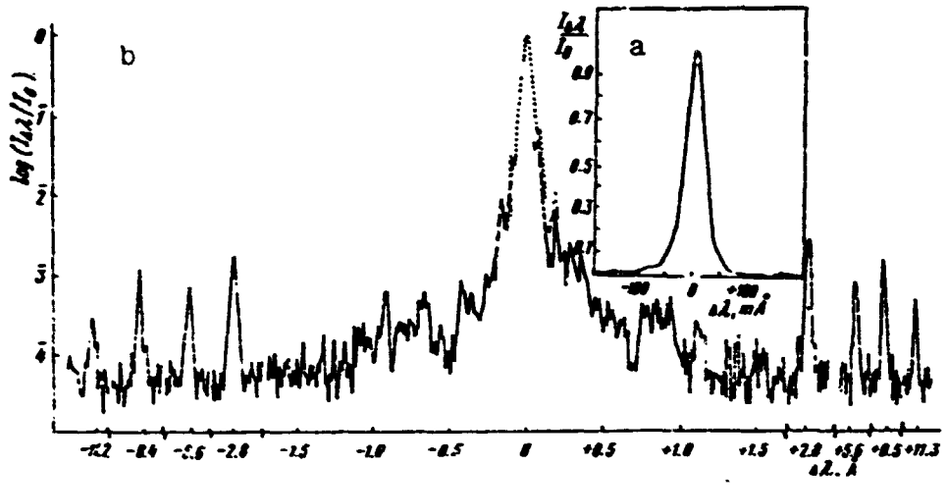

Figure 6. Instrumental profile in third order of grating:

a — nucleus of profile; b — nucleus of profile with remote wings and Rowland ghosts

of the profile, are plotted along the ordinate, the distance from the line center along the abscissa. As is seen, the nucleus of the profile is symmetric, the violet wing is slightly (≈0.005) higher than the red. There is a satellite with intensity ≈90 mÅ at a distance ≈0.03 from the center of the profile. The half-width of the profile equals 40 mÅ.

The complete profile with extended wings and Rowland ghosts of the first and second order is presented in Figure 5b. Here the logarithm of the relative intensity is plotted along the ordinate. The /97
wings stretch to 2 Å from the center of the profile, and consist of a large number of satellites. It is seen from Table 3, where the distance from the center of the profile to each satellite and the logarithm of its relative intensity are presented, that each satellite in the violet wing corresponds to a satellite in the red wing, except for four cases. These pairs of satellites in the two wings of the profile have approximately the same intensities.

Adjacent satellites are spaced at approximately equal distances, at 90 mÅ, on the average. As was noted, the visible satellite closest to the nucleus of the profile also appears at a distance

≈90 mÅ (from the center of the profile). Consequently, we are justified in concluding that the nucleus does not have satellites up to a distance of ±80 mÅ from the center. It is a symmetric profile and is a single central maximum of intensity of monochromatic radiation.

Rowland ghosts of first and second order, which are located at distances of ≈ ±4.2 Å and ≈ ±8.4 Å from the center of the line, respectively, are also traced in Figure 5b. The intensity of the ghosts decreases generally with increasing order. The violet ghosts are somewhat more intense than the red. The data on the Rowland ghosts are presented in Table 4.

The nucleus of the instrumental profile, obtained in the third order of the diffraction grating (Figure 6a) is symmetric; its half-width is h=23 mÅ. Here, the red wing is slightly higher than the violet. There is an appreciable satellite with an intensity 0.03 on the violet side at a distance of 85 mÅ from the center of the nucleus of the profile. This is evidently the same satellite which is seen in Figure 5a.

TABLE 3

Violet wing		Red wing	
$\Delta\lambda$, Å	$\log(I_{\Delta\lambda}/I_0)$	$\Delta\lambda$, Å	$\log(I_{\Delta\lambda}/I_0)$
0.12	$\bar{2}.36$	--	—
0.20	$\bar{3}.82$	—	—
0.25	$\bar{3}.75$	0.26	$\bar{3}.60$
0.34	$\bar{3}.05$	0.36	$\bar{3}.08$
0.44	$\bar{4}.77$	0.43	$\bar{4}.77$
0.50	$\bar{4}.76$	0.51	$\bar{4}.95$
—	—	0.57	$\bar{3}.00$
0.61	$\bar{4}.65$	0.64	$\bar{3}.85$
0.78	$\bar{4}.40$	0.75	$\bar{4}.64$
0.87	$\bar{4}.47$	0.88	$\bar{4}.50$
0.99	$\bar{4}.40$	—	—
1.06	$\bar{4}.42$	1.06	$\bar{4}.45$
1.14	$\bar{4}.40$	1.19	$\bar{4}.60$
1.25	$\bar{4}.42$	1.28	$\bar{4}.47$
1.37	$\bar{4}.74$	1.41	$\bar{4}.55$
1.63	$\bar{4}.36$	1.64	$\bar{4}.30$

The entire instrumental profile for the third order of the grating, with its extended wings and Rowland ghosts from first to fourth order, is reproduced in Figure 6b. Here we have constructed the central parts and the remote wings by using negatives differing greatly in density. They were joined to each other with the help of the violet satellite closest to the nucleus, which was found on the negatives differing in density within the limits of the characteristic curve. As is seen in /98

TABLE 4

Order of ghosts		Grating order II		Grating order III	
		Δλ, Å	log ($I_{\Delta\lambda}/I_0$)	Δλ, Å	log ($I_{\Delta\lambda}/I_0$)
I	red	+1.25	$\bar{4}$.93	+ 2.84	$\bar{3}$.42
	violet	−1.18	$\bar{3}$.01	− 2.62	$\bar{3}$.25
II	red	+8.45	$\bar{4}$.49	+ 5.64	$\bar{4}$.86
	violet	−8.35	$\bar{4}$.52	− 5.62	$\bar{4}$.82
III	red	−	−	+ 8.47	$\bar{3}$.19
	violet	−	−	− 8.44	$\bar{3}$.09
IV	red	−	−	+11.27	$\bar{4}$.63
	violet	−	−	−11.25	$\bar{4}$.46

Figure 6b, the wings consist of a large number of satellites. The satellites are arranged symmetrically in both wings, i.e., a paired satellite in the red wing corresponds to each satellite in the violet wing at the same distance from the center of the profile. Data about the most intense satellites of the instrumental profile in the third order of the grating are presented in Table 5.

TABLE 5

Violet wing		Red wing	
Δλ, Å	log ($I_{\Delta\lambda}/I_0$)	Δλ, Å	log ($I_{\Delta\lambda}/I_0$)
0.10	$\bar{2}$.50	0.08	$\bar{2}$.70
0.17	$\bar{3}$.90	0.18	$\bar{3}$.85
0.27	$\bar{3}$.00	0.28	$\bar{3}$.40
0.36	$\bar{4}$.80	0.35	$\bar{3}$.20
0.48	$\bar{4}$.90	0.46	$\bar{4}$.70
0.57	$\bar{4}$.35	0.54	$\bar{4}$.35
0.68	$\bar{4}$.80	0.63	$\bar{4}$.40
0.93	$\bar{4}$.80	0.94	$\bar{4}$.70
1.11	$\bar{4}$.40	1.11	$\bar{4}$.40
1.34	$\bar{4}$.25	1.32	$\bar{4}$.20
1.46	$\bar{4}$.18	1.37	$\bar{4}$.20

The distance between adjacent satellites is 0.09 Å, on the average. It should be noted that the relative intensity of the brightest satellite is 0.05, which of 5% of the central intensity of the line. To be sure, this satellite is not as appreciable as in Figure 6a. Data on the Rowland ghosts in the third order of the grating have already been presented in Table 4. Here the ghosts were found to be somewhat more intense than in the second order of the grating. The intensity of the ghosts, generally speaking, falls with increasing order, but in this case, the ghosts of the third order are more intense than the ghosts of

the second (cf. the last column of Table 4). The ghosts located on the red side of the profile nucleus are a little more intense than those located on the violet side. We note that such a distribution of the ghost intensity is opposite to that observed in the second order of the grating. As is seen from Figure 6 and Table 4, the Rowland ghosts in the third order of the grating are located closer to the central maximum than in the second order. We have noted above a small asymmetry of the wings in the instrumental profile; in Figure 5a, the violet wing is higher than the red, whereas in Figure 6a, the opposite is observed. This is probably caused by the difference in intensity of the short wavelength and long wavelength satellites. As is seen from Figures 5b and 6b, below the intensity level of /99
$\bar{3}.0$, the red wing is above the violet everywhere.

In Figure 7, we have constructed the medial cross section of the instrumental profile for the second order of the grating. The line OO passes through the peak of the profile. The wavelengths measured from this line, being the axis of symmetry of the profile, are plotted along the abscissa, the logarithms of the relative intensity are plotted along the ordinate. The points denote the positions of the middle of the profile at different intensity levels. As Figure 7 indicates, the red wing is higher than the violet below an intensity level of 0.001. Above the 0.001 level, the points cover wavelengths along the axis of symmetry, and their average value above 0.01 exactly coincides with this axis.

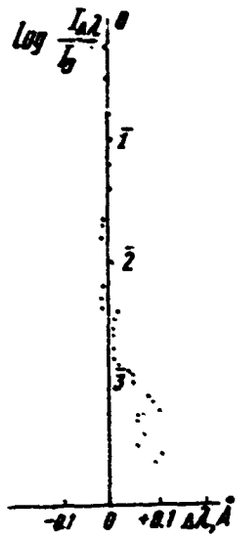

Figure 7. Medial cross section of instrumental profile in second order of grating. Points denote position of middle of profile at different intensity levels

Thus the nucleus of the instrumental profile is a single intensity maximum and has a symmetric shape. The wings consist of a large number of satellites located symmetrically in pairs relative to the nucleus, whose intensities differ somewhat. If, in the second left order of the grating, the satellite in the

violet wing is more intense that the satellite located at the same distance from the center of the profile in the red wing, then in the third right order of the grating, the opposite pattern is observed. The same change in intensity from the left orders of the grating to the right are observed in the case of the Rowland ghosts.

In order to study the effect of the entrance slit width on the half-width of the instrumental profile, we constructed profiles of the laser line, which were obtained for different entrance slit widths. The profiles obtained in the second order of the grating /100 for entrance slit width of 0.01, 0.02, 0.03 mm are presented in Figure 8a; the same for the third order of the grating for widths of 0.01, 0.02, 0.03, 0.04 mm are presented in Figure 8b. As is seen from Figure 8, a small broadening of the line profile is observed with increasing entrance slit width. It becomes particularly appreciable when the slit reaches a width of 0.04 mm. This is confirmed by the data of Table 6, where the half-width of the instrumental profile, obtained for different entrance slit widths, are presented.

The effect of the entrance slit width on the half-width of the profile is most notable on the first order of the grating, and least — in the third. As is seen from Table 6 and Figure 8, the instrumental profile is rather narrow for entrance slit widths up to 0.03 mm. The use of the slit within the limits of such widths is recommended for observations. In those cases when the incident light is insufficient, the slit can be increased to a width of 0.04 mm without great loss in the resolving power of the instrument. Profiles were obtained with a half-width narrower than those presented above. We will not reproduce them here. For slit widths within the range from 0.01 to 0.04 mm, the half-width of the instrumental profile, on the average, is 100 $\pm$ 29 mÅ in the first order of the grating, 44 $\pm$ 3 mÅ in the second, and 24 $\pm$ 2 mÅ in the third. However, the narrowest profiles were obtained for an entrance slit width of 0.02 mm. In this case, the half-width is h = 80 mÅ in the first order, h = 42 mÅ in the second, and h = 22 mÅ in the third.

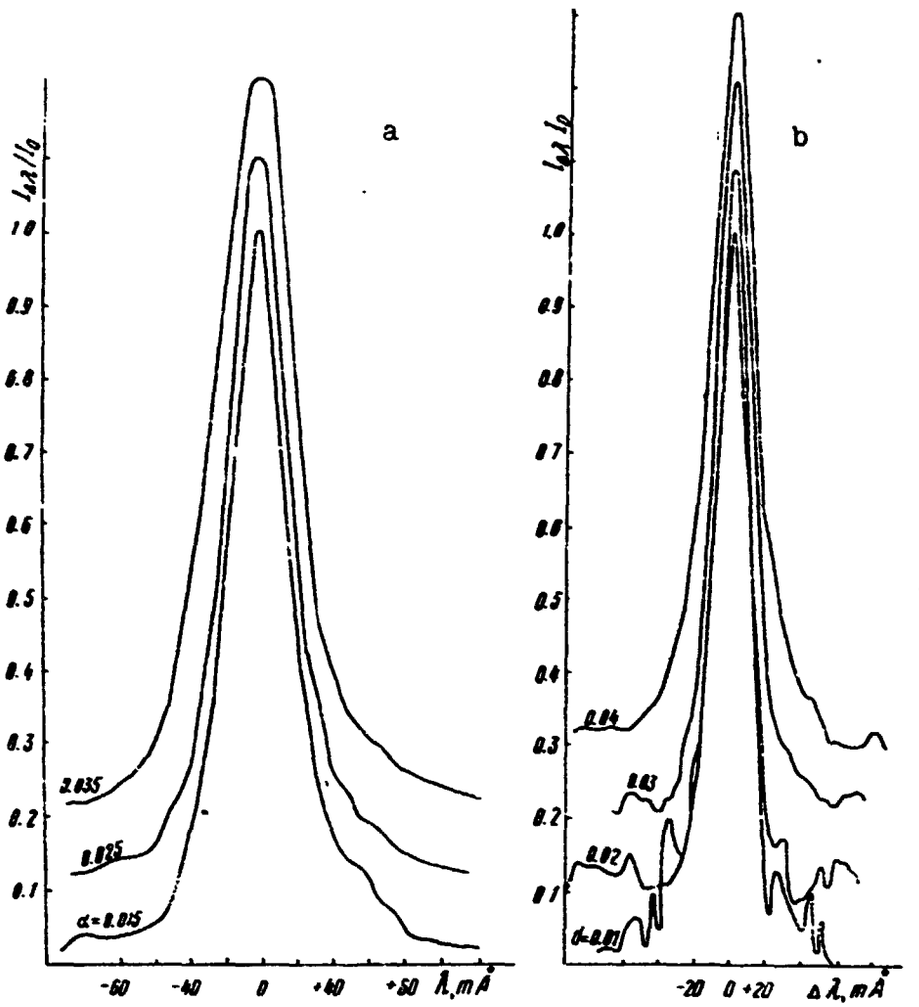

Figure 8. Instrumental profile in second (a) and third (b) orders of grating, obtained for different entrance slit widths

As follows from Figures 5, 6, and 8, the instrumental profile has a narrow nucleus and extended wings. The nucleus of the profile can be approximated by a Gaussian curve. The extended wings of the profile are close in nature to the effect of attenuation, and can be represented by the Lorentzian dispersion function. If we wish to represent the whole profile by one function, then it must involve the Gaussian and Lorentzian distribution functions. Such a function was first considered by Voigt [5], and has the form:

$$F(v) = \int_{-\infty}^{+\infty} L(v-x)G(x)\,dx.$$

TABLE 6

Entrance slit width, mm	Half-width of instrumental profile obtained in different orders of grating, mÅ		
	I	II	III
0.010	75	47	24
0.015	107	41	22
0.020	82	45	22
0.025	86	41	23
0.030	107	43	24
0.035	132	45	24
0.040	152	47	28
0.045	180	—	—
0.050	156	—	38

Here, $L(x)=\frac{1}{\pi}\frac{\beta_1}{\beta_1^2+x^2}$ is the Lorentzian distribution; $G(x)=\frac{1}{\sqrt{\pi}\beta_2}\times$ $\exp\left(-\frac{x^2}{\beta_2^2}\right)$ is the Gaussian distribution, β_1 and β_2 are parameters; $v = \Delta\lambda$ is the distance from the center of the profile in this case. The normalized Voigt function:

$$V(u, b_1)=\frac{F(u)}{F(0)}$$

is tabulated in [6], where $u=\frac{2\Delta\lambda}{h}$ and $b_1=\frac{\beta_1}{h}$ (h is the half-width of the profile). Making use of the tables of [6], we constructed the family of Voigt profiles (Figure 9) for the values of the parameter b_1 0.1; 0.2; 0.3; 0.4 [the quantities log V (u, b_1) are plotted along the ordinate, log u — along the abscissa]. The following graphic method was used to determine the parameters of the Voigt functions approximating the instrumental profiles of our spectrograph. The instrumental profile was represented on a logarithmic scale. For this, log ($I_{\Delta\lambda}/I_0$) was plotted along the ordinate, log $\Delta\lambda$ — along the abscissa. After copying the obtained curve on transparent paper, we superimposed it on the curves of the Voigt function so that the readings along the ordinate coincided. Then the observed profile was shifted along the abscissa until it coincided with one of the curves of the Voigt function. We took the value of

/101

/102

the parameter b_1 from the curve which best coincided with the observed profile. It was found that the instrumental profile in the second order of the grating of our spectrograph was most accurately represented by the Voigt function with the parameter $b_1 = 0.25$. The circles in Figure 9 refer to the violet, and the crosses to the red wing of the profile. The quantities $b_2 = \beta_2/h$, depending on b_1, are also tabulated in [6]. The value of the logarithm of the half-width log h is obtained on the abscissa of the instrumental profile at the point corresponding to log u = 0 on the abscissa of the Voigt profile, when the observed profile is superimposed on the calculated. By knowing h, it is easy to convert from b_1 and b_2 to β_1 and β_2.

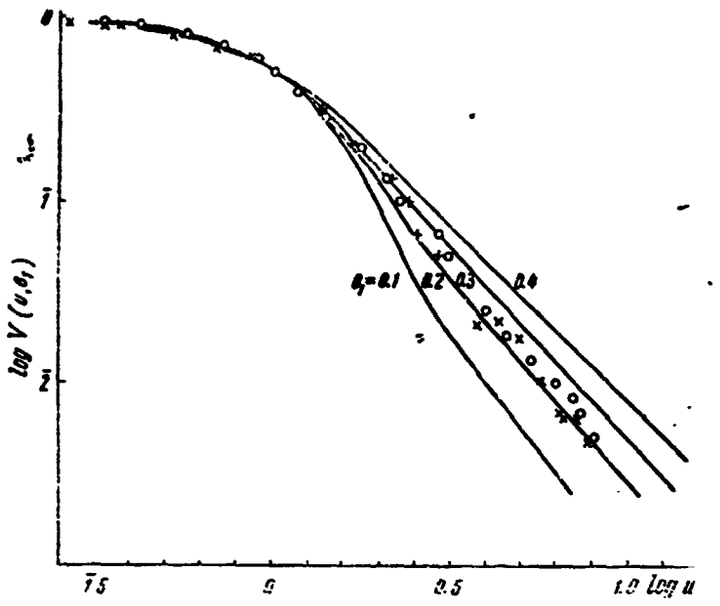

Figure 9. Comparison of the instrumental profile obtained in second order of grating with curves of the Voigt function. Crosses denote the violet, circles the red wings of the instrumental profile

Analagous comparisons of the observed profile with the calculated profile were carried out for the third order of the diffraction grating. The parameters b_1, b_2 and the half-width h were obtained as a result. The obtained data and parameters calculated from them are presented in Table 7. The half-width of the instrumental profile is indicated in the first row; the parameters b_1 and b_2, obtained from a comparison of the observed and calculated [6] profiles — in the second and fourth; the calculated parameters of the Voigt function which approximate the given instrumental profile — in the third and fifth. The parameters b_1 presented in Table 7 refer to the

average over the two wings of the profile. The parameters b_1, obtained separately for the red and the violet wing differ somewhat from each other.

TABLE 7

Parameter	Values calculated for II and III order of grating	
	II	III
h, mÅ	41	24
b_1	0.25	0.22
β_1, mÅ	10.2	5.3
b_2	0.417	0.443
β_2, mÅ	17.4	10.6

The profiles of the spectral lines are well represented by the Voigt function. The procedure for correcting the observed profile of the spectral line for the effect of the instrumental profile is technically as follows: The observed profile of the line is represented on a logarithmic scale; then, by comparing it with the calculated profiles of the Voigt function, the parameters b_1 (S), b_2 (S) and h (S) are found; β_1 (S), β_2 (S) and /103

$$p(S) = \frac{\pi}{2} \cdot \frac{b_2(S) \exp(-\alpha^2)}{\int_0^\infty \exp(-y^2)\, dy},$$

where $\alpha = \beta_1/\beta_2$. In [6], α and p are tabulated depending on b_1. Further, by knowing the parameters $\beta_1(A)$, $\beta_2(A)$ of the instrumental profile, we can easily calculate from the observed parameters of the spectral lines being studied β_1 (S) and β_2(S), its true parameters $\beta_1(W)$, $\beta_2(W)$. They are related in the following manner:

$$\beta_1(W) = \beta_1(S) - \beta_1(A), \quad \beta_2^2(W) = \beta_2^2(S) - \beta_2^2(A).$$

We determine α from the calculated parameters β_1 (W) and β_2 (W) and, by using Table 1 of [6], we find b_1 (W), b_2 (W) and p (W) from α. Then the true half-width of the spectral line is calculated from the formula:

$$h(W) = \frac{\beta_1(W)}{b_1(W)} = \frac{\beta_2(W)}{b_2(W)},$$

and the true central intensity c (W), from the formula:

$$c(W) = c(S)\,\frac{p(S)\,h(S)}{p(W)\,h(W)},$$

where c (S) is the observed central intensity of the spectral line.

Profiles of selected Frauenhofer lines obtained with the tested spectrograph. Central intensities, calculated on the basis of models of stellar atmospheres, even for the most intense lines, are less than the observed [8]. This divergence of theory and observations is explained partially by the imperfection of spectral apparatus.

Practice indicates that the effect of the instrumental profiles on the profiles of Frauenhofer lines is most strongly expressed in their central parts. As a result, the central intensity of the line is enhanced. Light scattered inside the spectrograph leads to an analogous phenomenon. With the appearance of spectrographs of high resolving power, the observed central intensities have approached closely to the theoretical calculations [9].

In order to compare the pratical potentialities of the ASP-20 /104
spectrograph with spectrographs used for solar investigations at other observatories, we selected several Frauenhofer lines of different intensities and investigated them with the help of the ASP-20. As was noted above, the optical system of the comparison bench permitted obtaining the spectra of the laser and Sun simultaneously. The radiation power of the laser was such that, to obtain the normal photographic density of the spectra of the laser and Sun in the second order of the grating, the same exposure time was required. We selected for photometry the section of the solar spectrum with the line λ 6246.3 Å on the same spectrogram on which the laser spectrum was obtained. The latter was used to derive the instrumental profile of the spectrograph. We recall that these spectrograms were obtained on the photographic plates WP-1 of the firm ORWO, and were developed in the fine grain developer A-44. As a result of the photometry of the section of the solar spectrum with the Frauenhofer

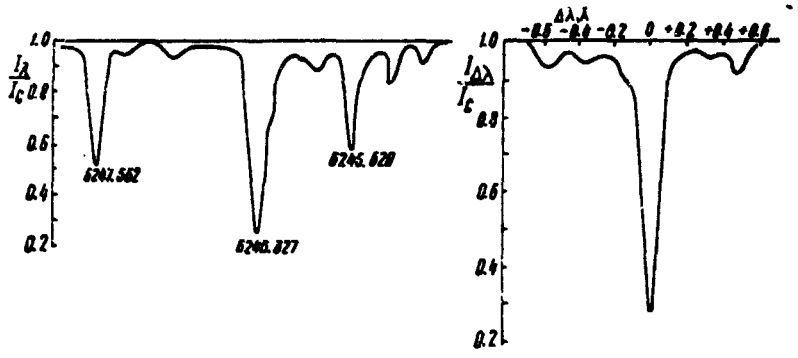

Figure 10. Portion of solar spectrum with Frauenhofer lines λ6247.5Å, λ6246,3Å, λ6245.6Å (left); profile of Frauenhofer line FeI λ5307.3Å (right)

lines Fe II λ 6247.5 Å, Fe I λ 6246.3 Å and Sc II λ 6245.6 Å, obtained in the second order of the grating, the profile of this portion of the spectrum was constructed. It is reproduced in the left part of Figure 10. Its comparison with the same section of the spectrum in the Utrecht Photometric Atlas [10] indicates that the lines in our spectrograms are characterized by a smaller central intensity. In Figure 10, the lines λ 6247.5 Å, λ 6246.3 Å, λ 6245.6 Å are approximately 18% deeper than according to the data of [10], and the depths of the weak lines is approximately ten times greater than the depths of these lines in the Utrecht Atlas. The central intensities of these lines are compared below with those obtained by other authors (Table 8).

The profile of the line Fe I λ 5307.3 Å, observed photographically in the third right order of the grating is shown in the right part of Figure 10. The photographic plates WP-1 of the firm ORWO were used. A number of weak lines, which decrease the level of the continuous spectrum, is seen in the vicinity of the line being studied. We found locations free of lines in the spectrum and took these sections as the level of the continuous spectrum. They correspond to the same sections in the solar spectrum which were considered in [9] as undistorted by absorption lines.

The line Fe I λ 5307.3 Å being studied is one of the narrowest and deepest in the visible portion of the solar spectrum. The observed profile of this line has, according to our data, a half-width /105

h (S) = 100 ± 4 mÅ, and a central depth of its profile c (S) = 0.72 ± 0.01. After correcting the observed quantities for the effect of the instrumental profile by the method described above, we obtained the true values of the half-width h (W) = 94 mÅ, and central depth c (W) = 0.79. This line was investigated photoelectrically in [7]. The fifth order of the double diffraction monochromator of the Pulkova Observatory was used. A profile of the line FeI λ 5307.3 Å, with a half-width h (S) = 96 mÅ and central depth c (S) = 0.696, was obtained as a result.

TABLE 8

Author	λ, Å		
	6246.327	5324.191	5307.369
Minnaert (Utrecht Photometric Atlas) [10]	0.440	0.170	0.310
Brault, et al. (Kitt Peak) [9]	0.278	0.135	0.230
I. Sattarov (Tashkent)	0.285	0.150	0.280

We also studied the profile of the line Fe I λ 5324.2 Å. The violet wing of the profile is strongly distorted by the presence of blending lines. The red wing, to a distance of Δλ=0.4 Å, is evidently distorted by the superposition of other lines. Thus, we present the data for it only:

Δλ, Å	$I_{\Delta\lambda}/I_0$	Δλ, Å	$I_{\Delta\lambda}/I_0$
0	0.150	300	872
0.025	235	400	925
50	335	500	945
75	440	600	956
100	525	800	964
125	590	1.000	970
150	648	1.500	0.983
200	747		

The line λ 5324 Å is of average intensity and has broad wings extending more than 1.5 Å from its center. The observed profile of this line, according to our data, has a half-width h (S) = 250 mÅ, and central depth c (S) = 0.85. As follows from our determinations, the half-width of the instrumental profile is 11 times narrower than

the half-width of the line λ 5324.2 Å. The tables of [6] do not permit expressing the profile of this line in the Voigt function. Thus we could not obtain the true values of h and c. However, taking into account the fact that the profile of the line λ 5324.2 Å is wider than the instrumental profile by far, one can assume that the correction for its effect probably does not exceed 2 - 3%.

We present in Table 8 the observed central intensities $r(S) = 1 - c(S) - (I\lambda/I_c)_{center}$ for three lines to compare the results of our investigations with the data of other authors. As is seen from this table, the central intensities determined by us are close to those obtained in [9], exception the line λ 5307.3 Å. We presented above the central depth of the line λ 5307.3 Å, corrected for the instrumental profile. By using it we arrive at the value of the true central intensity of this line $r(W)=0.21$, which is comparable with the values presented in [9]. Actually, in the case of the data in [9], the true central intensities corrected for the effect of instrumental profile differ from the observed intensities written in Table 8 by 1% at most. Hence, it follows that after correction for the effect of the instrumental profile, the observed central intensities of the Frauenhofer lines obtained on our spectrograph practically correspond to those determined on the vacuum spectrograph of the solar telescope of Kitt Peak Observatory. The corrections for the effect of the instrumental profile do not exceed 5 - 7%. '106

Thus, on the basis of this account, we are led to the conclusion that the ASP-20 spectrograph of the ATsU-5 horizontal solar telescope of the Astronomical Institute of the AN UzSSR has a sufficiently high resolving power, and can be successfully applied to the Investigation of Frauenhofer line profiles.

In conclusion, the author expresses thanks to colleagues of the Institute of Electronics of the AN UzSSR D. D. Gruich and T. U. Arifov for granting the temporary use of the gas laser.

References

1. Lipskiy, Yu. N. Astron. zh., Vol. 18, No. 3, 1941.

2. Garrison, J., R. Lord and J. Lufburow. Prakticheskaya spektroskopiya (Practical Spectroscopy). Moscow, Foreign Literature Press, 1950.

3. Van Bueren, H. G. and H. Hieuwenhuijze. BAN, Vol. 18, 1966, p. 3.

4. Gurtovenko, E. A. and L. U. Fedorenko. Solar Physics, No. 6, No. 3, 1969.

5. Voigt, W. Münch. Ber., 1912, p. 603.

6. Elste, G. Z. f. Aph., Vol. 33, 1953, p. 39.

7. Karpinskiy, V. N. Izv. GAO, No. 178, 1965, p. 84.

8. Sobolev. V. V. Kurs teoreticheskoy astrofiziki (Course in Theoretical Astrophysics). Moscow, "Nauka" Press, 1967, p. 138.

9. Brault, Y. W. et al. Solar Physics, Vol. 18, 1971, p. 3.

10. Minnaert, M, G. F. W. Mulders and I. Houtgast. Photometric Atlas of the Solar Spectrum. Utrecht, 1940.

TRANSMISSION OF INTERFERENCE-POLARIZATION FILTERS FOR H-ALPHA AND CaII K LINES

Z. B. Korobcva

ABSTRACT. Two Halle filters were investigated. The following characteristics were determined for lineshifter readings within ± 1 Å for the Hα-filter and ± 0.4 for the K-filter: the transmission at the band center (τ), the half-width of the band ($d\lambda$), the total intensity of the secondary maxima (ΣI_i) and the total intensity of these secondary maxima in each of the wings (ΣI_{iv} and ΣI_{ir}) were obtained. The corrections to the lineshifter readings ($\Delta \lambda_{meas} - \Delta \lambda$) were also obtained.

Narrow-band interference-polarization filters (IPF) are widely /107
used in solar research. The morphological, photometric, and dynamic characteristics of chromospheric formations are studied with their help. IPF are also used as a monochromatic guide for magnetographic observations [1].

Filters of V. Halle (FRG) with variable pass band, intended for solar observations in the H α line, have appeared in practice in recent years in the USSR and abroad.

The Division of Solar Physics of the Astronomical Institue of the AN UzSSR has available two Halle wide-angle interference-polarization filters. One of them transmits the H α line, the other — the K Ca^+ line. We have investigated the instrumental profile of these filters for various positions of the pass band.

The construction of the Halle IPF transmitting the H α line is described in detail in [2]. Without returning to it, we will discuss the optical design of the K-filter, since it differs from the design of the hydrogen IPF and, as far as we know, is not described in the literature.

The K-filter consists of 10 birefringent elements. Seven of them are fabricated from quartz, and three from Iceland spar (calcits). Thanks to the fact that the individual elements of the filter are made split, the number of polaroids is reduced from 11 to 7. This contributes to the increase of the IPF transmission.

Birefringent prisms of calcite and glass are used as five of the polaroids, from which several beams diverge at different angles to the optical axis. They form a series of secondary images. The angle between the principal and closest secondary images is 6°.3. Two polaroids (at the entrance and exit of the beam) are made from special polarcid films transmitting ultraviolet rays. These polaroids serve as the lineshifters. Their rotation with respect to the optical stack leads to a shift of the pass band of the two calcite elements with the greatest birefringence. Moreover, the three calcite and two quartz elements perform as wide-angle. This increases the monochromatic field of view to 5°. Thus, the filter can be placed in the converging beam of a telescope with an aperture 1:15.

The filters were analyzed by a technique similar to that described in [2 - 7].

To obtain the spectrograms of the passband, each filter was mounted at operating temperature in autocollimation in front of the slit of the ASP-20 spectrograph in the pavilion of the ATsU-5

horizontal solar telescope. The center of the solar disk served as the light source. For the correct installation of the filter, it was necessary to have the spot from its front surface coincide with the principal mirror of the telescope, and the entrance slit of the /110
spectrograph located in the middle of the spot from the rear surface of the filter. The hydrogen filter was placed directly in front of the spectrograph slit. The calcium filter was mounted so that the distance between its rear surface and plane of the entrance slit of the spectrograph, on which the solar image was focused, was not less than 170 mm. With this installation, the secondary images emerging from the filter do not overlap the main image.

Although each filter has a set of pass bands (0.5 Å and 1.0 Å for the Hα-filter, and 0.3 Å, 0.6 Å and 1.2 Å for the K-filter), we investigated them only for the narrowest band, the most effective for studying the fine structure of chromospheric formations. A contrast element was always inserted in the Hα-IPF.

The pass band of the filters was shifted along the spectrum by 0.1 Å. To determine the position of the pass bands for different shifts, the solar spectrum was photographed through the IPF and without it, with the same position of the photographic plate, with successive screening of different parts of the entrance slit of the spectrophotograph.

Calibration of the spectrograms was carried out from photographs of the center of the solar disk through an eight-stage attenuator and neutral light filter. In processing the spectrograms, these same photographs served for correcting the profile of the pass bands of the IPF for the Frauenhofer spectrum of the source. The region of the H α line was photographed on Kodak O-A-F plates, the K region — on WU-1.

The spectrograms were read photometrically on the MF-4 microphotometer, with recording on graph paper. The distance of the principal maxima from the center of the H α and K lines for all

readings of the lineshifter was measured on the UIM-23 coordinate computer.

The profiles of the pass band of the Hα-IPF, corrected for the Frauenhofer spectrum of the source, are presented in Figure 1. The intensity of all points of the profiles is expressed as fractions of intensity of the principal maximum. The wavelength of H a is taken as the zero on the abscissa.

The optical characteristics of the Hα-filter, presented in Table 1, were calculated from the profiles of Figure 1. The following designations are used here and below: $\Delta\lambda$ is the pass band shift according to the lineshifter scale; $\Delta\lambda_{meas}$ is the shift measured with respect to the position of the H α line; $\delta\lambda_{meas}$ is the half-width of the band measured on the profiles; $\sum I_i$ is the total intensity of the secondary maxima in percentages of the intensity of the principal maximum. This quantity, as in [2], was determined from the areas bounded by the profiles in the corresponding maxima; $\sum I_{iv}$ and $\sum I_{ir}$ are the total intensities of the secondary maxima shifted relative to the principal maxima toward the short- and long-wavelength sides of the spectrum; τ is the transmission of filter at the band center*.

It is seen from Figure 1 and Table 1 that the width of the main pass band of the filter is less in a majority of the cases than follows from the instructions, but the intensity of the secondary maxima rapidly increases with a shift of the band into the wings of the H α line. For a shift of the band into the short-wavelength side of the spectrum, the secondary maxima from the long-wavelength side predominate. The maximum, separated from the principal maximum by 2 Å, becomes the most intense. Its intensity for $\Delta\lambda$ - - 1 Å is /111

*V. Baturin, laboratory assistant for the Division of Solar Physics, participated in the processing of the spectrograms.

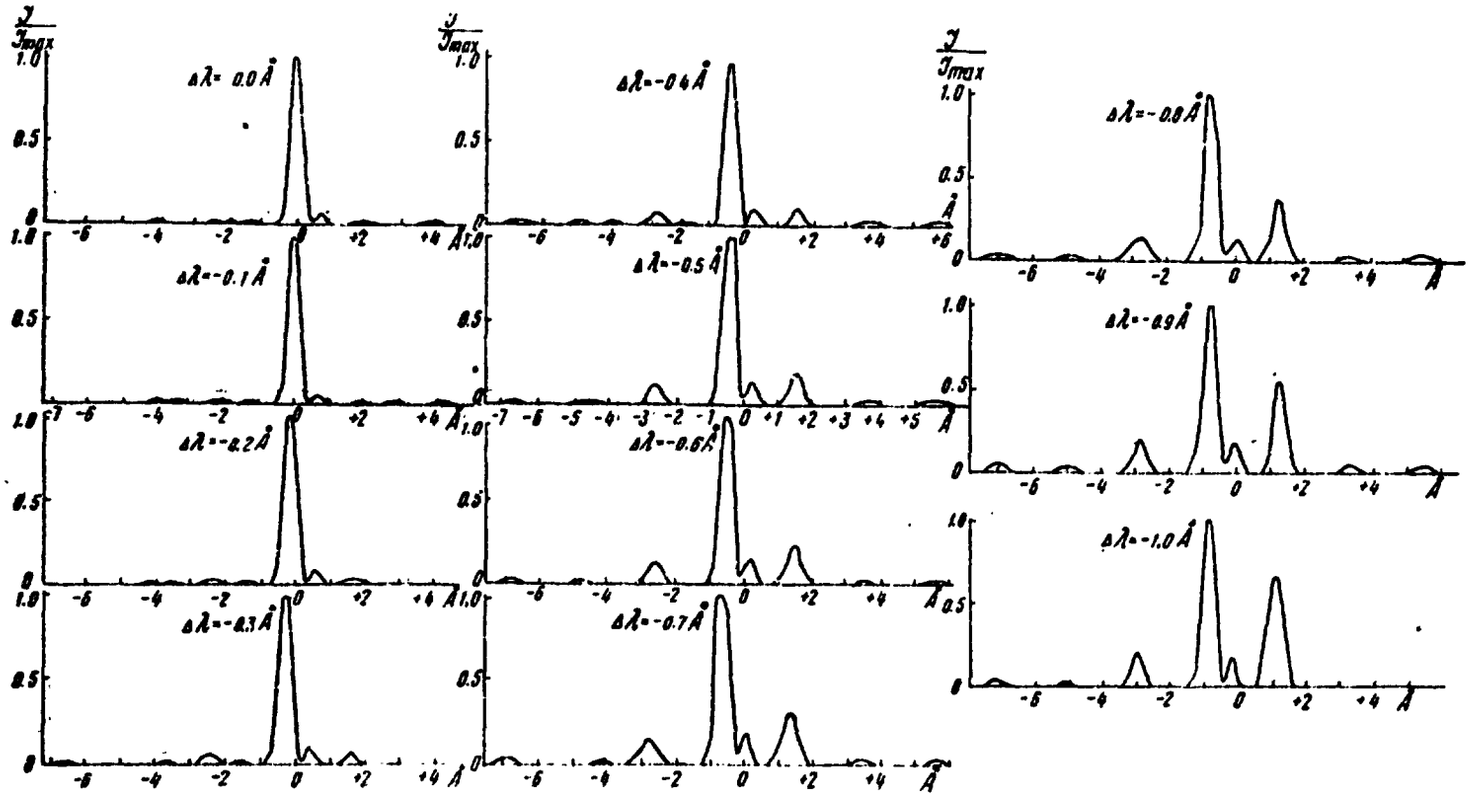

Figure 1. Transmission of hydrogen filter

(Figure continued on following page)

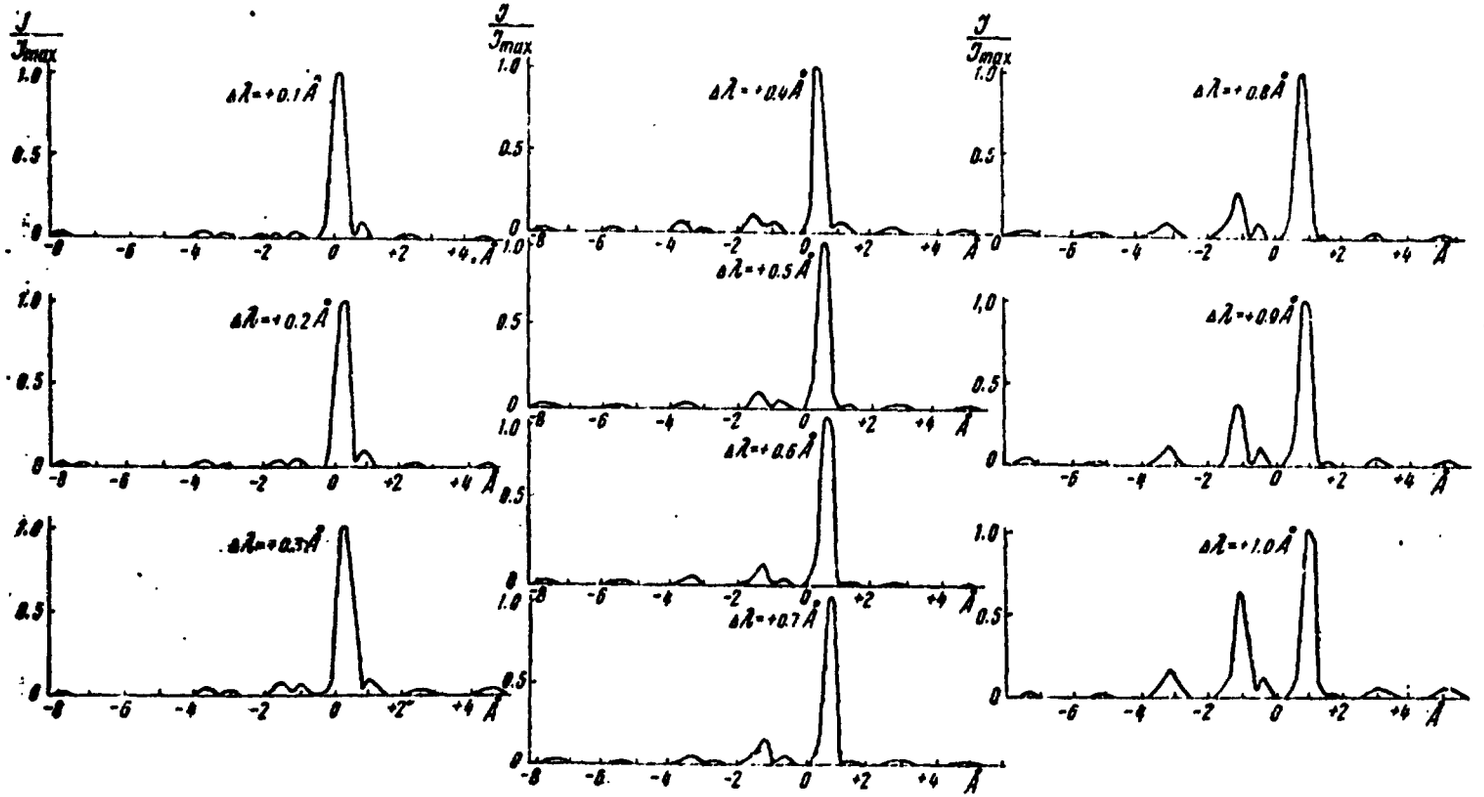

Figure 1. (continued)

TABLE 1.

$\Delta\lambda$, Å	$\Delta\lambda_{meas}$, Å	$\delta\lambda_{meas}$, Å	ΣI_1, %	ΣI_{1v}, %	ΣI_{1r}, %	τ, %
0.0	−0.01	0.40	8.7	3.5	5.2	7.0
−0.1	−0.06	0.40	10.7	3.9	6.8	6.4
−0.2	−0.18	0.44	11,8	4.3	7.5	6.0
−0.3	−0.28	0.45	18.4	5.6	12.8	5.8
−0.4	−0.40	0.43	26.3	8.8	17.5	5.5
−0.5	−0.47	0.50	39.0	11.7	27.3	5.5
−0.6	−0.55	0.50	47.0	14.4	32.6	4.1
−0.7	−0.64	0.50	57.5	15.1	42.4	3.6
−0.8	−0.73	0.47	68.2	20.0	48.2	3.5
−0.9	−0.80	0.45	93.0	25.4	67.6	2.3
−1.0	−0.89	0.45	124.4	25.7	98.7	2.0
+0.1	+0.16	0.50	14.2	6.7	7.5	5.2
+0.2	+0.27	0.52	20.5	11.3	9.2	4.9
+0.3	+0.38	0.54	21.6	13.3	8.3	4.6
+0.4	+0.46	0.50	25.7	18.1	7.6	4.4
+0.5	+0.55	0.43	18.6	15.3	3.3	4.5
+0.6	+0.63	0.42	22.1	19.0	3.1	4.4
+0.7	+0.70	0.43	30.5	26.2	4.3	4.2
+0.8	+0.77	0.48	48.8	42.7	6.1	4.2
+0.9	+0.86	0.47	69.8	60.7	9.1	3.7
+1.0	+0.93	0.47	99.4	88.6	10.8	2.8

82% of the intensity of the principal maximum. For a shift of the pass band into the long-wavelength side of the spectrum, the secondary maxima from the short-wavelength side predominate. The relative intensity of the largest (its distance from the principal is also 2 Å) is 60% for $\Delta\lambda$ = + 1 Å. It follows from the same table that it is necessary to introduce a correction into the value of the pass band shift taken from the lineshifter scale.

The conclusions were reached in [2, 7] that one can operate with similar IPF with pass band shifts up to $\pm$ 0.5 Å. In our case, ΣI_1 does not increase uniformly with band shifts to the long-wavelength and short-wavelength sides of the spectrum. While a shift of the band toward long wavelengths is probably tolerable up to $\Delta\lambda$ = + 0.6 Å, it should be limited to $\Delta\lambda$ = - 0.4 Å on the short-wavelength side. The transmission of Hα-IPF at the band center is 7% of the radiation incident on the filter at the given wavelength, and decreases with increasing $\Delta\lambda$, which agrees with the results of [2].

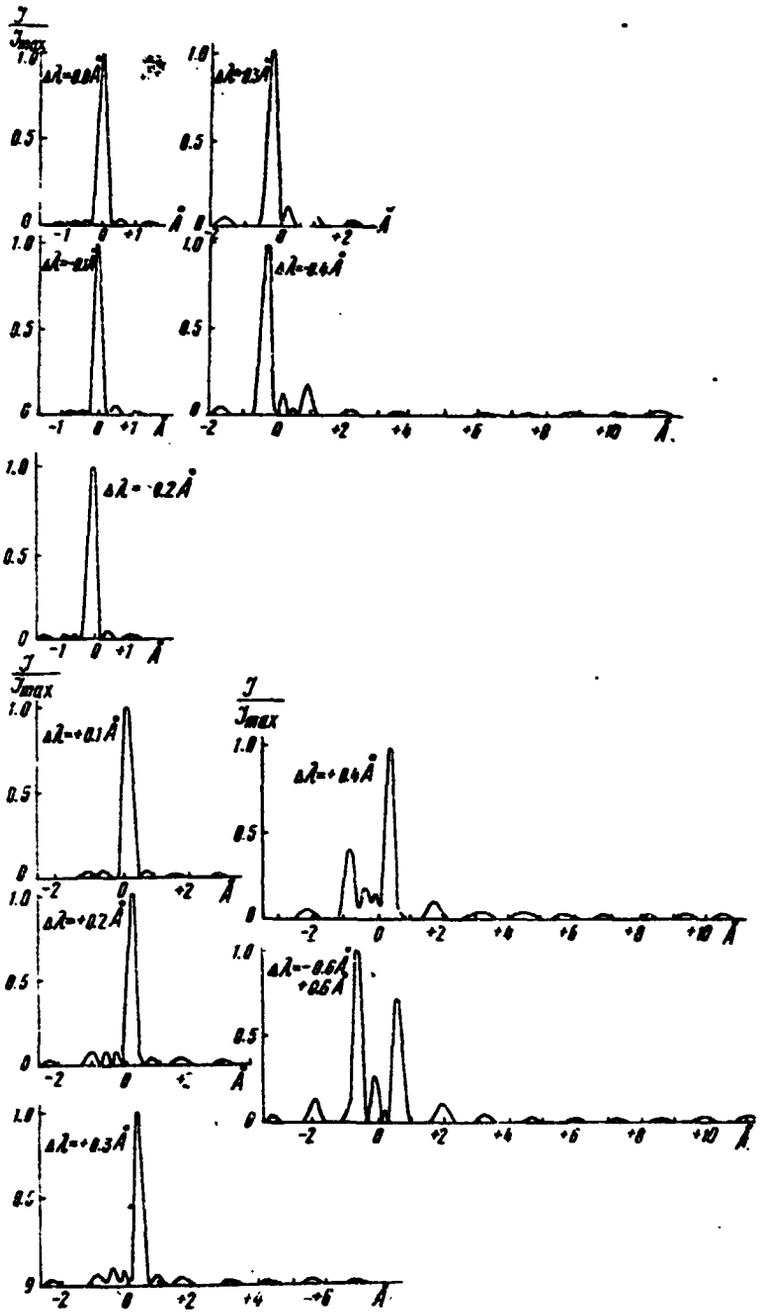

Figure 2. Transmission of calcium filter

Let us turn to the K-filter. The lineshifter scale of this filter is calibrated at ± 0.6 Å; however, appreciable secondary maxima appear as early as $\Delta\lambda = \pm 0.3$ Å. They intensify with increasing $\Delta\lambda$; thus, the filter was not investigated for $\Delta\lambda > \pm 0.4$ Å. When the lineshifter scale was rotated by 180° with respect to the zero mark, two pass bands appeared, separated with respect to K_3 and 1.2 Å.

TABLE 2

$\Delta\lambda$, Å	$\Delta\lambda_{meas}$, Å	$\delta\lambda_{meas}$, Å	ΣI_1, %	ΣI_{1v}, %	ΣI_{1r}, %	τ, %
0.0	0.00	0.30	10.3	5.6	4.7	5.9
−0.1	−0.11	0.28	8.7	2.7	6.0	5.3
−0.2	−0.20	0.28	12.4	5.6	6.8	3.9
−0.3	−0.28	0.35	29.0	6.8	22.2	2.6
−0.4	−0.35	0.30	37.0	0.5	36.5	2.8
+0.1	+0.13	0.35	14.2	8.1	6.1	5.2
+0.2	+0.19	0.25	40.1	25.*	14.3	3.7
+0.3	+0.25	0.25	45.9	27.2	18.7	3.4
+0.4	+0.40	0.32	102.1	74.7	27.4	2.3
−0.6	−0.62	0.28	83.2*	43.4*	39.8*	1.5
+0.6	+0.62	0.37				1.2

*With respect to violet maximum.

The results of the investigation of this filter are presented /113
in Figure 2 and in Table 2, from which it is seen that the actual values of the pass band width and its positions with shifts into the wings of the K-line, as in the case of the Hα-filter, deviate appreciably from the values indicated on the device. The secondary maxima for band shifts, beginning with $\Delta\lambda = -0.4$ Å and $\Delta\lambda = +0.3$ Å, form a series of uniformly spaced bands, extending on the long-wavelength side to more than 10 Å. One should obviously work with this filter with pass band shifts not exceeding $\Delta\lambda = -0.3$ Å and $\Delta\lambda = +0.2$ Å. The transmission of this filter is somewhat lower than the Hα-IPF.

In summarizing the results of the analysis of both devices, one should note that the K-filter differs favorably from the Hα-IPF by a narrower pass band, which permits obtaining filtergrams in K_3, K_2.

References

1. Ioshpa, B. A. Geomagnetizm i aeronomiya, Vol. 2, 1962, p. 172.

2. Vinogradova-Smirnova, T. A., M. V. Kushnir and A. A. Shpital'-naya. Bull. Solnechnyye dannyye, No. 2, 1970, p. 95.

3. Severnyy, A. B. and A. B. Gil'varg. Izv. Krymskoy astrofiz. observ., Vol. 4, 1949, p. 3.

4. Gurtovenko, E. A. Ir the collection: "Nablyudeniya Solntsa" (Observations of the Sun). Moscow, AN UzSSR Press, 1959, p. 25.

5. Van Griethuysen, I. G. and J. Houtgast. Bull. Astron. Inst. Netherl., Vol. 14, No. 490, 1959, p. 279.

6. Stenflor, J. O. Arkiv for Astron., Vol. 3, No. 34, 1965, p. 481.

7. Skomorovskiy, V. I. In the collection: "Resultaty nablyu-deniy i issledovaniy v period MGSS" (Results of Observations and Research during IQSY), Part 4. Moscow, "Nauka" Press, 1967, p. 105.

STUDY OF IMAGE QUALITY FROM THE PHOTOMETRIC PROFILE OF MERCURY ON THE SOLAR DISK

I. Sattarov

ABSTRACT. The role of scattered light and image smearing in spectrophotometric studies of the components of the solar surface is examined by using data of spectral observations of the transit of Mercury over the solar disk of May 9, 1970, which were obtained on the ATsU-5 horizontal solar telescope of the Astronomical Institute of the AN UzSSR. The observed profile of the image of Mercury on the solar disk is compared with those calculated under different assumptions about the image blurring function. The dependence of the values of the scattered light and the light caused by image blurring on wavelengths is studied.

1. Taking extraneous light into account with spectroscopic /114 study of components of the solar surface (spots, faculae, etc.) is one of the complex and unresolved problems of solar physics. We will call extraneous light here that which is projected, or however superimposed, on the image element being considered, but not actually belonging to the given element being studied. It has recently been ascertained that it can play an appreciable role, particularly in the case of the spectrophotometry of sunspots [1, 2]. Thus, the study of the characteristic properties of extraneous light is of definite interest.

Extraneous light can be divided into two components, according to the cause of its generation and by its nature. The first is caused by the processes of true scattering of sunlight from molecules and aerosol particles of the atmosphere of the Earth and by the scattering of light in the optics of the instrument. It produces a general background superimposed on the image, i.e., as if it were fogged. The intensity of the background at any point on the solar disk does not depend on the brightness of the region surrounding the given point. The second component includes extraneous light caused by non-uniformity (fluctuations of density) and instability in time of the optical properties of the atmosphere of the Earth, defocusing of the telescope optics and diffraction at the edges of the aperture, imprecision of the image direction and vibration of the instrument from local interference, scattering of light in the emulsion layer of photographic plates. This component leads to a decrease of contrast and to the redistribution of brightness of image components. For example, the brightness of a spot increases at the expense of a decrease of brightness of the photosphere surrounding the spot. We will subsequently call the first component of the extraneous light the scattered light proper, and the second — the blurring effect.

2. If $I(\xi, \eta)$ is the true intensity distribution over the illuminated surface, then the observed intensity distribution $I'(x, y)$ will be related to it by the following:

$$I'(x, y) = \int_{-\infty}^{+\infty}\int I(\xi, \eta) F(x-\xi, y-\eta)\, d\xi d\eta. \qquad (1)$$

The function $F(x-\xi, y-\eta)$ is called the distribution function of the extraneous light. This function is symmetric and must be normalized.

The graph of the function $F(x-\xi, y-\eta)$ has a narrow nucleus and extended wings [1]; the profile of the nucleus is principally determined by the blurring effect, and the wings are generated by scattered light. Thus the function F can be represented in the form of a superposition of two functions representing the blurring and scattering: /115

$$F = (1-\varepsilon) f_B + \varepsilon f_S. \qquad (2)$$

Here ε is the fraction of extraneous light caused by scattering. The normalized function f_B is the distribution function of the light caused by image blurring, and f_S is the distribution function of the scattered light.

In order to determine the true intensity distribution of the image element under consideration, one should solve Equation (1) for $I(\xi, \eta)$ in terms of the observed $I(x, y)$. It is required for this to find an analytic expression of the function F, which is a very difficult problem. Many authors [3 - 8] have tried to derive the function F empirically. To derive the function f_B, the observed profile of the edge of the solar disk is compared with some "true" assumed profile. The form of the function f_S is determined from observations of the halo around the image of the Sun.

The components of scattered light fall smoothly with distance from the center of the solar disk. It slightly affects the contrast of neighboring components, producing only a general background. For example, we can assume that the amount of scattered light is constant within groups of sunspots with a dimension $\approx$ 1 - 2'. The image blurring plays the determining role in the intensity distribution in this case.

The change in time of the optical properties of the atmosphere of the Earth, which leads to vibration of the image, has a random nature. The distribution function over the surface of the light source, caused by image blurring, was first proposed by Wanders [3], who represented it in the form of a two-dimensional distribution function of Gaussian random variables, i.e.:

$$f_B(x-\xi, y-\eta) \quad \frac{1}{\pi s^2}\exp\left[-\frac{(x-\xi)^2+(y-\eta)^2}{s^2}\right]. \qquad (3)^*$$

Here, s is the blurring parameter.

*Translator's note: The equation number — (3) — was inadvertently omitted from the original foreign text.

Michard [9] found that s depends on wavelength. However, Stumpff [10] did not observe such a dependence. Makita and Mo moto [8] indicated that the graph of the blurring function has a narrow nucleus and broad wings; thus, they represented it in the form of a superposition of two Gaussian functions with different parameters s.

When correcting the observed brightness of the umbra of sunspots for the effect of extraneous light caused by image scattering, several authors [3, 6, 8 - 10] have used the function f_B in the form of (3). They assumed that the true intensity within the umbra and penumbra have constant value, i.e., the true photometric section has a stepped shape. V. Ye. Stepanov [5] also assumed a stepped shape of the spot profile. But, according to his presentations, the intensity across the boundary nucleus-penumbra and penumbra-photosphere must not change discontinuously, but linearly. The corrections for blurring calculated by V. Ye. Stepanov [5] indicate their dependence on the wavelength of the radiation.

Thus, the results of the investigations of different observers clearly diverge. Perhaps this is partially explained by the difference of instruments used for the observations, and partially by the initial assumptions about the distribution of the true intensity in /116
the spot. In this respect, observations of the edge of the Moon during solar eclipses and transits of the inferior planets across the solar disk could be fruitful, particularly for clarifying the form of the function f_B.

3. We observed the May 9, 1970, transit of Mercury across the disk of the Sun, which began at 10:20 local time (i.e., at 4^h20^m U.T.), and ended at 18:13. It was overcast in the morning, but cleared after noon. The observations were interrupted from time to time by passing clouds. Nonetheless, the sky was not very clear.

The observations were carried out on the ATsU-5 horizontal solar telescope with the ASP-20 spectrograph of the Astronomical Institute of the AN UzSSR. The projection of Mercury on the solar disk was a

dark circular spot with a diameter of ≈ 12". In the focal plane of the telescope, where the spectrograph slit is positioned, the shadow of Mercury appeared as a dark circle of diameter ≈ 1 mm (Figure 1). The spectrograph slit was directed along the diameter of the shadow. The height of the slit was ≈ 8 mm, and its width was close to normal.

Figure 1. Projection of Mercury on the solar disk (indicated by arrow) obtained on the photoheliograph

The spectrum of the Sun intersected along the dispersion by the shadow of Mercury was reminiscent of the spectrum of sunspots (Figure 2). The observations were carried out in the first order of the diffraction grating with a dispersion ≈ 0.4 mm/Å. In this order, the camera permits taking a segment of the spectrum of length ≈ 800 Å, projected onto two 13 × 18 plates at the same time. Five such pairs of negative plates were obtained. On each pair we took ten spectra of the shadow of Mercury and a nine-stage attenuator, which covered the range

Figure 2. Portion of solar spectrum intersected by the shadow of Mercury in the middle

≈ 3700 - 6500 Å. Data on the obtained spectrograms are presented in the table. Fearing that the fraction of scattered light might be deficient because of underexposure, we used one of the transparent steps of the attenuator. The image of Mercury coincided with it, and

impressions of the attenuator were obtained with overexposure. However, as will be seen below, our fears were groundless, since the amount of scattered light was found to be sufficiently large to be produced on the spectra with normal exposure times. /117

No. of negative	t_{obs} (beginning-end)*	Wavelength region of spectrum, Å	τ_{exp}, sec
1	$15^h45^m-15^h52^m$	6600—4500	$0^s.3 - 0^s.4$
2	15 53 —16 00	6600—3700	0.3 — 0.6
3	16 44 —16 58	6600—3600	0.3 — 0.6
4	17 00 —17 10	6600—3700	0.3 — 0.6
5	17 35 —17 45	6500—3700	0.3 — 0.6

*In local time.

The WF-1 photographic plates of the firm ORWO were used, and were developed in the fine-grain developer A-44 for 8 minutes at a temperature of T-20° C.

The processing of the results of the observations were carried out on the MF-2 and MF-4 microphotometers with an automatic recorder of the type EPP-09. Photometric readings across the direction of the dispersion were carried out at about 30 sections of the spectrum free from absorption lines. The recordings obtained for the direct and reverse motion of the negative in front of the illuminating slit of the microphotometer were added, and the average taken. The photometric profiles of the projection of Mercury on the solar disk were constructed as a result.

4. The true surface brightness of the shadow of Mercury equals zero. The true photometric profile of the projection of Mercury on the solar disk must have a rectangular stepped shape. Deviation from this shape is caused by extraneous light. Let us consider the effect of extraneous light on the photometric profile of the projection of Mercury on the solar disk. We set the origin of the coordinate system at the center of the shadow of Mercury. The distribution

function of the extraneous light is specified by Formula (2). The observed intensity I (x, y) at some point M is related to the true intensity I (ξ, η) at point N in terms of the function F (x - ξ, y - η) by Formula (1). If we substitute (2) into Formula (1), then we obtain:

$$I(x, y) = (1-\varepsilon)\int_{-\infty}^{+\infty}\int_{-\infty}^{+\infty} I(\xi, \eta) f_B(x-\xi, y-\eta)\,d\xi d\eta + \\ + \varepsilon\int_{-\infty}^{+\infty}\int_{-\infty}^{+\infty} I(\xi, \eta) f_S(x-\xi, y-\eta)\,d\xi d\eta. \qquad (4)$$

We keep in mind that the intensity of the radiation I (ξ, η) and the amount of scattered light ε changes slowly over the disk of the Sun. In the shadow of Mercury and beyond the solar disk, I (ξ, η) = 0, so that the limits of integration in Formula (4) are arbitrary. Within 0'.5 - 1'.5 from the edge of the shadow of Mercury, one can assume that the intensity of the photospheric radiation is constant, and equals the average intensity of the photosphere $\bar{I}_{ph}$. Consequently, one can assume within these limits that I (ξ, η) = $\bar{I}_{ph}$. This assumption is illegitimate only near the edge of the disk of the Sun, where darkening is severe. Then the second term on the right side of Equation (4) will equal $\varepsilon\bar{I}_{ph}$. /118

We now convert to a polar coordinate system whose origin is placed at the center of the shadow of Mercury. We denote the radius of the shadow by ρ_0. The blurring function is taken in the form of (3). We substitute for I (ξ, η) in the first integral of Formula (4) its average value $\bar{I}_{ph}$; we take this constant out from under the integral. We divide both sides of the obtained equation by $\bar{I}_{ph}$; then we finally obtain:

$$\frac{I(r, \varphi)}{\bar{I}_{ph}} = \varepsilon + (1-\varepsilon)\frac{1}{\pi s^2}\int_{\rho_0}^{\infty}\int_{0}^{2\pi} \exp\left[-\frac{r^2 + \rho^2 - 2r\rho\cos(\varphi-\theta)}{s^2}\right]\cdot\rho\,d\rho\,d\theta. \qquad (5)^*$$

*Translator's note: Equation (5) is inadvertently unnumbered in the original foreign text.

Here, as above, the upper limit of the first integral is infinite. This is assumed purely arbitrarily; in reality, the upper limit is the boundary of the solar disk. When the projection of Mercury on the disk of the Sun is not located on the very edge of the disk, Formula (5) is valid, since for the assumed values of ρ_0 and s, the integral converges rapidly. After some transformations, the double integral on the right side of Formula (5) can be written in the form of the following series:

$$\frac{I(r,\varphi)}{\bar{I}_{ph}} = \varepsilon + (1-\varepsilon)\exp\left(-\frac{r^2}{s^2}\right)\left[\exp\left(-\frac{\rho_0^2}{s^2}\right) + \frac{r^2}{s^2}P\left(\frac{2\rho_0^2}{s^2}, 4\right) + \right.$$
$$\left. - \frac{1}{2!}\left(\frac{r^2}{s^2}\right)^2 P\left(\frac{2\rho_0^2}{s^2}, 6\right) + \cdots + \frac{1}{n!}\left(\frac{r^2}{s^2}\right)^n P\left(\frac{2\rho_0^2}{s^2}, 2n+2\right) + \cdots\right]. \qquad (6)$$

Here, $P\left(\frac{2\rho_0^2}{s^2}, 2n+2\right)$ is the analog of the probability integral. Replacement of the finite sum in Formula (5) for the infinite in deriving Formula (6) does not introduce significant inaccuracies in the final result, if the projection of Mercury on the solar disk is separated from the edge of the disk by a distance of $\gtrsim 1'$, i.e., by 0.06 of the radius of the solar disk. The observational material completely satisfies this condition. We found the values of the function $P\left(\frac{2\rho_0^2}{s^2}, 2n+2\right)$ by using the tables of probability integrals from [11].

The series in Formula (6) converges rather rapidly for possible values of s. For example, it was sufficient to limit the series to 30 terms to achieve an accuracy of 0.001 for r/s = 4. We calculated the series in the brackets in Formula (6) for values of r/s from 0 to 5 in steps of 0.5. Then, by specifying the different values of ε, we calculated I (r, ϕ) and constructed the photometric profile of the shadow of Mercury for different values of s. The value of ε was taken for the value of the scattered light, and the value of s — for the blurring parameter, for which the calculated profile coincided best with the observed profile. As a result, a pair of values of ε and s was obtained for each observed profile. Comparison of the calculated and observed photometric profiles of the shadow of

Mercury indicates that the blurring function is sufficiently accurately represented by Formula (3). Consequently, the image blurring process is analogous to the distribution of Gaussian random variables.

The photometric profiles of the shadow of Mercury are presented in Figure 3a, where the solid curve represents the observed, and the dashed curve represents the calculated profiles for values of s = 2", 3", 4". The negatives Nos. 1 and 2 were taken when the Sun was visible through the haze of high cloudiness. Thus, the amount of scattered light ε is ≈ 50% of the photospheric intensity. We should point out that in this case, the blurring parameter was precisely equal to 2". For s = 2", the calculated and observed profiles coincide. The edge of the shadow of Mercury is very clear, the intensity changes rather sharply from the photosphere into the shadow. The quantity s = 2" is less than the blurring parameters obtained from ground-based observations by other authors [3 - 10]. Although the quantity ε is large, the resolution of details in this case is relatively high.

/119

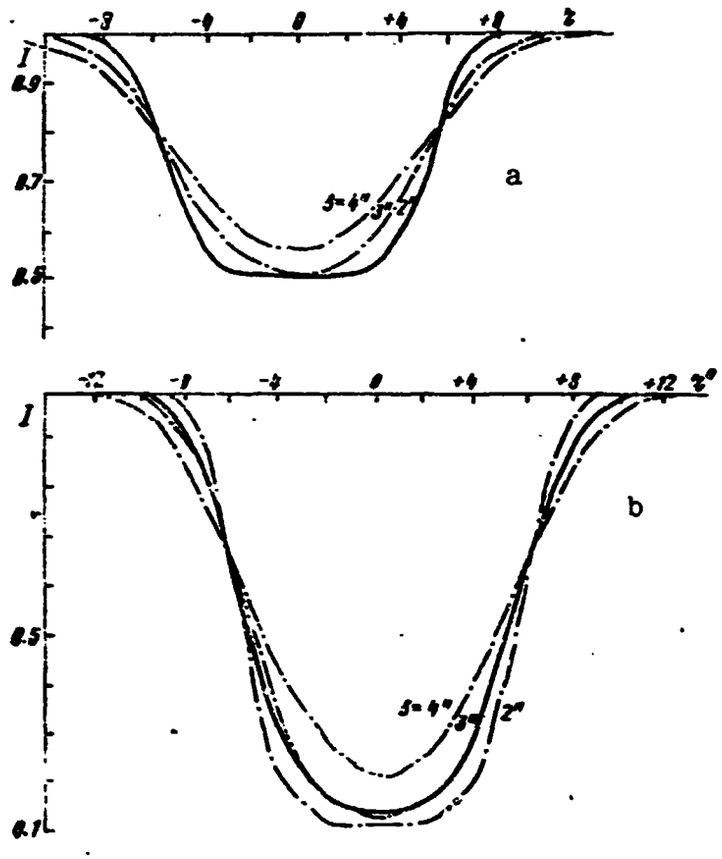

Figure 3. Spectrophotometric profiles of the projection of Mercury on the solar disk obtained from the data:

a — negative No. 2; b — negative No. 5

At the moment negative No. 5 was obtained (cf. Figure 3b), the sky cleared up. However, the amount of scattered light here was also rather appreciable. The minimum value of ε, which is observed in the green part of the spectrum, is $\approx$ 8% of the intensity of the photosphere. The parameter s varied over the limits 2"5 - 3"5, on the average scarcely less than 3". Two good spectra with sharp boundaries of the shadow of Mercury were obtained on negative No. 3. The values of the scattered light and the blurring parameter are about the same here as in Negative No. 5. At the time when negative No. 4 was obtained, the projection of Mercury was superimposed on a group of sunspots; thus, it was not processed. /120

As is seen from Figure 3, the observed intensity at the center of the shadow of Mercury is caused mainly by scattered light. The contribution of the blurring effect is negligibly small. This is indicated by the flat bottom of the photometric profile of the shadow. But the profiles presented in Figure 3 are the best. There are spectra of the shadow where a sharp boundary between the shadow and photosphere is not observed. In these cases, the blurring parameter exceeds 3", and the blurring effect introduces a significant contribution to the observed brightness of the shadow of Mercury. Spectra with the sharpest shadow of Mercury were selected for photometric processing.

The photometric profile of the shadow of Mercury was constructed for different portions of the spectral region $\lambda\lambda$ 3700—6500 Å. The obtained results indicate that the profiles for different portions of the spectrum differ little from each other. The blurring parameter and the amount of scattered light for each profile were obtained after comparing the observed profiles with the calculated. It is seen from Figure 4 that the amount of scattered light (we obtained it from the shadow profiles) varies over the spectrum, depending on wavelength. The minimum value of ε is observed in green light at the short wavelength side, from which the value of ε increases. The dependence of the form $\varepsilon \sim \frac{a(\lambda_0)}{\lambda}$ (solid curve) and $\varepsilon \sim \frac{b(\lambda_0)}{\lambda^4}$ (dashed curve) is also reproduced in Figure 4a. Here, a (λ_0) and b (λ_0)

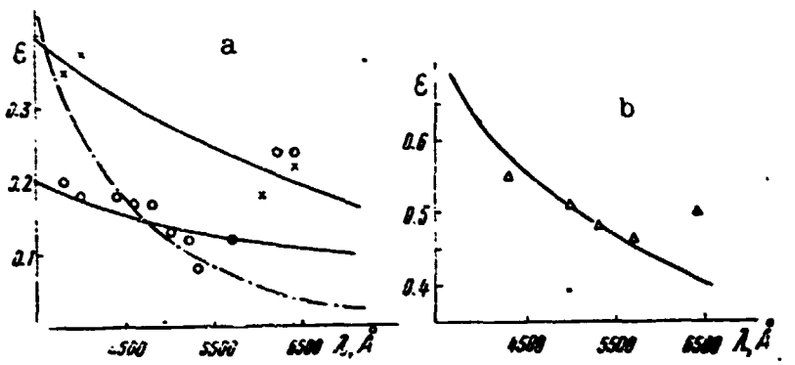

Figure 4. Dependence of the amount of scattered light ε on wavelength from the data:

a — negatives No. 3 (crosses) and No. 5 (circles); b — negative No. 2

are constants, λ is the wavelength. The first dependence of the amount of scattered light ε on wavelength occurs if the scattering in the atmosphere of the Earth is caused by aerosol particles, the second — if Rayleigh scattering occurs from molecules of the atmosphere of the Earth. As is seen from Figure 4, in the regions of the spectrum with wavelengths shorter than 5800 Å the observational data is better described by $\varepsilon \sim \frac{a(\lambda_0)}{\lambda}$ than by Rayleigh scattering. In the red part of the spectrum, the value of ε is greater than would be obtained from extrapolating the distribution curve of ε (λ) for the blue-green portions of the spectrum. Such a pattern is observed on the spectrograms of the negatives No. 2 and 5, although the levels of ε (λ) differ greatly here.

The value of ε obtained from negative No. 2 is 0.45 - 0.55, /121 whereas ε obtained from negative No. 5 lies in the interval 0.10 - 0.25. It is difficult to explain the growth of the value of ε in the red part of the spectrum.

It is difficult to trace any dependence of s on λ (Figure 5). A straight line parallel to the abscissa is obtained in the case of negative No. 2; one might judge from negative No. 5 some growth of s in the red and violet portions of the spectrum, and its minimum in

the blue part. But this dependence lies within the errors of measurement. The scatter of points in Figure 5 is greater in the long-wavelength portion of the spectrum.

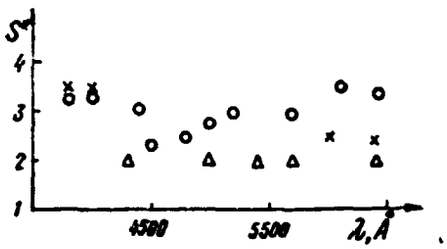

Figure 5. Relation between the blurring parameter s and wavelength from the data of negatives No. 5 (circles), No. 3 (crosses) and No. 2 (triangles)

The obtained results refer to the specific moment of observation. The parameters ε and s can change with time in accordance with the changes of the optical properties of the atmosphere of the Earth. If we could observe simultaneously a sunspot and a screen similar to the shadow of Mercury taken outside the atmosphere of the Earth and projected onto the solar disk, we could easily and quickly determine and take into account the effect of extraneous light on the surface brightness of a sunspot. One could successfully use the edge of the lunar shadow during solar eclipses for this purpose. In this case, one could divide the extraneous light into that caused by blurring and that caused by scattering of sunlight from areosol particles of the atmosphere of the Earth and in the instruments.

Conclusions

1. Determination and consideration of the effect of extraneous light on the surface brightness of solar formations (sunspots, faculae, etc.) and evaluation of image quality can be successfully performed during solar eclipses and transits of inferior planets across the solar disk.

2. The brightness in the center of the shadow of Mercury in this case, and also sunspots with radii $\gtrsim 5''$ (in general, under the condition $s \leq 3''$) is not distorted by image blurring.

3. The effect of image blurring is well described by the distribution law for Gaussian random variables.

4. The minimum value of the amount of scattered light is 8% of the intensity of the surrounding photosphere, and the maximum (under conditions of high cloudiness) reaches 50%.

5. The spectral distribution of the amount of scattered light indicates that scattering is caused mainly by aerosol particles in the atmosphere of the Earth.

6. The image blurring parameter s does not depend on wavelength.

7. Although the observations were carried out under the worst atmospheric conditions for this location, spectrograms of good resolution were successfully obtained.

References

1. Zwaan, C. Rech. Astron. Obs. Utrecht, Vol. 17, 1965, p. 4. /122

2. Sattarov, I. (a) Bull. Solnechnyye dannyye, No. 6, 1967; (b) Leningradskovo gosudarstvennovo universiteta (LGY), Vol. 19, No. 4, 1967.

3. Wanders, A. I. M. Z. f. Aph., Vol. 8, 1934, p. 108.

4. Krat, T. V. Astron. zh., Vol. 25, No. 5, 1948.

5. Stepanov, V. Ye. Gosudarstvennova astronomicheskovo instituta im. P. K. Shternberg (Soobshcheniya GAISh), No. 100, 1957.

6. Birkle K. and W. Mattig. Z. f. Aph., Vol. 60, 1965, p. 4.

7. Kozhevnikov, N. N. Astron. zh., Vol. 41, 1965, p. 1.

8. Makita, M. and Morimoto, M. Publ. Astr. Soc. Japan, Vol. 16, 1964, p. 1.

9. Michard, P. Ann. d'Aph., Vol. 16, 1954, p. 4.

10. Stumpff, P. P. Z. Aph., Vol. 52, 1961, p. 72.

11. Bol'shev, L. N. and N. V. Smirnov. Tablitsy matematicheskoy statistiki (Tables of Mathematical Statistics). Moscow, "Nauka" Press, 1965.

Translated for National Aeronautics and Space Administration under contract No. NASw 2483, by SCITRAN, P. O. Box 5456, Santa Barbara, California, 93108